NOVA SCHOOL OF SCIENCE & TECHNOLOGY

DEPARTAMENT OF CHEMISTRY

AFONSO MIGUEL DOS SANTOS GONÇALVES

BSc in Biochemistry

Blue biotechnology on the Coast of Portugal: a prospection of neurological bioactive compounds from marine sponges

MASTER IN BIOTECNOLOGY

NOVA UNIVERSITY Lisbon

MARCH, 2022

NOVA SCHOOL OF SCIENCE & TECHNOLOGY

DEPARTAMENT OF CHEMISTRY

Blue biotechnology on the Coast of Portugal: a prospection of neurological bioactive compounds from marine sponges

AFONSO MIGUEL DOS SANTOS GONÇALVES

BSc in Biochemistry

Adviser: Pedro Afonso dos Santos Baltazar Lima, Assis-tantProfessor, NOVA University Lisbon,
CEO, CSO and co-founder at Sea4Us

Co-Advisers: André Emanuel Pinheiro Costa Bastos,R&D Ma-nager at Sea4Us

Carlos Alberto Gomes Salgueiro, Full Professor,
NOVA University Lisbon

Examination Committee:

Chair: Ana Rita Cruz Duarte, Full Professor,
NOVA University Lisbon

Rapporteurs: Ana Isabel Moura Santos, Associate Professor,
NOVA University Lisbon

Advisers: Pedro Afonso dos Santos Baltazar Lima, Assistant Professor, NOVA University Lisbon,

CEO, CSO and co-founder at Sea4Us

André Emanuel Pinheiro Costa Bastos, R&D Manager at Sea4Us

MASTER IN BIOCHESMESTRY

NOVA UNIVERSITY Lisbon

MARCH, 2022

Blue biotechnology on the Coast of Portugal: a prospection of neurological bioactive compounds from marine sponges

To the Oceans

ACKNOWLEGMENTS

Gostaria de demonstrar o meu agradecimento a todas as pessoas e instituições que de alguma forma contribuiriam para a realização desta tese. Mencionando ainda que, a concretização da mesma não teria sido possível sem o seu apoio.

Ao **Doutor Pedro Lima,** o meu orientador, que desde o primeiro dia, no mergulho em Sagres, me facilitou a entrada no mundo da neurofisiologia em biotecnologia, um obrigado por parte do Diogo/Gonçalo/Afonso, ou, o que me quiseres chamar. Obrigado, pela motivação que me transmitiste para questionar não só ciência, mas como o mundo à minha volta, alargando a minha curiosidade e vontade de aprender. Por me deixares integrar numa empresa de investigação com o melhor ambiente/atitude/simpatia que já experienciei. O gajo "Da" Quarteira só te tem a agradecer.

Ao **Doutor André Bastos,** o meu co-orientador, Mr Miyagi, que dedicou dias da sua vida para me ensinar. Não sei ao certo por onde começar. Foste sem dúvida um dos melhores professores que já tive, não só pela paciência tremenda (enfâse no tremenda) como pela simplicidade lógica das tuas explicações. Contudo, a maior razão pela qual te agradeço prende-se no facto de seres também um grande amigo, que desde conversas, a doutrinas sobre a vida, brincadeiras, mas também das noitadas a trabalhar, nunca perdeste a boa disposição. Obrigado por tudo, especialmente, porque sem ti tanto a minha tese como a minha presença na empresa não teriam sido remotamente semelhantes.

Ao Miguel, Rosa, Diego tenho claramente a agradecer a disponibilidade para me ajudarem, sugerindo novas perspetivas científicas que me permitiram avaliar e melhorar a metodologia em torno da minha tese. Todavia, também tenho a agradecer todas as pausas, conversas e bullyings/brincadeiras que tornaram o meu estágio na empresa uma experiência inigualável. Muito obrigado por me tornarem o vosso "Barista oficial", relembrando que sem mim vocês não bebiam café de excelência.

Ao pessoal do Lab e à Cristina (ITQB), tenho a agradecer a ajuda nas mais variadas situações e à alegria que davam ao ambiente do laboratório, eliminado qualquer estado de tristeza ou monotonia.

Aos meus pais (mums e pups) e irmã (nês) por acreditarem em mim e me indicarem o melhor caminho a seguir, aparando sempre as minhas quedas, por mais frequentes que fossem. Por todas as chamadas de telefone só para "checking up", cafés no posto2, conversas motivacionais sobre o futuro, carinho, tiktoks, paciência e muito amor, MUITO OBRIGADO. O vosso apoio incondicional, foi o meu

porto seguro e não teria conseguido atingir este objetivo sem vocês. Um obrigado será sempre pouco para demonstrar o que sinto, mas MIL obrigados está um bocadinho mais próximo.

À Eva tenho a salientar a força, determinação e paciência que teve de ter para me conseguir aturar durante este período, onde insaciavelmente compreendeu a situação e me ajudou a ver o lado positivo, acreditando sempre em mim. Por todos os momentos partilhados, por me dares casa ao pé do mar durante dias a fio, pelos filmes, pelos chocolates, por sete rios, pelas tostas do mac e, especialmente, por me tornares melhor pessoa, muito obrigado.

Aos meus amigos que foram como família durante este tempo, ajudando-me sempre nos momentos de maior pressão e stress, quer seja na rua a beber uma cerveja, em casa ou ao telefone. Muito obrigado ao Miguel, Tomás, Nísia, Mariana, Luz e Diana, Johnny.

"The essence of knowledge is, having it, to apply it; not having it, to confess your ignorance"
(Confucius)

ABSTRACT

Marine environments are vastly unexplored territories, being considered an untapped resource of chemical and biological molecules. Chances of new opportunities are emerging and likewise, the discovery of new potential pharmaceuticals. These bioactive compounds are present in a variety of invertebrates, such as the sponges (Porifera) studied in this project, found on the Coast of Sagres, south of Portugal. The extracts and fractions obtained from this organism were submitted to neuronal bioactivity evaluations by determining their possible effects on both potassium (K^+) and sodium (Na^+) currents of small diameter dorsal root ganglion neurons (sdDRG), dissected from naïve rats. The most active sample in assessed resorting to electrophysiology studies, was elected to undergo bio guided fractionation process, to reach a purified fraction (99% purity) of the most prominent peak (S4U1).

Under the presence of S4U1, *whole-cell voltage-clamp* were conducted to screen S4U1 against a platform of voltage-gated K^+ and Na^+ channels present at the surface of a well-established pain sensing cell model: sdDRG neurons (*ex vivo* testing). *Ex vivo* experiments recordings in rat sdDRG neurons showed decreased mean current density values in the presence of S4U1, mostly observed in the slow component of K^+ currents (I_K), suggesting a specific effect over I_K, and in peak Na^+ current. These results might be chiefly supported by a facilitation of the inactivation of K^+ and Na^+ currents, observed in the hyperpolarizing shift of both steady state inactivation curves, and in the increasing rate of the decaying phase of K^+ currents.

Thus, by ensuring the absence of S4U1 toxicity in human and animal cell lines (MTS), the biotechnological value of S4U1 was further analyzed through a study of its potential analgesic effect in animal (chronic) pain models (*Chronic Constriction Injury*- CCI; *in vivo* testing). Through the intravenous administration of S4U1 (*in vivo* testing) the reduction of pain was effectively observed, since, following an evaluation method in animal models, %MPE, there was an increase in the force applied by the von Frey monofilaments (vFF) in the ipsilateral side, in each period of time.

The results showed a neuronal bioactive effect of S4U1 on pain sensing model cell (sdDRG), which was translated into a potential analgesic value verified in chronic pain models. Despite, the need to increase the experimental sample size, S4U1 is here presented as a possible new therapeutic drug for chronic pain treatment.

Keywords: Sponges, Neuronal Bioactivity, Analgesic Potential, Electrophysiology

RESUMO

Os ambientes marinhos apesar de serem considerados como recursos naturais de grande relevância para moléculas químicas e biológicas, são ainda territórios vastamente inexplorados. Contudo, novas oportunidades estão a surgir relativamente ao interesse marítimo e, consequentemente, à descoberta de potenciais novos produtos farmacêuticos. Estes compostos bioativos estão presentes numa variedade de invertebrados, tais como as esponjas (Porifera), podendo ser encontradas ao largo da Costa de Sagres, sul de Portugal e, intrinsecamente ligadas ao propósito desta dissertação. Os extratos e frações obtidos de um organismo colhido foram submetidos a avaliações da bioatividade neuronal para determinar possíveis efeitos tanto em correntes de potássio (K^+) como de sódio (Na^+) em small diameter Dorsal Root Ganlions (sdDRG) neurons, dissecados de ratos *naïve*. A amostra eleita com a mais proeminente em termos de bioatividade, no decorrer das análises eletrofisiológicas, foi subjugada a um processo de fracionamento bioguiado, com a intenção de atingir uma fração purificada (99% de pureza) do pico mais saliente (S4U1).

Posteriormente, estudos de *whole-cell voltage clamp*, recorrendo ao mesmo modelo celular (testes *ex vivo*), foram realizados com e sem a presença de S4U1, estabelecendo assim uma compreensão mais concreta dos seus efeitos nos canais de K^+e Na^+. Assim, com registos experimentais foi possível observar um decréscimo de valores médios de densidade de corrente aquando presença de S4U1, observados principalmente na componente lenta das correntes K^+ (IK) e nas correntes de Na^+, sugerindo tanto um possível efeito específico em IK como no pico das correntes de Na^+. Após uma análise detalhada dos resultados foi também possível cimentar a sugestão anteriormente mencionada, relativamente à existência de efeitos a nível da neuroexcitabilidade dos canais, complementada pela facilidade observada de inativação das correntes de K^+ e Na^+, através de uma consequente deslocação das curvas de inativação para estados mais hiperpolarizantes. Tais conclusões permitiram inferir um possível efeito terapêutico em modelos de dor.

Deste modo, ao garantir a inexistência de toxicidade de S4U1 em linhas celulares humanas e animais (MTS), o valor biotecnológico de S4U1 foi aprofundado através de um posterior estudo do seu potencial efeito analgésico em modelos de dor (crónica) em animal (*Chronic Constriction Injury- CCI*; testes *in vivo*). Através da administração intravenosa de S4U1(testes *in vivo*) a redução de dor foi efetivamente observada, uma vez que, seguindo um método de avaliação em modelos animais, %MPE,

registou-se um aumento da força aplicada pelos monofilamentos de von Frey (vFF) no lado ipsilateral, num determinado período de tempo.

Os resultados demonstram um potencial bioativo neuronal associado a S4U1 em modelos celulares de sensibilidade à dor (sdDRG), que foi traduzido num potencial valor analgésico verificado em modelos de dor crónica. Apesar da necessidade de aumentar o tamanho da amostra experimental, o S4U1 é aqui apresentado como um possível novo medicamento com fins terapêuticos para o tratamento da dor crónica.

Palavras chave: Esponjas, Bioatividade Neuronal, Potencial Analgésico, Eletrofisiologia

INDEX

LIST OF FIGURES

LIST OF TABLES

LIST OF ABREVIATIONS

ASIC1	Acid sensing Ion Channel Subunit 1
AP	APs
ATP	Adenosine triphosphate
C	Capacitance
CCI	Chronic Constriction Injury
Cm	Whole-cell membrane capacitance
CNS	Central nervous system
G	Conductance
G/Gmax	Conductance normalized to maximum conductance values
HPLC	High-performance liquid chromatography
I	Current Amplitude
I/Imax	Current normalized to the maximum value
I_{fast}	Transient current (I_k)
I_{slow}	Sustained current (I_A)
I_K	Voltage-gated potassium currents
I_{Na}	Voltage-gated sodium currents
I_{peak}	Current amplitude taken at the peak of the current traces
$I_{sustained}$	Current amplitude taken at the sustained of the current traces
I-V	Current-Voltage relationship
J	Current Density
Kv	Voltage-gated Potassium Channel
K^+	Potassium Ion
Nav	Voltage-gated Sodium Channel
Na^+	Sodium Ion
PNS	Peripheral Nervous System
pA/pF	Current amplitude normalized to cell capacitance
RMP	Resting Membrane Potential

SdDRG	small-diameter Dorsal Root Ganglion
SEM	Standard Error of the Mean
SPE	Solid Phase Extraction
TrkA	Tropomyosin receptor Potential Channel
TRPA	Transient Receptor Potential Channel, sub-family A- Ankyrin
TRPM	Transient Receptor Potential Channel, sub-family M- Melastin
TRPV	Transient Receptor Potential Channel, sub-family V- Vanilloid
TTX	Tetrodotoxin
V_H	Voltage of half activation or inactivation
vFF	von Frey Filament
Vm	Voltage pulse current
V_S	Slop constant
τ	Time constant

1. INTRODUCTION

1.1. Marine Sponges and their influence on Blue Biotechnology field

Since the 1960s, over 10000 different natural products have been identified from marine sources, mainly from invertebrates such as sponges, tunicates and bryozoans. The first have been often reported as the most prolific marine producers of natural products (Faulkner et al., 2004). These organisms provide complex structures, such as, secondary marine metabolites that serve as a great source for the search and development of new therapeutics (Buchanan, 2015). This characteristic inherent to these types of organisms is attributed to the lack of physical or fast movement defense, acting as morphological defense mechanism to protect them (Helber et al., 2018). The accumulation of toxic natural products can be linked with an effective approach for protection against predators or even dispel neighbors (Lindquist et al., 1992), using them as a form of chemical war (G. Wang, 2006).

Sponges are also known for their symbiotic relations with abundant and diverse quantity of microorganisms, such as bacteria and fungi, which can even compose up to 40% of their tissue volume (Taylor, Radax, et al., 2007). This association allows provisions such as nutrients, water transportation, chemical bioactive defense, and structure stabilization (Hudspith et al., 2021). Their involvement in the production of secondary metabolites has been a widely studied topic, contributing, at some extent, to the production of bioactive compounds (G. Wang, 2006; Taylor, Hill, et al., 2007; Thomas et al., 2010; Hardoim & Costa, 2014).

For this reason, it was conjectured the existence compounds that are active in human cell, in Porifera for pharmaceutical purposes (Rocha et al., 2011), which, over the last three decades of research aroused as one of the most promising source of new drugs. According to Marine Pharmacology web page provided by Prof. Alejandro M. S. Mayer, (*Index @ Www.Marinepharmacology.Org*, n.d.) by 2021, there are at least 17 marine-derived pharmaceuticals approved globally with 29 more in Phases I, II and III of clinical development, with an expectancy of increasing in the following years. As

previously mentioned, these drugs are related to a variety of body dysregulations such as tumors, viruses, neuronal diseases and chronic pain, instigating economical and scientifical curiosity.

1.2. The Biotechnology process – from the sea to the laboratory

As an emerging industry, the search of possible new compounds not only brought many companies investments but also led to the creation of scientific center/companies aiming for the research, development and innovation of bioactive marine compounds or products for therapeutic needs. One example is Sea4Us, a company with a designed methodology following a scuba diving sampling program off the coast of Sagres, aiming at exploring the biotechnological value of marine organisms, such as porifera. So far, at Sea4Us, potential therapies to many medical indications have been evaluated, with the most prominent one relying on the field of neuropathic chronic pain.

Marine sponges are presented as complex organisms from where the prospected bioactive compounds may be extracted (Varijakzhan et al., 2021).

Taking into consideration the diversity of these molecules, the extraction should depict parameters that aim for their withdrawal, like solvent polarity, temperature, and pressure (Fernando et al., 2021). New technologies, such as microwave-assisted extraction, ultrasound-assisted extraction and pressurized solvent extraction target every single aspect regarding high performance extraction, normally including an extreme number of running cycles, bringing an increment of the quantity of extracted material (Varijakzhan et al., 2021). Nonetheless, the traditional methods serve as an optimal resource for this type of experiments, consisting primarily in solvent extraction, with methods such as maceration or percolation (Zhang et al., 2018). However, the latter ones are associated with a lack of simplification and purification of the extracts, consequently, needing a more precise method of separation, which can be attained by coupling a secondary extraction/differentiation method. For such, solid phase extraction (SPE) arises as a viable procedure, separating composites through different polarity fractions (Cutignano et al., 2015).

Not every compound possesses bioactive properties, however, as described priorly, marine sponges alongside microorganisms, are a great source of possible new therapeutics. Thus along the years was determined that there can be found some recurrent activities observed such as anti-bacterial, antiviral, antifungal, anti-parasitic and analgesic (Varijakzhan et al., 2021).

At Sea4Us, novel analgesic compounds targeting chronic neuropathic pain has been the main source of investigation from the company´s pipeline. Accordingly, determination of bioactive properties related to the extracts can be accessed by using patch clamp electrophysiological techniques in a

pain sensing cell model substrate: small diameter Dorsal Root Ganglion (sdDRG) neuron. This model is widely used for the determination of analgesic properties of compounds in peripheral neurons, in specific diseases like neuropathic pain disorders (Ahimsadasan et al., 2021). The established comprehension of the sdDRG neurons cell models can help improve the understanding and treatment of neuropathic pain syndromes. Therefore, evaluation of possible bioactive effects on this neurons allows an accurate understanding of the effect upon neurological chronic pain in the peripheral system (Ahimsadasan et al., 2021). Here, it is important note that by studying the sdDRGs, neuropathy is addressed only in what the peripheric phenomena is concerned (not central). In the present work, sdDRG neurons were used to assess the neuronal activity properties of the compounds.

1.3. Dorsal Root Ganglion (DRG) and Nociception

The Dorsal Root Ganglion (DRG) are a collection of cell bodies from an afferent peripheral nerve that enervate the body (Buckton et al., 1969). These structures can be found linked to the afferent fiber homologue in the adjacent vertebrae (Ramachandra et al., 2012). There is a connection established with the sciatic nerve from either the left and right leg to the DRG, encountered in the lumbar vertebrae L4 through L5 or L4 through L6, depending on the rat strain (Rigaud et al., 2008). Ensuring, therefore, the transmission of the synaptic information to the spinal cord, where it reaches the central nervous system (CNS) and travels to the brain (Fernando et al., 2021).

DRG neurons structure relies on a pseudo-unipolar architecture demonstrated in the figure bellow (Krames, 2015; Fernando et al., 2021) (Figure 1.2), meaning their axon is split into two sections, one that runs from the peripheral to the cell body and the other aiming towards the spinal cord, both of which are joined to the soma by a shared axonal stalk in the shape of a T-stem axon (Serrão, 2015; Fernando et al., 2021). This neuroanatomy allows a regulation of the electrical pulse information from the periphery to the CNS, reducing the transmission of activity that can arise from ectopic situation, therefore serving as defense mechanism for unnecessary pain (Gemes et al., 2013).

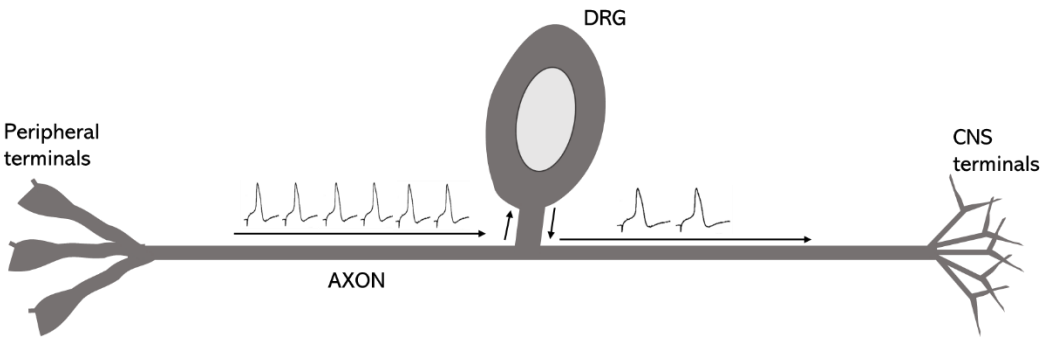

Figure 1.1 Schematic representation of dorsal root ganglion (DRG) structure. The sensory neurons cell bodies are located within the DRG, with peripheral and central axon extensions. Action potentials (Aps) pulses are represented for a better understanding of the regulatory effect behind these structures, with an observable reduction in the central axon in comparison to the peripheral axon. Adapted from Krames (2015).

The stimulus that develops pain can open a cascade of chemical reactions, which in turn results in the activation of a certain type of primary neuron sensors (nociceptors), this mechanism being denominated "Nociception" (Tominaga et al., 2003; Davis & Davis, 2020; Giniatullin, 2020).The main difference between nociceptors and other neurons from the nervous system stands on the process of stimuli detection and its transition to the peripheric nervous systems being combined in the same cell. For such, different types of stimuli are decoded and transmitted by three different nociceptive fibers, whose cell bodies are bundled in the DRG (Davis & Davis, 2020; Renthal, 2020). Hence, DRG neurons can be divided into three categories based on overall soma diameter: large, medium, and small. A large diameter (40-50 μm) relates to A-fibers and transmit vibratory and location sensations (Hong & Wiley, 2006). Medium diameter DRG neurons (31-40 μm) relate to Aδ-fibers while small diameter DRG neurons (27-31μm) are associated with C-fibers, (De Hert et al., 2014). Nociceptive data are normally determined by both Aδ-fibers and C-fibers (Hong & Wiley, 2006; Ramachandran, 2018).

1.4. Pain

Pain prevails as one of the principal evolutionary characteristics that facilitated the creation of medicine, even more than any other type of symptom/disease (Raffaeli & Arnaudo, 2017). The fundamental knowledge behind this statement is associated with the vital importance of maintaining an organism's life (Haefeli & Elfering, 2006; Fitzgerald, 1991). As it can happen, due to genetic modifications, the lack of pain or the lack of sensory signal mechanism, impairs the awareness of the environment around the being, therefore not allowing a cognitive response upon a noxious stimulus, possibly leading to its decadence or even death (Acharya et al., 1991; Fitzgerald, 1991). Therefore, we can assume that although nefarious, pain presents itself as a positive evolutionary acquired sensation (Pogatzki-Zahn et al., 2020).

There are numerous categories in which a certain described pain can fall on to, yet it is considered that all the known forms of pain can be gathered up into two groups: acute and chronic pain. However, it is also possible to find a type of pain associated with medium- and long-term cancer situations and its treatments (Lavand'Homme, 2011; McCormick & Law, 2016).

As stated above, despite being an indispensable characteristic acquired by organisms, it is feasible that pain may not cease, leading to the development of a painful condition that persists beyond the normal healing time, established to be more than 3 months: chronic pain (Russo & Brose, 1998;

Aziz et al., 2015). It is believed to be caused by an ongoing stimulation of the nociceptor, as a possible result of a neurophysiological change at multiple levels along the nervous system and related nerves (Roberts & Kramis, 1990).

1.5. Chronic pain syndrome

In normal conditions, once the noxious stimuli are over and the body has mended, the type of associated pain (acute) will be reduced (Acharya et al., 1991; Raffaeli & Arnaudo, 2017). Nevertheless, pain may outlive its usefulness and develop into a chronic condition (Raj & Birring, 2007).

Chronic pain is distinguished from acute pain not just by its persistence, but also by the body's failure to return to homeostatic values of physiologic function. Chronic pain severity appears to be unrelated to original acute inflammation. Trauma, metabolic or autoimmune problems, infection, antiretroviral therapy, and chemotherapy are among factors that contribute to the development of Chronic pain (Tsantoulas & McMahon, 2014).

Primary and secondary hyperalgesia (an exaggerated sensation to a painful stimulus) and allodynia (pain perception in response to non-painful stimuli) are caused by abnormally amplified signals in the CNS because of central sensitization (an increment of spinal sensitivity neurons) (Michels et al., 1983; Campbell & Meyer, 2006; Tsantoulas & McMahon, 2014).

1.6. Cellular mechanisms of neuropathic pain

Neuropathic pain syndromes are chronic pain conditions generated by a defect or pathology in the regions of the nervous system that typically signal pain (Baron 2006). Upon nerve damage, the expression of a specific type of plasma membrane proteins, named voltage-gated ion channels, can be either up or down regulated. The dysregulation of potassium (Kv) and sodium (Nav) voltage-gated channels expression, verified under nerve damage conditions, potentiates ectopic discharges in neurons involved in the somatosensory signaling(Saab, 2012; Laedermann et al., 2013; Baskozos et al., 2019). As a result, a myriad of deleterious phenomena may arise, such as an ongoing numbness, pain, and new evoked pain. There is an occurrent secretion of nerve-growth factor (NFG) throughout this process, which meets the surrounding undamaged fibers through the axons, increasing levels of Nav, TRPV1 channels and adrenoreceptors, ramping up the sensitivity among those fibers that have not been affected (Baron & McDonald, 2006). Due to the loss of potassium channels, that are known to regulate neural

activity, remaining fibers will be hyperexcitable, resulting in a state of nociceptors with low threshold to irritability, which turns into sleep disturbances, anxiety, depression, bringing a more impaired quality of life to these patients (Campbell & Meyer, 2006).

1.7. Type of fiber involved

The fibers involved in the neurosensory system can be divided in a multitude of groups, however there are three main classifications for these groups: a) A-α and A-β, b) Aα and c) C-fibers (Manzano et al., 2008). They are described by having different signal transmission velocity, due to their differentiated content in myelin. A-fibers are the fastest given their high content in myelin and C-fibers are the slowest, as they contain no myelin sheath (Waxman, 1980). A-α and A-β are not considered to be involved directly with pain, but with muscle sense (proprioception) or touch, and no nociception exactly (Li & Bak, 1976). On the contrary, Aα and C-fibers underly the nociceptive processes conveying their signaling to the spinal cord (Baron, 2006), under different velocities, given, once again, the content of myelin encountered in both fibers. Aα fibers, named as medium diameter fibers, have a faster transmission being around 20 m/s, and C-fibers, known for their small diameter fibers, display a velocity around just 2m/s (Suer & Sehgal, 2021) (Figure 1.3).

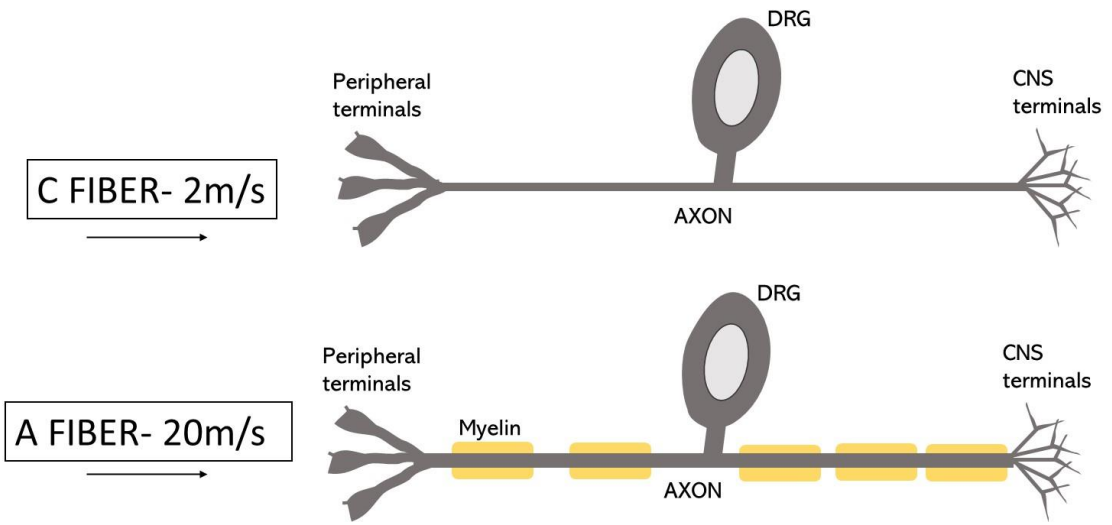

Figure 1.2 Peripheral nerves include small-diameter unmyelinated afferent fibers (C fibers) and medium to large-diameter myelinated (myelin identified by yellow squares) afferent fibers, known as (A fibers. Their different conduction velocities (20 m/s and 2 m/s, respectively) account for the first (fast) and second (slow) pain responses to injury.

The thickness of a nerve fiber and the presence of a myelin coating both influence the pace at which it produces Action potentials (APs) increasing the conductivity velocity of the peripheral nerve, as mentioned by Campbell & Meyer (2006) and Helber et al. (2018). In most cases, the presence of

both types of fibers, Aα and C, allows a “double pain sensation”(Agarwal et al., 2016), since they differentiate in time, one pain being the fast one and the other one retarded and diffuse. The differentiation between both APs and physiology related to each fiber led to naming the Aα “fast sharp pain” and C “slow pain” (Basbaum et al., 2009). For the relevance of the present study, important to stress that C-fibers are the ones with closer relationship with chronic pain.

1.8. Transduction and transmission of pain signaling

To achieve the nociceptor activation, the minimum intensity of the threshold must be reached by the frequency of the stimuli, which leads to an inward movement of calcium ions (Ca^{2+}). Subsequently, the cellular membrane potential depolarizes, activating the voltage-gated Na^{+} channels. This will allow the influx of Na^{+}, building up the conditions to initiate an APs, that flows from the nerve terminal, through the nerve fiber, reaching the spinal cord, where the same noxious information is passed to the next neuron (Waxman & Zamponi, 2014). Nociceptors are mainly found outside the spinal cord, in the DRG, in the afferent pathway, from where numerous sequential synapses take place in the secondary neurons in the column dorsal horn, reaching the CNS (Mazzocchio & Caleo, 2015). The production of these electrical impulses that transmit nociceptor signals to synapses in the dorsal horn is dependent on voltage-gated Kv and Nav (Costigan & Woolf, 2000). The nociceptive sensorial signal eventually comes across the neuronal circuits in the dorsal horn, through pseudo-unipolar first order neuron establishing connection with the spinal cord and afterwards ascending through the spinothalamic pathway. To aid the process, a specific category of neurons, the interneurons, connects the afferents with the CNS (Powley, 2021), allowing the stimulus to travel from the inflicted area to the brain, where the pain signaling is processed.(Figure 1.4).

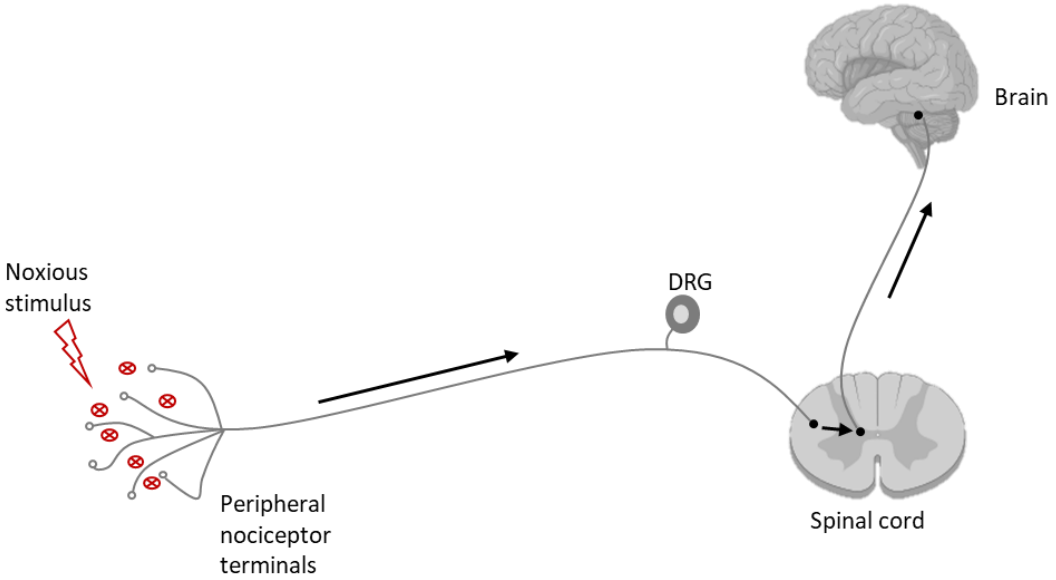

Figure 1.3 Cellular pathway in pain transmission from the peripheral to the CNS. Noxious stimuli (thermal, high pressure, mechanical, chemical) are first detected by the receptors located at the level of free nerve endings of the peripheral system fibers. The electrical signaling, conveyed by the axon fibers until the dorsal horn of spinal cord, is regulated by the cell bodies of the DRG neurons. At the spinal cord, the information is transmitted to the dendrites of secondary sensory neurons, which, subsequently, passes it to the hypothalamus in the brain cortex.

1.9. Voltage-gated ion channels and neuroexcitability at the periphery

Focusing on the cellular mechanisms involved in nociception and pain neuroexcitability, it is in demand to understand the basic knowledge that underlies the signal transmission.

Voltage-gated Na^+, K^+, and Ca^{2+} channels, leak channels, and ligand-gated channels govern the excitability of neurons and other excitable cells. These channels can control the resting membrane potential (RPM), APs initiation, depolarization and repolarization, and the refractory period between APs, as well as neurotransmitter release (Waxman & Zamponi, 2014) (Figure 1.4).

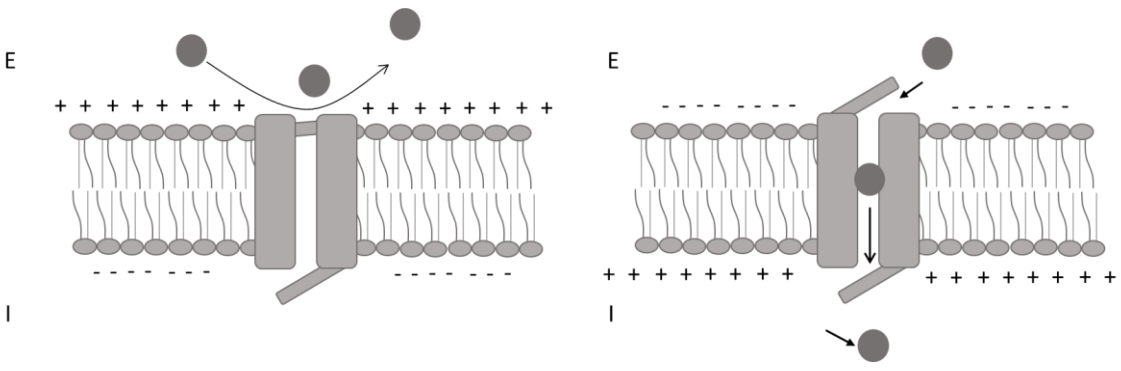

Figure 1.4 Diagram showing an example of voltage-gated channel in the cell membrane at a resting state and under depolarization, more specifically in sodium currents. With a membrane potential at approximately -70 mV there is no influx of the Na^+ (circles), with the interior (I) negatively charged when comparing with the exterior (E), on the left. Upon activation, thanks to an increasement of the membrane potential up to the threshold, leaving E of the cell comparatively more negative than in I, a depolarization occurs, allowing the gate opening and the entrance of Na^+ ions, on the right.

The importance of ion channels in nociception is related to the production of the APs upon the receptors triggering, created after depolarization of the potential threshold of the membrane (Hille, 2001). The impulses from the nociceptors to the other end of the axon can travel quickly and without distortion due to their nature. The APs is formed across the neuron's membrane, which subsequently transmits an electrical impulse through the axon's membrane (Yu et al., 2005). However, the firing frequency of the APs is restricted by the refractory time during which Na^+ channels are recuperating from the inactivation state, not promptly generating a second APs (Hille, 2001).

In RMP, the extracellular composition of neurons consists significantly of Na^+ when compared to the intracellular side, mainly composed by K^+ (Cooper et al., 1998). This chemical gradient along the plasma membrane axis, promotes the influx of Na^+ and the efflux of K^+. However, since the neuronal membrane displays a greater permeability for K^+ when comparing to Na^+, the RMP of the neurons is pushed towards the K^+ equilibrium potential ($E_K \sim$ -90mV), thus, presenting a value of RMP close to -70mV. Such basal conditions will limit the neuronal excitability, keeping membranes away from the depolarized firing threshold (Hodgkin & Huxley, 1952; Hille, 2001; Yu et al., 2005).

1.10. Why potassium channels? - K_v and nociceptive pain mechanisms

Electrical signals are produced by brief localized changes that cause the membrane potential to deviate from its resting value and are conveyed throughout a neuron or nerve fiber. These changes are mediated by ion channels (Rasband et al., 2001; Wulff et al., 2009).

Ion channels are classified into families based on their structure and function. K channels are the most diverse and widely distributed class of membrane proteins (Yu et al., 2005). K_v are the most varied of them, with 12 families (Kv1-Kv12) representing them (Babcock et al., 1992; Kubo et al., 2005). K_v are crucial in membrane potential stability in excitable cells because they align the RPM to the K^+ equilibrium potential, decreasing it and staying away from the APs firing threshold (Bosma & Hille 1992). They are also involved in the reduction of enhanced activity, maintaining the temporal difference between recurrent spikes, effectively reducing excitatory inputs in the cell (Babcock et al., 1992). Sensory neurons express a variety of K_v, comprising members of the Kv1, Kv2, Kv3, Kv4, Kv7, and Kv9

families. Immunochemical investigations indicate that DRG neurons express many K_v from the Kv1 and Kv2 families (Ishikawa et al., 1999), with Kv1 family channels playing a crucial role in neuronal excitability (Doyle et al., 1998). Hence, in what concerns nociceptive pain phenomena, they are important players on the underlying mechanisms that regulate the intrinsic electrical behavior of neurons (Luján, 2010).

After nerve damage, DRG neurons can exhibit atypical firing characteristics or cross-excitation by nearby neurons, resulting in inappropriate impulsive activity that may support unpleasant feelings (Yu et al., 2005). Particulary, C-fibers are usually silent, only firing with pain. Because research has mostly concentrated on Na^+ and Ca^{2+} channels, the role of K^+ channels in pain signaling has been underappreciated over the years (Rasband et al., 2001; Wulff et al., 2009; Du & Gamper, 2013) . However, new evidence suggests that nerve damage or inflammation affects K^+ channel function in neurons of the pain pathway, which plays a significant role in DRG hyperexcitability, indicating its potential as a therapeutic target (Rasband et al., 2001; Wulff et al., 2009; Cao et al., 2011; Tsantoulas & McMahon, 2014).

1.11. Why sodium channels? – Nav and nociceptive pain mechanisms

Na_v are required for the creation of APs. Its capacity to transit from a closed to an open conformation in milliseconds in reaction to a depolarization of the membrane potential generates a rapid inward Na^+ current in sensory neurons, permitting the ascending phase and transmission of the APs to occur. The inward Na^+ current causes the membrane potential to become even more depolarized, resulting in the opening of more Na_v. Subsequently, the natural inactivation process flickers the Na_v to an inactivated, non-conducting, state. Following the refractory time during which the membrane is repolarized, the channel returns to its rest conformation, being available to be triggered again (reaching a closed-active state). This Na_v conformational cycle enables AP firing to be repeated (Bhattacharya et al., 2009; H. J. Wang et al., 2011), bestowing upon Nav a pivotal role on neuroexcitability studies.

In mammalian cells, 9 Na_v isoforms were discovered, ranging from Nav1.1 to Nav1.9, and were shown to be dispersed differently among excitable cells. Nav1.1, Nav1.2, Nav1.3, and Nav1.6 are mostly expressed in the CNS, whereas Nav1.7, Nav1.8, and Nav1.9 are primarily expressed in the Peripheral Nervous System; and Nav1.4 and Nav1.5 are primarily expressed in adult skeletal muscle and cardiac muscle, respectively (Yu et al., 2005).

Na_v are further categorized based on their susceptibility to tetrodotoxin (TTX), a natural toxin that inhibits Na_v. As a result, TTX-sensitive Na_v (Nav1.1, Nav1.2, Nav1.3, Nav1.4, Nav1.6, and

Nav1.7) are inhibited at nanomolar doses of TTX, but TTX-resistant Na^+ channels (Nav1.5, Nav1.8, and Nav1.9) are only disrupted at micromolar concentrations of TTX (Gilchrist et al., 2014).

The different approaches of Na_v isoform expression provide varied electrical properties to excitable cells. As previously stated, Nav1.7, Nav1.8, and Nav1.9 are mostly expressed in periphery neurons (Dib-Hajj et al., 2009; Shah et al., 2010). Nav are produced in the DRG neurons' soma and delivered to their peripheral destinations via axoplasmic processes (Coward et al., 2000).

Nav1.7 is expressed primarily in sensory neurons, including all DRG neurons. (Dib-Hajj et al., 2013). Associated with a rapid activation and inactivating Na^+ current (Klugbauer et al., 1995), a long recovering from inactivation, and a slow closed-state inactivation, which limits its ability to sustain high frequency repeated firing (Ramachandra et al., 2012).

The TTX-resistant channel Nav1.8 is mostly expressed in DRG neurons and their axons A and C-fibers (Cummins & Waxman, 1997; Waxman & Zamponi, 2014). Recognized by allowing the inward Na^+ current in DRG neurons even during AP upstroke and allows for recurrent firing (Renganathan et al., 2001). Nav1.8 has also been linked to inflammatory and neuropathic pain disorders (Coward et al., 2000; Minett et al., 2014).

Nav1.9, a TTX-resistant channel, mainly present in C-fibers, generates a substantial continuous current that is progressively triggered at hyperpolarized potentials near the membrane resting potential. The overlap among activation and inactivation causes Nav1.9 Na^+ currents to persist, which intensifies and intensifies tiny depolarizations and, as a result, enhances DRG neuro excitability (Renganathan et al., 2001; Waxman & Zamponi, 2014).

1.12. Electrophysiology recordings of ion currents

The ion currents measured off an excitable cell result from the ion net flow across the membrane, which is caused by the activity of the ion channels located at the cell membrane (Rush et al., 2007). Proceeding a depolarization of the cell membrane, caused by the stimulation of the nociceptor's receptors, voltage Na_v are enlisted, allowing an inflow of Na^+. Consequently, the membrane potential increases up to the APs threshold, thus generating an APs. With this, K_v with high thresholds of activation are recruited, expelling K^+ from the inside of the cell, to achieve a repolarization (Hille, 2001; Tsantoulas & McMahon, 2014). Thus, both families of channels are important mediators of the electrical properties of neurons (Rush et al., 2007; Luján, 2010).

DRG neurons arise as a fruitful cell model for the determination of the electrogenic roles of these channels (Rush et al., 2007). Voltage-gated channels can either be a) activated, with an open conformation allowing flow of ions, or b) inactivated, a non-conducting stable state, adding that each type of

channel presents a wide variety of families that can be expressed, each one with its unique electrophysiological, pharmacological and biophysical characteristics (Black et al., 2004; Yu et al., 2005; Bezanilla, 2007; Shah et al., 2010). The currents mediated by these channels can be studied in terms of conductance and kinetics properties, from activation and inactivation processes(Akins & McCleskey, 1993; Gold et al., 1996; Ocaña et al., 2004; X. L. Zhang & Gold, 2009; Zemel et al., 2018). In case of whole-cell potassium currents, two different types of currents can be dissected in terms of kinetics. Firstly, a transient one (I_A), described by fast activation and inactivation processes, followed by a sustained one (I_K), usually assigned to potassium delayed rectifier channels, with slow activation and inactivation processes. (Akins & McCleskey, 1993; Gold et al., 1996). (Figure 1.5)

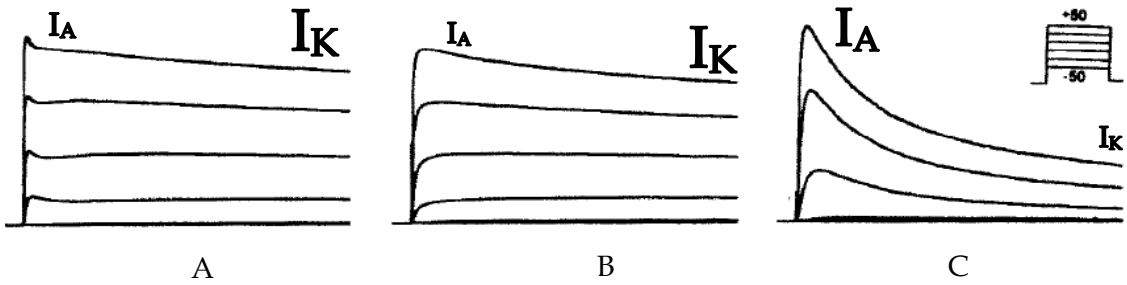

Figure 1.5 Representative potassium current decaying traces elucidating the two different types of currents studied in the present dissertation: fast (I_A) and slow (I_K) currents, taken at the peak, and at the steady state regions of the traces, respectively. A) and B) depict a conspicuous presence of IK and a less prominent contribution of IA. C) mainly fast currents presented. Adapted from Akins & McCleskey (1993).

Regarding whole-cell Na^+ currents of DRG neurons, these can be modulated by two types of channel populations, characterized by their sensitivity to tetrodotoxin (TTX): TTX-sensitive and TTX-resistant Na^+ channels (Figure 1.6). The former group of channels present currents with fast kinetics of inactivation, with a rather sharp profile (Figure 1.6C). The latter group of channels refer to currents with slow kinetics of inactivation, and a much broader current profile, contributing to the presence of sustained currents at the end of the command pulse of the voltage protocol (Figure 1.6B)(Akins & McCleskey, 1993; Jonas et al., 2015). In addition to their differential response to TTX application, these channels also display different electrophysiological characteristics, which allows to isolate the respective Na^+ currents. Indeed, TTX-R channels have a more depolarized threshold of activation compared to that of TTX-S channels (Blair & Bean, 2002; Bennett et al., 2019).

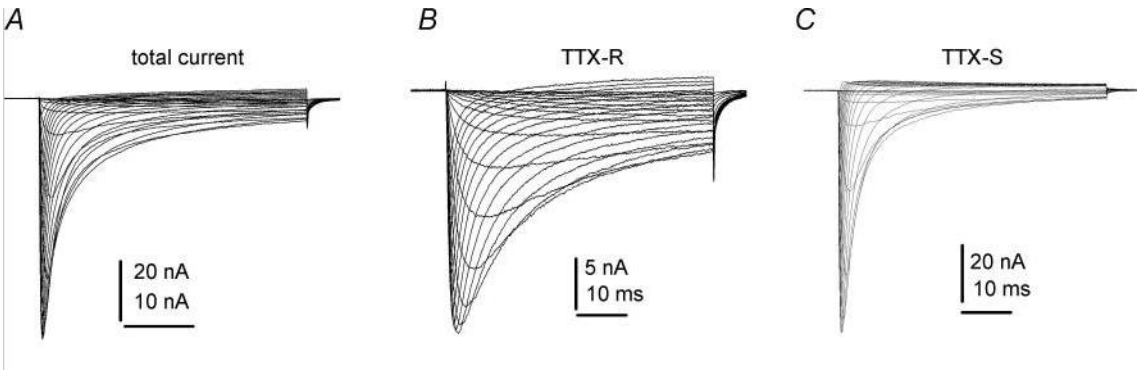

Figure 1.6 Total sodium current in this DRG cell elicited using a holding potential of −100 mV and 25 ms step depolarizations to voltages ranging from −80 to +40 mV (*A*) can be pharmacologically separated on the basis of sensitivity to TTX (100 nM), allowing isolation of TTX-R currents (*B*) and by subtracting *B* from *A*, TTX-S currents (*C*). Reproduced from (Rush et al., 2007).

1.13. Animal chronic pain models

To address the mechanisms of nociception in a pathophysiological context, rodent behavioral models are a viable source to better understand nociception and pain physiology (Mogil, 2015).

The use of rodents to investigate chronic pain is a well-accepted method since medications, that have shown some benefit in human patients, have showed positive results in pain animal models (e.g., gabapentin/pregabalin) (Coward et al., 2000; Liu & Wood, 2011). Chronic Constriction Injury (CCI) neuropathic model is extensively described in the literature as a reliable pain model (Colloca et al., 2017). This model is achieved normally with surgical intervention in one sciatic nerve, constricting it with three or four loose ligations, as seen in the figure 1.7, thus resulting in a site inflammation, which will in turn lead to neuropathic chronic pain in L4, L5 and L6 (lumbar vertebrae) DRGs. (Bennett & Xie, 1988; Austin et al., 2012)

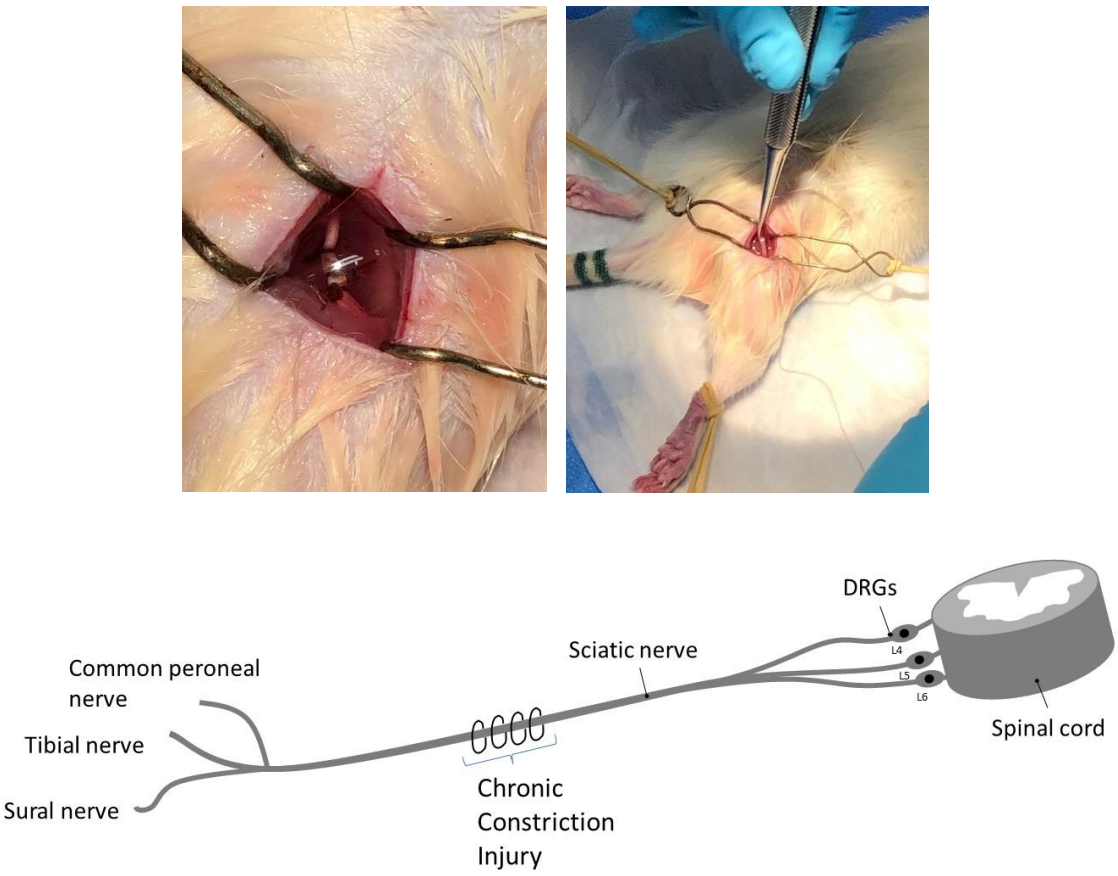

Figure 1.7 Upper panel contains photographs of a CCI surgical procedure conducted on the mid-thigh sciatic nerve. Bottom panel is a schematic representation of surgically implanted CCI with 4 loose ligations on mid-thigh sciatic nerve. Adapted from Bennette e Xie 1988.

In pain research, typical behavior are just responses or intrinsic reactions (e.g., paw withdraw, licking the sensitized zone, tail flick (Jänig, 2009). Mechanical, pharmacological, or radiation stimuli can indeed be delivered to the rat's paw through the mesh on the floor of the behavioral cage (Austin et al., 2012). Mechanical withdrawal threshold is one of the methods used to measure and compare the paw sensitivity between both injured and not injured hindpaw (Austin et al., 2012).

The number of withdrawal reactions from rats can be used to assess mechanical allodynia and hypersensitivity using calibrated von Frey monofilaments (vFF) (De Sousa et al., 2014). Acute stimulation of the glabrous surface of the hind paw (figure 1.8) with the filament in spaced repeating presentations provides a reliable assessment of the animal's sensitivity and permits pain quantification (Hudspith et al., 2021).

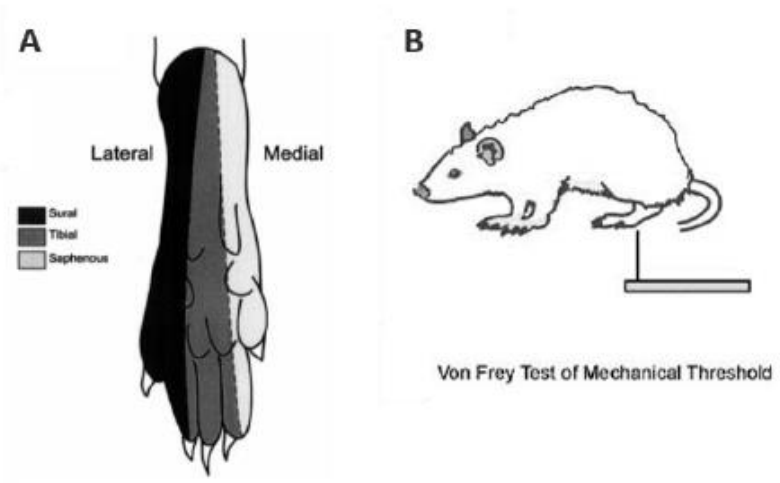

Figure 1.8 Measurements of mechanical sensibility on the hind paw from rats. A- The plantar surface of rats hind paw is enervated by the sural, tibial and saphenous nerves. B- Pain and sensitive may be assessed by stimulation of the surface of hind paws of rats with a variety of calibrated von Frey filaments and observing the withdrawals evoked. This was the approach followed in Serrão (2015).

2. Objectives

Marine environments, despite being considered one of the most important natural resources in terms of chemical and biological molecules, are still vastly unexplored territories. However, new opportunities are emerging in relation to the maritime interest and, in the same way, the discovery of potential new pharmaceutical products. These bioactive compounds are present in a variety of invertebrates, such as marine sponges (Porifera). The overall goal of the present dissertation was to disclose of candidate metabolites with inherent neuronal bioactive properties related to nociception, from marine sponges found in submarine caves off the coast of Sagres. More specifically, this study aimed to:

- Extract and purify fractions from the matrix of sponge samples collected from the 'Cathedral Cave' in Sagres;

- Determine the bioactive potential of the fractions, by studying of K^+ and Na^+ currents in small diameter Dorsal Root Ganglion neurons from rats, through the whole-cell voltage-clamp technique;

- Hypothesize, upon bioactivity determination, the possible analgesic effect of the bioactive metabolite on CCI pain model in rats, with prior establishment of non-toxic characteristics of the compound of interest.

3. Methods

This study was conducted in the startup Sea4Us, a biotechnology company focusing on the discovery and development of new drugs based on novel marine compounds for clinical purposes.

3.1. Sampling and diving conditions

Prior to the sponge's species selection, a study was conducted to determine the viability of its sampling. The performed evaluation was carried mainly following a Sea4Us approach, which cannot be disclosed, due to professional/confidential agreement between all parties involved.

From the research done, a submerged area was determined as a possible hotspot for the existence of sponges of interest. Then a dive was scheduled for 12 of September of 2020.

On the day, conditions were underlying perfection, with only a small swell and good visibility. Two species of sponges were collected manually by scuba diving at depths ranging from 9 to 12 m inside Cave 'Cathedral', on the coast of Sagres, Portugal (37.00 N and 8.93 O) (Figure 2.1). Sponge samples were transferred underwater into sealed plastic bags containing seawater, then brought to the surface and quickly to shore. In the Sea4Us laboratory in Sagres, specimens were stripped of any materials/parasites and frozen at -4 ºC. Subsequently, the sponge samples were transferred to the main Sea4Us laboratory, in Nova Medical School, in Lisbon, in an ice box container, then kept at -4ºC, until the compound extraction procedure.

Figure 3.1 Underwater photography taken during the diving session to collect the marine sponges. Samples searching was done at depths ranging from 9m down to 12m inside the "Cathedral Cave" on the coast of Sagres.

Determination of the freeze weight, of 313 g, was preformed, from which 106 g were cut off and inserted in the freeze dryer. Here it went through the process of lyophilization reaching a mass of 27.90 g (dried sponge sample), meaning that the sponge was constituted of *ca.* 74% water. Resorting to a mortar, the sponged was reduced to pieces just before proceeding with the extraction of its compounds. The reduced sponge was then divided into three separate groups, one that went through the process of maceration, another through a total extraction method and a final one that was kept in the freezer.

3.2. Extraction of compounds from the sponge

3.2.1. First Method (Maceration extraction)

The first method used is adapted from Kumar & Ravikumar (2014)

Following lyophilization, the sample is reduced into small pieces and then weighed (7.39 g).

The maceration process can be adjusted, in terms of time, to each different sponges, in this case being collect a sample of 25 ml. For that same reason stirring was needed, to improve the results afterwards (figure 3.2).

Figure 3.2 Maceration extraction method. The sponge inside a 500 mL shot containing 96% ethanol/ H2O (3:1). On the left, a stabilized viewing of the sponge inserted into the solvent and on the right, the same sponge allowing the perception of the extracts acquired. Afterwards, upon stirring, 25mL of the extract solution is retrieved to proceed with the experimental work.

After the completion of each maceration, a filtration was done recurring to a filter paper method, eliminating any type of contamination. The filtrate was subsequently concentrated in rotavapor, collected to a pre-weighed sample vial (7.660 g). To ensure a complete drying of the samples, the vial containing the extracts would be dried out under N_2 flux and then reweighed (8.855 g). Finally, the dried extract was kept at 4 ºC.

To calculate the extraction percentage, the following equation was used:

$$Extraction\ (\%) = \frac{mass_{vial+residue} - mass_{vial}}{mass_{sponge\ material}} \times 100 \qquad \text{Equation 1}$$

$$Extraction\ (\%) = \frac{8.855 - 7.660}{7.39} \times 100$$

$$Extraction\ (\%) = 16\ \%$$

3.2.2. Second Method (Total extraction)

The second method used was adapted from Goiris et al. (2012)

The basic principle of this method relies on the fact that the used solvent allows the extraction of polar and (some) nonpolar compounds. The marine sample must be frozen and lyophilized to prepare

the extraction. Afterwards, the sample must be reduced to small pieces, ideally to powder, and then weighed (7.39 g).

Figure 3.3 Total extraction method. Image of two falcons (50 mL), containing the sponge sample bathing in 96% ethanol for 30 min. Both falcons combined contained the total mass of sponge determined for this method, divided into two tubes, to achieve a greater sample- solvent contact area.

The solvent can be composed by ethanol 96%, being added 2 mL for every 200 mg of sample. After letting it settle for 30 min (with often stirring periods), it was centrifuged for 10 min, at 4000 rpm; consequently, pellet was resuspended in ethanol 96% (2 mL), after which, the whole process was repeated for a second time, for 30 min.

After centrifugation, the extract was collected (Figure 2.4).

Figure 3.4 Total extraction method. Following the bathing, a centrifugation at 4000 rpm (for 10 min.), separating the compounds of interest is applied. The process is repeated twice.

At the end, the sample is concentrated using a rotavapor, transferred to a previously weighed sample vial (7.700 g), and dried, if necessary, under nitrogen flux. Following, weight the vial containing the extract (8.453 g) and store it at 4 ºC.

To calculate the extraction percentage, the following equation was used:

$$Extraction\ (\%) = \frac{mass_{vial+residue} - mass_{vial}}{mass_{sponge\ material}} \times 100$$

$$Extraction\ (\%) = \frac{8.453 - 7.700}{7.39} \times 100$$

$$Extraction\ (\%) = 10\%$$

3.3. Fractionation of Extracts

3.3.1. First method

The first method was adapted from Cutignano et al. (2015) and Blunt et al. (2018)

Due to the aqueous/organic composition of the extract retrieved from the sponge, and to obtain active metabolites of the whole extract, the elected extraction process sample (maceration) undergoes a fractionation with different polarities, which leads to a better polarity understanding of the active

compound(s) and/or which fraction expresses the greater interest. Once the extract is dried, a chromatography column was required for this type of process (fractionation). In the present work, it was prepared a poly (styrene-co-divinylbenzene) resin (CAS: 9003-70-7). To obtain separation, it was used 3 g of resin for each 10 mg of extract, approximately. For a higher resolution of the process, samples were dissolved in small volumes (ex: 800 µL) and sonicated (Figure 3.5).

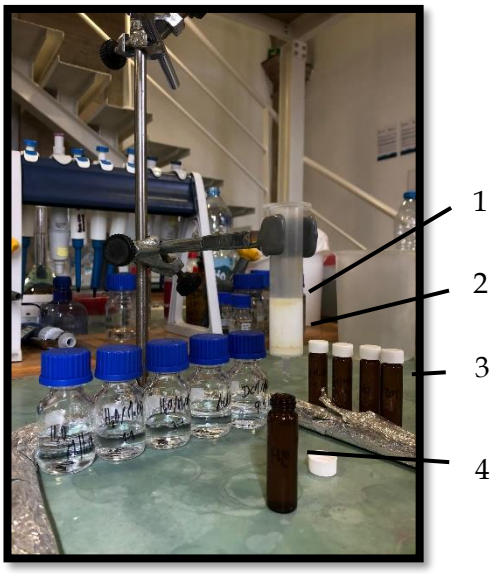

Figure 3.5 Fractionation method with in-house manufactured chromatography column. 1- sample extract; 2 – resin column; 3 – collecting vials; 4 – collection vial corresponding to the first fraction. An overview of the beginning of the method used with 3 g of poly (styrene-co-divinylbenzene) resin (CAS: 9003-70-7), being compacted with MeOH and H_2O (9 mL each). After applying 100 mg of extract, identified by the light yellow colour, a sequential placing of the defined eluents is initiated with H_2O, H_2O/MeOH (1:1), H_2O/MeOH (3:7), ACN and DCM/MeOH (9:1), collecting the resulting liquid in the vials.

Then, the sample was loaded. At that point, collection of samples begins, according to the eluent being used. The elution is made as bellow:

A fraction) 1*v* (4.5 ml) of H_2O

B fraction) 2*v* (9 ml) of 1:1 H_2O/MeOH

C fraction) 2*v* (9 ml) of 7:3 MeOH/H_2O

D fraction) 2*v* (9 ml) of ACN

E fraction) 2*v* (9 ml) of 9:1 DCM/MeOH

Difficulties were found while evaporating fraction A and B, as described by previous studies mentioned above, due to their higher content in non-organic component, H_2O, which is less volatile, therefore harder to dry out. For this apparent reason, prior to transferring the fractions correctly to their final vial, with the aid of MeOH, for the N_2 flux, water was evaporated in the rotavapor. However, from the steps 'C' to 'E', only the N_2 flux was needed.

3.3.2. Second method

The first method was adapted from Cutignano et al. (2015) and Blunt et al. (2018)

Similarly, to the first fractionation, this method also takes in account the aqueous/organic composition, only differing in the nature of the column used, which have a higher resolutions and reproducibility.

Due to the aqueous/organic composition of the extract retrieved from the sponge, and to obtain active metabolites of the whole extract, the elected extraction process sample (maceration) undergoes a fractionation with different polarities, which leads to a better polarity understanding of the active compound(s) and/or which fraction expresses the greater interest. Once the extract is dried, a chromatography column was required for this type of process (fractionation). In this case, were used Sep-Pak® C18 Cartridges. To obtain great separation, approximately 3 g of resin for each 10 mg of extract was used. For a higher resolution of the process, samples were dissolved in small volumes (ex: 800 µL) and sonicated (Figure 3.6).

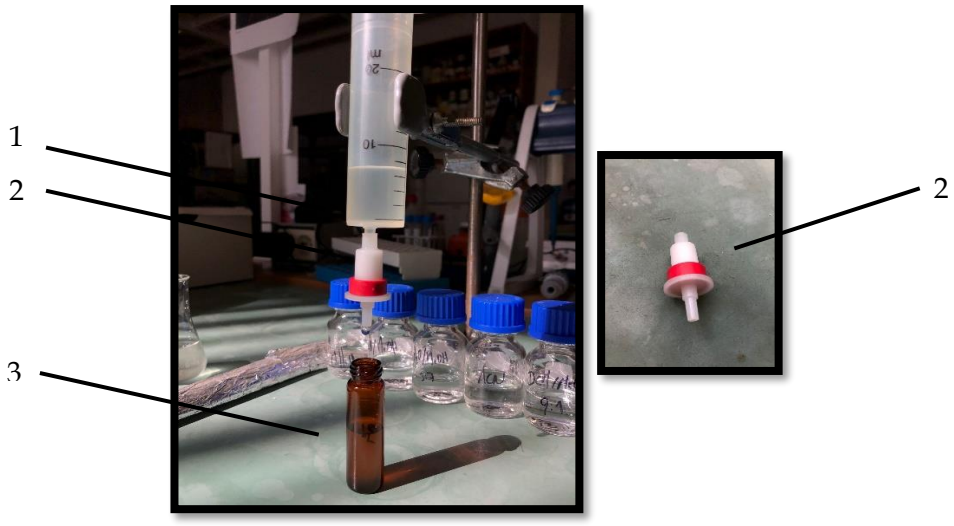

Figure 3.6 Fractionation method performed with a commercial chromatography column. 1- sample extract; 2 – cartridge column; 3 – collection vial corresponding to the first fraction. A specific illustration depicting the difference between both fraction methods. Principal differentiation in the used column, relying on a premade Sep-Pak® C18 Cartridge, allowing a more reproductible process. Column aside, identical procedure was carried out in both fractionation methods. Compaction with MeOH and H2O (9 mL each). Employing 100 mg of extract, dissolved in a mixture of MeOH/H_2O. Following then the same sequential solvents insertion with H_2O, H_2O/MeOH (1:1), H_2O/MeOH (3:7), ACN and DCM/MeOH (9:1), collecting the resulting liquid in the vials. This fractionation method provided the best separation/isolation results in this thesis.

Finally, similarly to the previous protocol, a collection and separation of the sample compounds occurred following a reverse phase chromatography with the same eluents.

3.4. High- Performance Liquid Chromatography (HPLC)

The method was adapted from Tanaka et al. (1978), Faulkner et al. (2004) and Wang (2006)

With the objective of studying the constituents of the isolated fractions and, thus, encountering possible compounds for evaluation, it was pivotal to use the high-performance liquid chromatography (HPLC) technique. First, after gathering all the fractions and determining their weight, the pool of fractions was diluted in methanol (1:10), achieving a 10 µg/ml concentration. These samples were run on a Waters HPLC System with a 2707 Autosampler, a 1525 binary HPLC pump with a column oven, and a 2998 Photodiode Array Detector. A Nucleodur C18 HTec (Macherey-Nagel) reverse phase column (5 µm particles), at 26 ºC. Data were acquired using Empower 2 software, 2006 (Waters Corporation). Sample injections of the fractions with 50 µL were made using a 100 mL loop operated in partial loop mode. The mobile phase, at a flow rate of 0.9 mL min^{-1}, consisted of a 30 min. linear gradient from 5% to 95% acetonitrile in water, followed by a 10 min isocratic flow of 95% acetonitrile, and 10 min of

column conditioning to the initial parameters. Absorption was monitored between 190 and 400 nm, and the chromatogram obtained at 208 nm was extracted.

3.5. Bioactivities

3.5.1. Animals monitorization and ethical approval

All the procedures involving animal subjects (*Rattus novergicus Wistar Han)*, namely neuron and brain preparations, were carried out at the rodent house of NOVA Medical School/Faculdade de Ciências Médicas(NMS|FCM), in accordance with the institution's Ethics Committee and Directive 86/609/EEC (14/2015/CEFCM), and with the European and Portuguese guidelines for the protection of animals used for scientific purposes (European Union Directive 2010/63/EU, transposed to Portuguese Legislation by the Decrete DL 113/2013). 14 female Wistar Han rats, 60 days old, were accommodated in 12 h Light/dark cycle cage, with room temperature of 21 $\pm$ 3° C and an adequate quantity of food and water (Comissão das Comunidades Europeias, 2008) (Isbn et al., 1991). Two different groups of animals were used: naïve control and chronic constriction injury (CCI). The former group was used for *ex vivo* electrophysiology experiments and the latter group was thought to test the possible analgesic effect of the fractions/compounds obtained. The complexity of the pain underlying physiological mechanisms, and the lack of non-animal models that can mimic such phenomena, justified the usage of these 14 animals throughout the present thesis. Indeed, these models (here used and others), still present themselves as a resourceful tool to study human pathologies and new therapeutics. Animal handling, namely animal behaviour, pain assessment and animal sacrifice, was carried out by certified operators who followed SPCAL guidelines.

3.5.2. Acutely isolation of Dorsal Root Ganglion (DRG) neurons (*ex vivo* preparations)

Procedures aiming the isolation of the DRG neurons follow work previously done at Sea4Us. Firstly, subjects were anesthetized with sodium pentobarbital (100 mg/kg i.p) by a certified operator (SPCAL). The harvesting was adapted from the method described in Malin et al. (2007). Briefly, once the animal is laid facing down, a cut is made with an iris scissors, focusing on the separation of the skin/muscle with the intent of exposing the cervical, hence cutting thoracic and lumbar spinal regions. With a Littauer bone cutting forceps, a transversal cut was performed in the backbone at lumbar L1

level. The spinal cord was exposed by cutting each vertebra at a time, from one side of the vertebra canal to the other all the way to the caudal end of the rat.

The spinal cord and dura mater were pulled away from the inside of the backbone gently with tweezers to expose the DRG roots. The delicate dorsal root was grasped with a tweezer and by pulling it, both roots of the DRG ganglia become accessible for the spring scissor to cut it and remove from the vertebra canal. The DRG ganglia from L4 to L6 were collected.

Harvested DRG ganglia were collected and placed in cold Krebs dissociation solution consisting of (in mM): NaCl 120, KCl 5, PIPES 20, CaCl2 1, MgCl2 1 and glucose 25 saturated with oxygen (pH 7.4, NaOH). Next, all ganglia were incubated for 45 min. at 32°C in collagenase 3 mg·mL-1 (type IA, Sigma C9891) prepared in Krebs dissociation solution. At 20 min. of digestion, the pieces of DRG ganglia were mechanically dissociated with a fire-polished Pasteur pipette and at 45 min., they were again mechanically dissociated with a smaller diameter fire- polished Pasteur pipette. By that time, trypsin was added to a final concentration of 2.5 mg/mL-1 (Sigma T9201). After 40 min., digestion with trypsin, an additional mechanical trituration was performed with an even smaller diameter fire-polished Pasteur pipette; 1.5 mL of Krebs dissociation solution was added to the cell suspension; which was centrifuged for 5 min. at 2000 rpm at room temperature. After digestion, the supernatant was discarded, and the cell pellet re-suspended in 2 mL of Krebs dissociation solution. All recordings were performed within 7 hours of dissociation.

3.6. Electrophysiology

DRG neurons were selected with a graduated microscope eyepiece, taking into consideration the size and other phenotypic characteristics: small diameter cells (around 15 and 25μm) , with some brightness under the microscope light, as an indication of healthy appearance and viability. Membrane currents were recorded in whole-cell voltage-clamp configuration, at room temperature (20-24°C), bathed in the external solution that could be either designed to record potassium currents (in mM): NaCl 140; KCl 4; CaCl2 1; MgCl2 1.5; HEPES 10; Glucose 5; pH 7.4 titrated with NaOH; 300 mOsm) or sodium currents (in mM): NaCI 40; KCl 5: HEPES 10; CaCl2 1.8; MgCl2 1; TEA-Cl 30; NMG 60; glucose 25; pH 7.4 titrated with HCl; 290 mOsm.

Voltage-activated K^+ and Na^+ currents were determined with and electrometer (*Axon Instruments*, Axopatch 200B), which was stored in an analogue/digital signal converter (*Axon Instruments*, DigiData 1200 interface) and recorded with a Clampex 6.0.3 software (*Axon Instruments*), at 20-25º C of temperature.

Microelectrodes, with a pipette resistance around 2.0-3.8 M were made from borosilicate glass tube (Science Products GMBH) in a micropipette vertical puller (Science Products GmbH, GB150T-8P). Micropipettes were filled with an internal solution, whose composition differed depending on the type of ion current under evaluation. In case of whole-cell K^+ currents, the solution was as follows (in

mM): KF 140; MgCl2 1; HEPES(1/2Na) 10; EGTA 10; CaCl2 1; Na2-ATP 2; Na-GTP 0.5; pH 7.3 titrated with KOH; 290mOsm. As for whole-cell Na^+ currents, the pipette solution was composed of (in mM): NaCl 10; CsF 140; HEPES 10; EGTA 5; pH 7.2 titrated with CsOH; 280mOsm.

Upon the contact between the tip of the micropipette and the cell surface, a continuous negative pressure was gently applied creating a high resistant seal. The whole-cell can be achieved by gently applying more negative pressure, to rupture the cell membrane, only on the patch where the micropipette is located (hence the name 'patch clamp').

With a holding potential of -70mV and eliminating any transients, series resistance and capacitance compensated up to 80%, low pass filtered at 5kHz sampled at 10 kHz, using a Digidata 1200 AC converter. Holding current and series resistance were monitored throughout all experiments. For the case of the recordings of Na^+ currents, leak subtraction was performed online by P/4 subtraction with pCLAMP 5 software (Axon Instruments®).

Once achieved the whole-cell configuration, application of the voltage protocols would be carried out 5 min after this process, therefore allowing the dialysis of the solution inserted in the micropipette into the intracellular part of the patched cell.

3.6.1. Whole-cell voltage-gated K^+ currents

K^+ currents were evoked by applying voltage protocols that started with the depolarizing pulses through the whole-cell membrane with minimal disruption of other ions equilibrium.

Voltage Dependence of Activation- From the established holding potential (-70 mV), a pre-pulse of -120mV, which removed any type of inactivated channel, was followed by a step of 14 command pulses from -80 to +50 mV, in 10 mV steps, that evoked K^+ currents.

Voltage Dependence of Inactivation- From the holding potential (-70 mV), a double pulse protocol was designed, containing a conditioning pre-pulse ranged from -140 to +10 mV, followed by the command pulse to a voltage where full activation is obtained (+10 mV). This protocol allows to study the steady state of inactivation of peak K^+ currents evoked at the command pulse, enabling to assess the fraction of K^+ channels available to respond to activation at a certain membrane potential.

3.6.2. Whole-cell voltage-gated Na^+ currents

Na^+ currents were evoked by applying protocols that started with the depolarizing pulses through the whole-cell membrane with minimal disruption of other ions equilibrium.

Voltage Dependence of Activation- From the established holding potential (-70 mV), a pre-pulse of -110 mV, which removed any type of inactivated channel, was followed by series of depolarizing command pulses from -50 to +1 0mV, in 10mV increment, evoking Na^+ currents.

Voltage Dependence of Inactivation- From the same holding potential (-70 mV), a pre-pulse ranged from -120 to +0 mV was tested, followed by the command pulse to a voltage where full activation is obtained (+10 mV). Therefore, allowing the evaluation of the potential in which the channels close the inactivation gate.

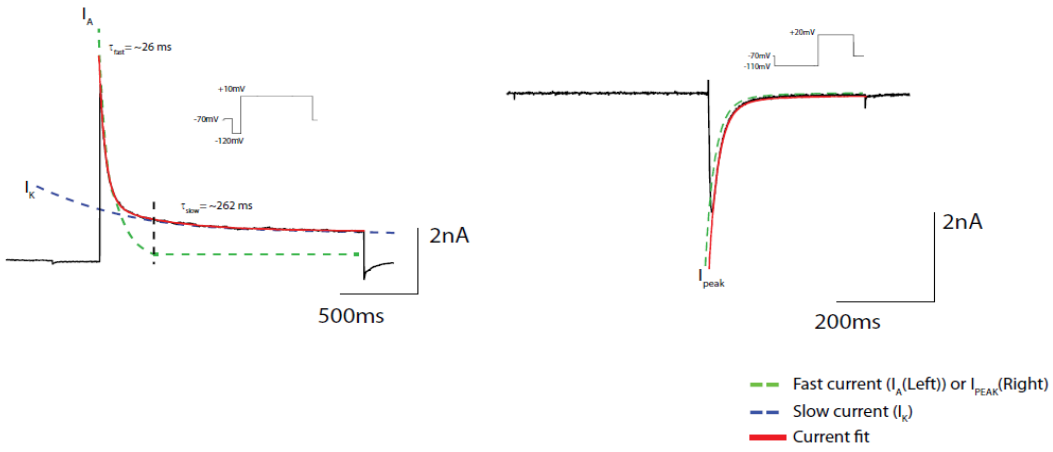

Figure 3.7 Decaying phase of whole-cell K^+ and Na^+ currents. Representation of current traces following activation protocols (see inset), applied to potassium and sodium currents, on the left and right, respectively. K^+ currents are typically described by a decaying phase fitted with two exponentials, enabling to breakdown the total potassium currents into two different types of currents: a rather fast current, with fast activation and inactivation processes, designated as A-type currents (I_A), and a slow current, with slower activating and inactivating processes, usually assigned to delayed rectifier K^+ channels (I_K). These two types of K^+ currents are separately analyzed in this thesis. Identified by colors are the fast current phase (I_A) in dashed green, slow current phase (I_K) in dashed blue and full current trace fitting exponential in red. Values obtained from the fitting function are associated with each current phase. On the potassium, τfast=26

3.7. Data analysis

For electrophysiology data analysis, a combination a different softwares, such as Clampfit 10.3(Axon Instruments®), Microsoft Excel (Microsoft Office 2013 Professional Plus®), Origin Pro 8 (Microsoft Software®) and PRISM (GraphPad software, Inc. ®), was used.

A set of channels named as the voltage-gated ion channels control the diffusion of ions through the cell membrane. Thus, expecting changes in the occurrence of bioactivity it was proceeded an evaluation of this characteristics. In other words there was a determination of the Current Density (J), in which the current is divided by the capacitance (pA/pF), that remains constant in patch clamp recording (Cm=1µF/cm2)((*The Axon Guide. (n.d.). 2500.The Axon Guide*, n.d.)). These values can be found upon whole-cell, being presented in the amplifier after current transients (The Axon Guide, n.d.). Afterwards it is used the following equation for the Current Density determination:

$$J = \frac{\mathrm{I}}{\mathrm{C}} \qquad \text{Equation 2}$$

Where current density (pA/pF) is represented by J, current then is I (pA; being intrinsically all depolarizing pulse of the activation protocol, at each time). Finally, capacitance (pF) is characterized by C.

Conductance (G) currents were studied after transforming Ifast and the Islow currents, which followed this equation:

$$G = \frac{\mathrm{I}}{\mathrm{E} - \mathrm{Vm}} \text{ (having E as } E_{Na} \text{ or } E_K) \qquad \text{Equation 3}$$

Where I is the current amplitude (in each current (fast or slow) in whole-cell potassium currents and peak in whole-cell sodium currents), E is the reversal potential of Na^+ estimated from the extrapolation of the rising phase of the current-voltages (*I-V*) relationship curves for each cell, while in terms of K^+, is calculated by Nernst equation (E_K=-87mV) and Vm, which is the voltage of the pulse command (Ribeiro & Costa, 2000). The conductance values are normalized for the maximal response ($G/Gmax$) and plotted against step command potential. The voltage dependence of activation can be studied by fitting the activation curves with a Boltzmann function, as follows:

$$G/G_{max} = \frac{(\mathrm{A1} - \mathrm{A2})}{1+\exp\frac{\mathrm{Vm} - \mathrm{VH}}{\mathrm{VS}}} + A_2 \qquad \text{Equation 4}$$

Where Vm remains as the pulse potential, VH is the half-activation potential or, in other words, the potential need to activate half of the channels, Vs is the slope constant or, the number of charges needed to open the channel (Standen & Stanfield, 1978), A1 and A2 are associated with the Boltzmann curve, describing the minimum and maximum, respectively.

For current density (J), after the normalization of this one dividing the current amplitude by the whole-cell capacitance, its values, that correspond to the average current density were plotted against the step command pulse.

To study the kinetics of inactivation of Na^+ and K^+ currents, each sweep of the activation protocol was fitted by an exponential curve, as follows:

$$i_t = \sum_{i=1}^{m} a_i e^{-t/\tau i} + c, \qquad \text{Equation 5}$$

Where τi is the time constant, ai is the exponential amplitude coefficient, c is a constant. The inactivation phase was fitted into a double exponential function (m = 2) with a fast and slow component; τi and ai were noted.

To study the voltage dependence of steady state inactivation, the fraction of channels available for activation is obtained by normalization of the currents obtained at the command pulse to its maximum value (I/I_{max}). Values of normalized currents were plotted against pre-pulse potentials, and data points from each cell were fitted a sum of sigmoid, as in 6:

$$\frac{I}{I\,max} = \frac{a1}{1 + \exp\frac{Vh\,1 - Vm}{Vs\,1}} + \frac{1 - a1}{1 + \exp\frac{Vh\,2 - Vm}{Vs\,2}} \qquad \text{Equation 6}$$

3.8. Bio-guided fractionation evaluation method

Concerning the process of bio-guided fractionation, it was needed to evaluate the bioactivity of the compounds obtained (Pasquet et al., 2011). Consequently, electrophysiological test protocols were design for this purpose. Following an activation test protocol with only one command pulse, at 0mV, for potassium currents, and, at +20mV for sodium recordings, currents were continuously evoked, every

30s, and for a period of around 20min, before and under the application of the fractions to the bath solution. The results are shown in form of percentage (%) current inhibition or enhancement of the slow/steady state component of potassium (Islow) and differentiation that resulted in the Ipeak in sodium. Fractions that appeared to have produced at least 20% increase or decrease of current trace were considered interesting for further investigation. Finally, those fraction that produced at least 40% increase or decrease of current trace can be considered highly interesting extracts/fractions. In view of the isolation and identification of the compound/molecule accountable for such bioactivity, these samples are preferentially selected to undergo a thorough process of bio-guided fractionation.

3.9. MTS assays

All tests were done using Tetrazolium inner salt assay (MTS) to measure viability of cells cultivated (and maintained in flasks) after application of S4U1 (24 hours exposure). MTS reagent is useful to quantify the amount of formazan produced by living cells. After application of 20 µl mixtures (MTS: PMS 19:1) to 100 µl of medium with cells, plates were incubated at 37°C, 5% CO_2. After 1h to 1 h 30 min, absorbance was measured at 492 nm, by using a multi-well plate reader (O'Toole et al., 2003).

3.10. Evaluation of cell viability on human cell lines

Cell toxicity was tested against MRC-5 human cell line and Melanoma cell line A2058. MRC-5 is a cell line from ATCC (CCL-171) of human fibroblast adherent cells derived from normal lung tissue. Melanoma cell line from ATCC (A2058 – Ref CRL-11147) are human skin adherent cells derived from metastatic site. Culture maintenances was performed accordingly to ATCC specifications. Cells were maintained in 75 cm^2 flasks in the incubator at 37 ºC with controlled CO_2 and humidity conditions. For the assays, cells were seeded in 96-wells plates, 24 hours previously to applications of testing compound. For seeding, media was removed from the flask and cells were washed with PBS. Enough trypsin was added to cover the cells, and after 3-5 min incubation at 37C for cell detachment, 15 ml of fresh media was added. Cells were counted at the microscope in a hemocytometer using a volume of 10 µl of a cell suspension containing 100 µl and 100 µl of trypan blue. The proper volume of cell suspension

was added to fresh RPMI media for 100 µl added in each well at the 96 plate to contain about 7500 cells/well for MRC5 and 4000 cells/well for A2058. S4U1 was added at maximum concentration of 50 µg/ml at the well, diluting progressively by 1:2 for the last concentration of the same extract to be 1.56 µg/ml (spent media was removed and substituted with 100 µl of fresh RPMI media to all wells containing cells). S4U1 was tested in triplicate at the following range of concentrations (µg/ml): 50, 25, 12.5, 6.25, 3.125 and 1.56. After 48 hours incubation period, the cell viability was addressed using a CellTiter 96 Aqueous Non-Radioactive Cell Proliferation Assay (MTS) from Promega. To each well containing 100 µl of media with cells, 10 µl of MTS solution was added, and plates incubated at 35ºC for 1 hour. The absorbance of the formazan product was measured at 485 nm directly from 96-well assay plates in a Biomek minicore multimode plate reader system, from Beckman Coulter. Triton was used as positive control (0% viability) and untreated cells as negative control (100% viability). Percentage of cell viability for each extract tested were calculated. % Survival is calculated from the formula:

$$\%\ Survival\ = \frac{(\text{Sample} - \text{positive control})\ x\ 100}{(\text{Negative control} - \text{positive control})}$$ Equation 7

3.11. Cardiac toxicity on rat cells

Cardiomyocyte cells are used as model of cardiac cells thus representing a preliminary evaluation of cardiotoxicity for testing compounds. Neonatal (P2-3) cardiomyocyte cells were provided by Helena Vieira´s group under a cooperation with Sea4Us and were extracted from rats using their standard protocol. The same number of cells were seeded in each plate for testing S4U1 at 50 µg/ml in DMSO (in triplicate). A negative control using DMSO and an impure fraction containing S4U1 were also tested after 24 hours of incubation at 37 °C, 5% CO_2, the cell viability was addressed using MTS assays.

3.12. Animal behavior

Animals were left for one week for habituation with the equipment and operator prior to the establishment of the pain models. Experiments were carried out by experienced operators with animal testing licenses from the Portuguese Society of Sciences in Laboratory Animals (SPCAL). The operator was blind for each group of rats. A baseline for mechanical sensitivity was obtained in the last two days

of the habituation week. Behavioral tests were performed between 9 and 12 a.m. at the same weekday, for the entire course of establishment of the pain models. After the establishment of pain chronicity, 0.6 mg (compound)/kg (rat) was intravenously administered in the rat tail vein.

3.12.1. Mechanical sensibility

To assess mechanical sensitivity in rats, the hind paw withdrawal thresholds were observed using calibrated von Frey Filaments vFF (Bio-VF-M, Bioseb®). Briefly, animals were let to habituation 15 to 20 min. in the behavioral cage, until cage exploration and grooming activities ceased (Chaplan et al., 1994). Next, the medial plantar surface of both contralateral and ipsilateral hind paws was stimulated by individual vFF with an increasing bending force (6, 8, 10, 15 and 26g), according to their sensitivity at the habituation week. Each monofilament was presented 5 times until a withdrawal response was observed, with at least 5 s of interval between measurements (Hulse et al., 2011).

The withdrawal threshold was the filament with the weakest force (g) that gave at least 3 withdrawal responses in the 5 presentations of the filament (Hori et al., 2013).

MPE% is commonly used in studies of behavioral pharmacology, once it is based on cutoff characteristics, stipulated force/time, normally under conditions that allow it to be considered control, where subjects can be evaluated before suffering real tissue damage (Keyhanfar et al., 2013). Therefore, once many nociceptive (type of model pain serving as input) assays have a hard cutoff, this represents as a reliable method for these types of studies. For instance, for this study calibrated vFF were used, meaning that throughout habituation a cutoff diameter/force of the filament on the left leg (normal leg) was defined. The baseline is considered as the filament upon which the contralateral leg reacts at any given moment, the %MPE is calculated with this equation, towards a better understanding of the analgesic behavior of the compound when applied:

$$\%\ MPE = \frac{(\text{reaction pressure after treatment} - \text{control reaction pressure})\ x\ 100}{(\text{cutoff pressure} -\ \text{control reaction pressure})}$$

Equation 8

3.13. Statistical analysis

Statistical analysis was performed with GraphPad Prims 6.01 (Windows, GraphPad Software, San Diego California USA, www.graphpad.com) and Adobe Illustrator 15.0.2 (CS5) was used to compose the final images and graphics.

Mean differences were compared by the nonparametric Mann-Whitney rank sum test, when samples did not have a normal distribution and by application of a parametric t-test, when it did not have a parametric distribution. Differences were not assumed as significant when $p>0.05$ and significant when $p<0.05$(*) and highly significant $p<0.01$ (**). Results are presented as mean ± S.E.M. (standard error of the mean) for several n samples.

4. Results

4.1. Sampling and Extraction process

The first stage of this thesis concerned the harvesting of the raw material. Figure 3.1 illustrates the two marine sponges collected from the submarine cave "Cathedral", on the Coast of Sagres, Algarve (here termed 'black sponge', found at a depth of 12m, and 'grey sponge', retrieved from a depth of 9m). The selection of these organisms followed the rationale of "underwater screening" developed by Sea4Us. With empirical evidence acknowledged from both previous host company studies and in situ observations, thus, endorsing the biotechnology study developed in the present thesis. Despite both harvested specimens (Figure 3.1) were considered as good candidates to proceed with the bioactivity studies, only the grey sponge was processed.

Figure 4.1 Photographs of the samples collected from the underwater Cave 'Cathedral', on the coast of Sagres, Portugal. Samples were named according to their phenotypic characteristics: ′black sponge' (on the left) and 'grey sponge' (on the right). The bioactivity studies presented in this thesis concern the metabolites extracted from the sample on the right (grey sponge).

Two extraction processes were undertaken and compared to optimize the quantity, in mass, of total extract on this first step of sample processing. Each extraction procedure began with a sponge sample with a mass of around 7.39 g, enough to compare the yield of both extraction methods. The

higher percentage of extraction (Equation 1) was associated with the maceration method with 16% for the maceration and 10% for total extraction method. From these results, it is concluded that the maceration method is slightly more efficient, therefore, elected as the standard extraction method to be used throughout this thesis.

4.2. Bio-guided Fractionation

A single process of fractionation was carried out to separate the secondary metabolites within the crude extract, samples went under two types of chromatography column, here termed fractionation 1 and fractionation 2, both rendering different outcomes (see Figure 4.2).

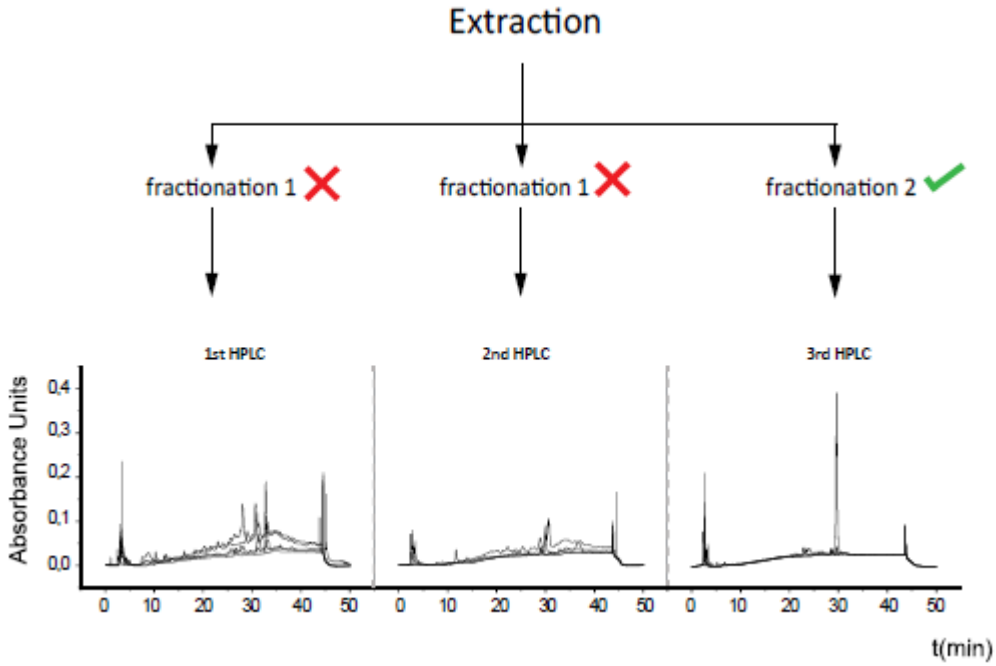

Figure 4.2 Increasing the efficacy of the fractionation method. The crude extracts obtained from the grey sponge using a maceration process, which implies a combination of polar and nonpolar solvent with mechanical assistance from lodestone, allowing an increased separation of the metabolites from the matrix. However, the intended separation was still insufficient for an adequate testing for bioactivity. Samples needed therefore an additional solid phase extraction with a polar reverse phase column, to separate the amalgamates. For these purpose, two methods were tested, a homemade column and a premade cartridge with similar constitution. Identical quantities of extract (100 mg) were loaded into two types of chromatography column (here represented by 'fractionation 1' and 'fractionation 2'), both differing on the composition and manufacturing of the stationary phase. In the fractionation 1, homemade columns were packed with poly (styrene-co-divinylbenzene) resin, whilst in fractionation 2 the separation process was secured by a commercial chromatography column. The first and second HPLC chromatograms show that the fractionation 1, when replicated, rendered a poor separation of the fractions, with low resolution and reproducibility (note the inconsistencies observed between the two chromatograms). The third HPLC chromatogram (fractionation 2) illustrates a more efficient separation process, with the detection of a prominent peak in one of the fractions. Given its consistency and reproductible results, the fractionation 2 was selected to collect the bioactive fractions obtained throughout the present work. In both fractionation methods,

the mobile phase consisted of 5 solvents with different polarity properties. The elution followed a gradient principle, by starting with the most polar solvent and finished with the most nonpolar: H2O, 1:1 H2O/MeOH, 7:3 MeOH/H2O, ACN, 9:1 DCM/MeOH. In the HPLC chromatograms displayed, the 5 fractions are superimposed.

In a first instant, 10 mg of the crude extract were eluted with 5 different solvent combinations - H2O, 1:1 H2O/MeOH, 7:3 MeOH/H2O, ACN ,9:1 DCM/MeOH – through a homemade column packed with 3 g of poly (styrene-co-divinylbenzene) resin (9003-70-7). The respective fractions were then analyzed by HPLC (Figure 3.2, 'fractionation 1'). By analyzing the HPLC chromatograms of the fractionation 1 conducted in two different instants - 1st HPLC and 2nd HPLC -, one can observe a) a poor definition of the peaks, suggesting an ill-defined separation of the compounds, and b) a lack of reproducibility when comparing the outputs of HPLC 1 and of HPLC 2. This was possibly due to an error attributed to the different/not reproducible packing of the columns used. Consequently, to reduce the probability of error, a prepacked chromatography cartridge was introduced – fractionation method 2. The HPLC chromatogram of the fractions obtained with this column (3rd HPLC, figure 4.2) showed more reliable results, illustrating a more efficient separation process, allowing a peak collection between 28 and 31 min. for every fraction, with the detection of a prominent peak (MeOH/H2O (7:3); see figure 4.3). Also given the reproducibility of this method (data not shown), it was therefore selected as the reference method for posterior experiments.

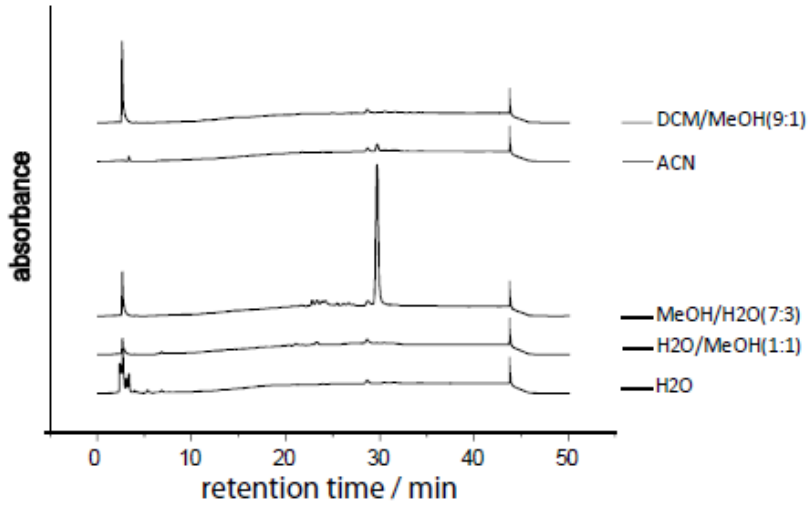

Figure 4.3 HPLC chromatograms of the fractions obtained with the fractionation 2 method. The HPLC separation method was performed with a gradient elution starting at 0min with 95% ACN and 5% MeOH and ending at 40min with 100 % MeOH, with a subsequent washing of the column until the end of the protocol (lasting for up to 50min). The chromatograms of the 5 fractions collected in the fractionation method are sequentially shown from bottom to top: H2O; H2O/MeOH (1:1); MeOH/H2O (7:3); ACN; DCM/MeOH (9:1). The fraction eluted with MeOH/H2O (7:3) solvent presented the most prominent peak.

The neuronal bioactivity of the 5 fractions depicted in figure 4.3 was evaluated by screening their effect against a platform of potassium (K^+) and sodium (Na^+) currents present at the surface of rat small

dorsal root ganglion (sdDRG) neurons. The results presented in Table 3.1 relate to the assessment of the bioactivities tested, those performed for the slow component of K^+ current (IK), as well for the peak Na^+ current (INa peak), approach of which is developed in the following section 3 (see figure 3.7 for further explanation)

Table 4.1 Bioactivity effects of the fractions collected- inhibition in % of potassium and sodium currents recorded from DRG neurons acutely dissected from naïve animals

	% current inhibition for every fraction				
	H_2O	H_2O/MeOH(1:1)	MeOH/H2O(7:3)	ACN	DCM/MeOH(9:1)
K^+	4.80%	15.73%	42.18%*	30.77%*	15.41%
Na^+	8.12%	6.94%	16.82%*	21.17%*	1.30%

*(n=2)
Average between both

Fractions collected with the solvents MeOH/H2O (7:3) and ACN presented the greater percentage of IK and INa current inhibition (IK: 42.18% and 30.77%, for MeOH/H2O (7:3) and ACN; respectively, and INa: 16.82% and 21.17%, for MeOH/H2O (7:3) and ACN, respectively, n=2). A greater inhibition on K^+ currents by the MeOH/H2O (7:3) is highly significant as such currents have been associated with analgesic proprieties during the analgesic program of Sea4Us. Together with the fact that the HPLC chromatogram of MeOH/H2O (7:3) presents the most prominent peak, prompted me to select this fraction as the elected fraction to continue with the biotechnological studies. Accordingly, the prominent peak of such fraction was collected and purified (hereafter defined as 'S4U1') (Figure 4.4).

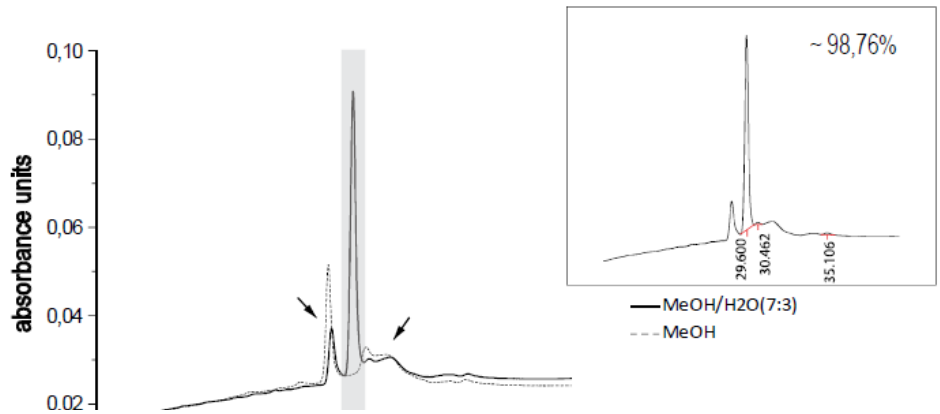

Figure 4.4 HPLC chromatogram of the fraction of interest (here in termed 'S4U1'). The sample trace (MeOH/H2O, 7:3; line) shows a major peak with a retention time around 30min (grey area) and two smaller peaks highlighted with arrows (retention times of 27min and 31min), which are also detected in the blank trace (MeOH, the eluent used in the HPLC run; dashed line). By ruling out the arrowed blank peaks, one can estimate the purity grade of the peak of interest in the sample trace (see inset). From peak area comparison, a purity of about 98.76% is attributed to the peak of interest.

Figure 4.4 shows visual representations of the resulting collection and purification of S4U1. The retention time presented is limited to period range 20 until 40 min once there were no other peaks visible. The straight line represents the result of the collection and purification, while the dashed line represents the blank trace of MeOH, that ran with the same HPLC protocol, to discard the two possible stray peaks flanking the peak of interest. Indeed, those two arrow pointed peaks match with the peaks from MeOH alone. Ruling out these blank peaks, and considering the remaining peak areas, it is possible to estimate the purity of S4U1 around 98.76% (see inset of figure 4.4).

4.3. Characterization of K^+ currents

Before delving into the effect of S4U1 on voltage-gated potassium (K^+) and sodium (Na^+) currents, it is important to firstly conduct an electrophysiological characterization of those currents from rat sdDRG neurons acutely isolated from naïve animals (control conditions). Starting with K^+ currents, the following results concern the study of the voltage dependence of activation and inactivation of whole-cell K^+ currents.

4.3.1. Voltage dependence of Activation

To study the activation of whole-cell voltage clamp K^+ currents of rat small DRG neurons, a voltage protocol to study the voltage dependence of activation was used, as follows: currents were evoked and recorded by a series of depolarizing pulses from -80mV until +50 mV, in steps of +10mV, preceded by a pre pulse at -120 mV, and with a holding potential of -70 mV. Figure 4.5A depicts an illustrative example of the whole-cell voltage clamp K^+ currents recorded with such protocol (see inset). K^+ current decay follow two different phases, a fast spontaneously decay current (IA) and, a slow inactivating current (IK) (Kostyuk et al. 1981; Standen et al., 1987; Costa, 1996; Everill et al. 1998; Mathie et al. 1998; Sah et al.,1998; Vreugdenhil et al., 1998; Bruehl & Witte, 2003; Yang et al. 2004; Ketelaars et al., 2011b; ,); Both current-components , in what the current decay is concerned, those are better fit with exponential functions described in figure 3.7 (methods section, for further details). These two components are supposed to be underlined by two different channel-type populations. Hence, current amplitude was taken at two different time points: at the beginning of the pulse (current peak), as a measure of IA, and at the end of the pulse, as a measure of IK (Figure 4.5A). The amplitude of these components, separately analyzed throughout this thesis, were normalized for the cell capacitance values

(pA/pF), as a measure of the size of cell membrane (1µF – 1cm2; (Hodgkin & Huxley, 1952)) and data was plotted in a current-voltage relationship (I-V) (Figure 4.5B). The voltage dependence of activation was studied by plotting the conductance, calculated from current values (equation 3) and then normalized to the maximum value (G/Gmax), against the voltage potentials of the command pulse (Figure 4.5C).

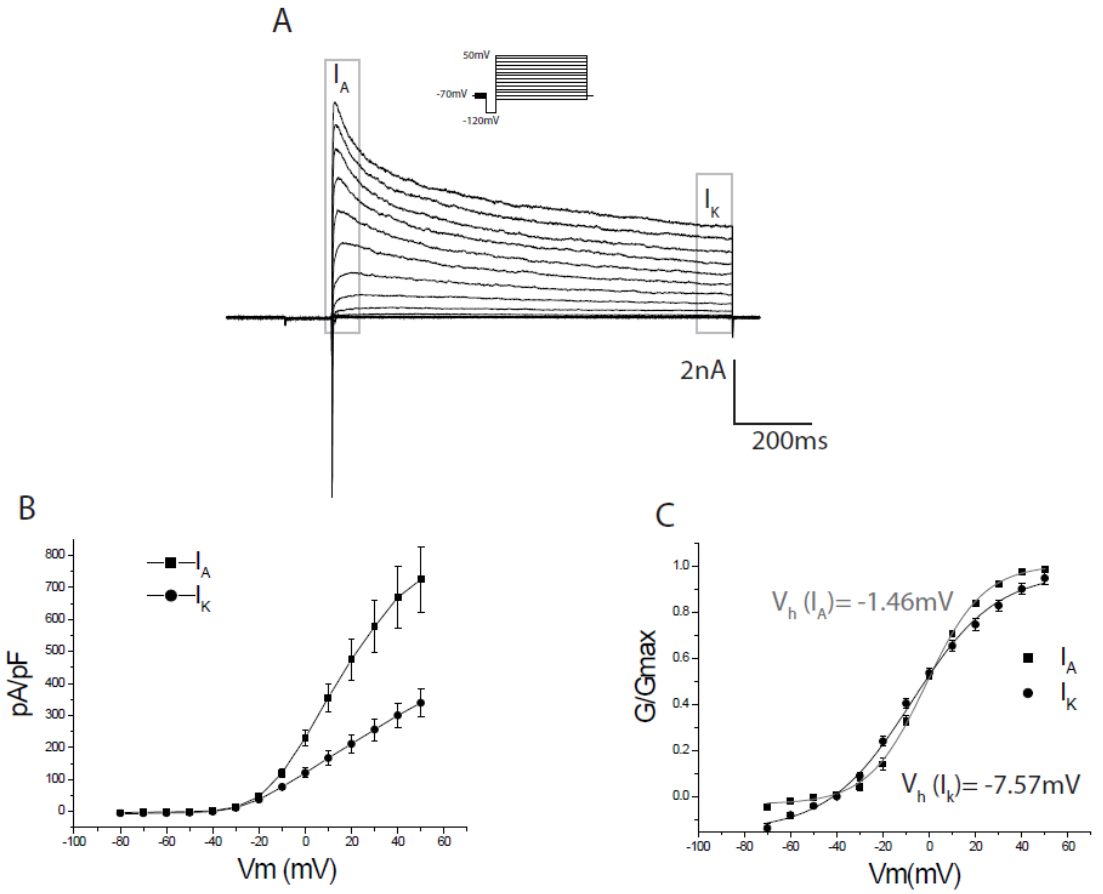

Figure 4.5 Voltage Dependence of Activation of potassium currents. Whole-cell voltage clamp K^+ currents were recorded in small diameter DRG neurons isolated from naïve rats. A) Representative potassium current decaying trace elucidating the two different types of currents studied in this work: fast (I_A) and slow (I_K) currents, taken at the peak, and at the steady state regions of the trace, respectively. K^+ currents were evoked by an activation protocol (see inset) of depolarizing command pulses, in steps of +10mV, from -80 mV up to +50mV, following a hyperpolarizing conditioning pulse at -120 mV. Holding potential was set at -70 mV.B) Mean I_A (squares; n=18 cells)) and I_K (circles; same n=18 cells) amplitudes were normalized to the cell capacitance as a measure of the current density. C) Mean conductance values of both currents were normalized to their maximum values (G/Gmax) and the data points were fitted with a Boltzmann (Equation 4: Vh (I_A)=-1.46mV and Vh (I_K)=-7.57mV). Error bars are ±S.E.M.

Figure 4.5A is a representative illustration of whole-cell K^+ currents recorded in this thesis with a typical decaying phase that comprehend two different current components, demonstrative of fast inactivating and slow inactivating currents – IA and IK, respectively. The I-V relationship curve (Figure 4.5B) plots the difference between the mean current density values of IA and IK (at 50mV: 724 ± 396

pA/pF and 339 ± 163 pA/pF, for IA and IK, respectively (n=18)). Figure 4.5C depicts the voltage dependence of activation of IA and IK, whose activation curves were fitted by a Boltzmann function (equation 4). Both current components have similar mean half-maximal activation potential (Vh (IA)= -4.67 ± 1.4mV and Vh (IK)= -8.73 ± 1.38mV, n=18, presenting no statistical significant difference (p-value > 0,05) (Everill et al., 1998;Szwarc, 2017); see also table 4.2).

Table 4.2 I_A and I_K activation fitting parameters Vh (mV) and Vs (mV/e-fold) and corresponding *p*-values (Equation 4) for sdDRG neurons of naïve animals. Values are mean ± S.E.M.

	Voltage dependence of activation of potassium		
	V_h (mV)	V_s (mV/*e*-fold)	*n*
I_A	-4.67 ± 1.40	13.6 ± 0.82	18
I_K	-8.73 ± 1.38	22.0 ± 1.41	
P-value	0.2502	0.0617	-

4.3.2. Voltage dependence of Inactivation

The process of inactivation of whole-cell K^+ currents imply the study of voltage dependence of steady state of a determined population of channels available for conduction at certain membrane potentials (Serrão, 2015). To achieve this, a double pulse voltage protocol, composed by a command pulse of +10mV, and conditioning pre pulses ranging from -140 mV until +10 mV, in steps of +10 mV, with a holding potential set at -70 mV, lasting 10360ms, were used. Following the same rationale used in the activation analysis, K^+ currents elicited by the command pulse were analyzed according to the existence of two current components (IA and IK), taken at the beginning and at the end of the command pulse (Figure 4.6A). IA and IK amplitude values were normalized to the maximum (I/Imax) and the mean values were plotted against the pre pulse voltage potentials (Figure 4.6B).

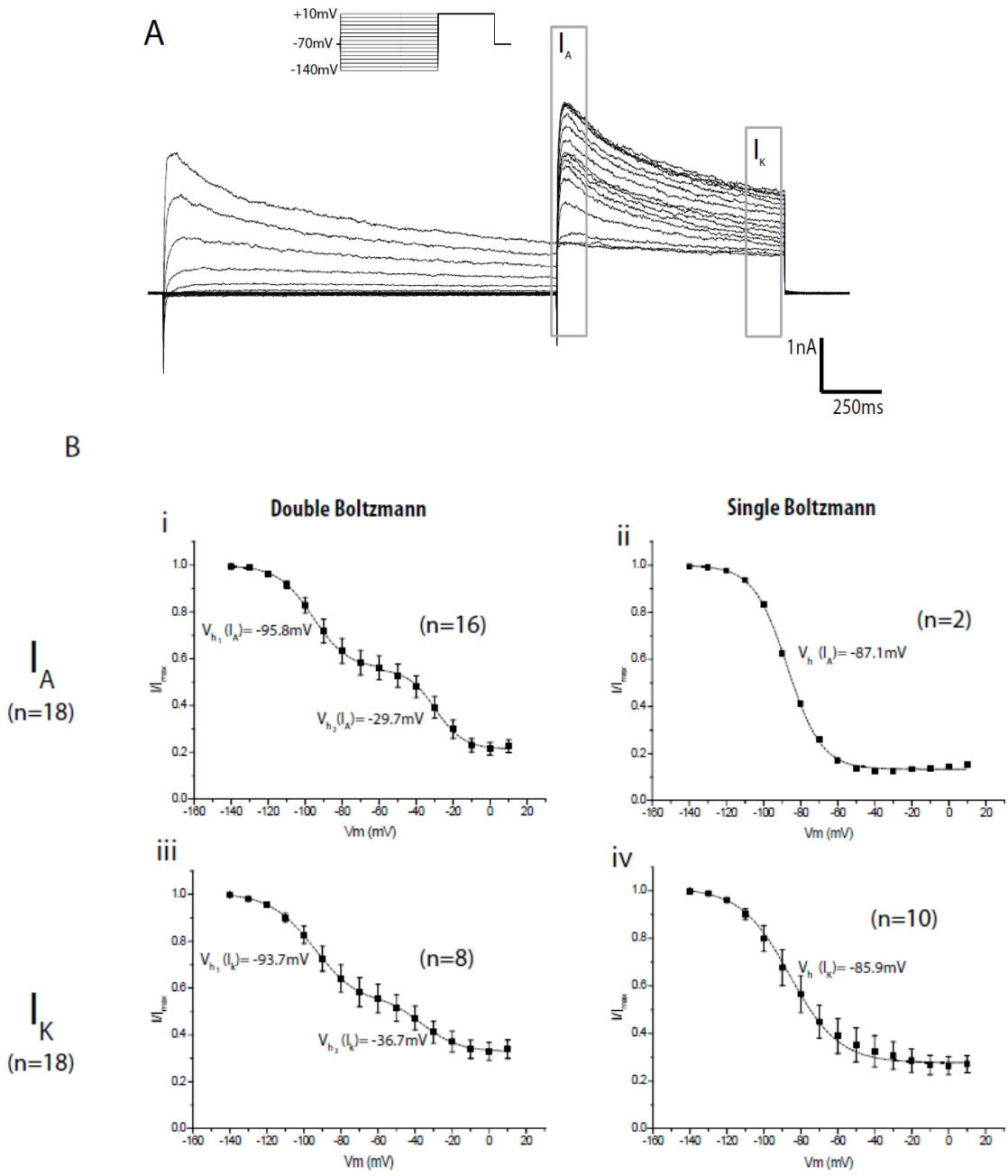

Figure 4.6 Voltage-Dependence of Steady-State Inactivation of voltage-gated K^+ currents. Whole-cell voltage-clamp K^+ currents were evoked by a command step pulse to +10mV, following a series of pre-pulses ranging from -140mV to +10mV, in steps on +10 mV, and with a holding potential of -70mV. A) Representative whole-cell potassium current recorded in sdDRG neurons of naive animals, elicited by the inactivation protocol (see inset). Two different types of currents were analysed: fast (I_A) and slow (I_K) currents, taken at the peak and at the end of the command pulse, respectively. B) Mean I_A and I_K values were normalized for the maximal response (I/Imax), as a function of pre-pulse potentials, to draw the steady state inactivation curves of sdDRG neurons (n=18) isolated from naïve animals. The data points related to I_A (Bi and Bii) and I_K (Biii and Biv) were both fitted by a double Boltzmann function (Equation 6; Bi: Vh1 = -95.8mV and Vh2 = -29.7mV, n=16, and Biii: Vh1 = -93.7mV and Vh2 = -36.7mV, n=8) and by a single Boltzmann function (Equation 4; Bii: Vh = -87.1mV, n=2, and Biv: Vh =-85.9mV, n=10). A larger fraction of I_A was described by a double Boltzmann equation (16/18), whereas I_K tended to be better described by a single boltzmann (10/18). Error bars are ± S.E.M..

Figure 4.6A illustrates representative K^+ currents recorded from a single rat sdDRG neuron. The voltage dependence of the steady state inactivation of the fast activating and slow inactivating K^+ currents of the command pulse were studied by plotting the current amplitudes for their maximum value (I/Imax) against the pre pulse voltage potentials. The respective inactivation curves were described by a single (equation 4) or a sum of two Boltzmann functions (equation 6). From the pooled data presented for IA in Figure 4.6B, one can observe that 16 out of 18 cells are better fitted with a double Boltzmann, and, consequently, 2 out of 18 cells are described with a single Boltzmann. As for IK, this distribution is more even, with a slighter tendency towards the single Boltzmann fitting (Double = 8 cells and Single = 10 cells). Despite this difference, the mean half-maximal inactivation potential (Vh) values are similar, corroborated by not possessing statistical significance upon its comparison (p-value > 0.05). The first and second components of the inactivation curves of IA and IK with a biphasic response present the following parameters of inactivation: Vh1 = -91.3 ± 2.2 mV and Vh2 = -29.9 ± 1.63mV, for IA (n=16), and Vh1 = -90.9 ± 3.84 mV and Vh2 = -33.6 ± 3.04mV, for IK (n=8). The mean Vh of the single fitted data inactivation curves are as follows: -86.8mV (n=2) and -80.5 ± 6.02mV (n=10), for IA and IK, respectively. These results, along with slope constants of the inactivation curves (Vs), are gathered in Table 4.3.

Table 4.3 Steady-state inactivation fitting parameters (single and double Boltzmann; equation 4 and 6, respectively) for I_A and I_K recorded in sdDRG neurons of naïve animals and corresponding *p*-values. Values are mean ±

	Voltage dependence of inactivation of potassium currents							
	Double Boltzmann					Single Boltzmann		
	V_{h1} (mV)	V_{s1} (mV/*e*-fold)	V_{h2} (mV)	V_{s2} (mV/*e*-fold)	*n*	V_h (mV)	V_s (mV/*e*-fold)	*n*
I_A	-91.3 ± 2.2	11.1 ± 1.08	-29.9 ± 1.63	6.99 ± 0.39	16	-86.8	8.87	2
I_K	-90.9 ± 3.84	12.9 ± 1.74	-33.6 ± 3.04	8.21 ± 0.98	8	-80.5 ± 6.02	16.8 ± 2.85	10
P-value	0.9758	0.4742	0.2826	0.2569	-	-	-	-

4.4. Neuronal bioactivity – Effect of S4U1 on K^+ currents

The present section of this thesis relates to the electrophysiological results obtained for K^+ currents upon the application of the purified fraction (S4U1). Aiming at studying the influence of concentration over the current output, a range of 3 different concentrations was superfused on rat sdDRG neurons under analysis.

4.4.1. Inhibition of K^+ currents

To study the effect of S4U1 on K^+ current inhibition, an activation voltage protocol with a single command pulse at +20mV, preceded by a pre-pulse at -120mV (from a holding potential of -70mV), was applied. This aimed a simplified view of the K^+ current inhibition by S4U1. This protocol was repeated, in intervals of 30 s, until the stabilization of IA and IK amplitude, which was usually ensured after 5min without current run-down. At this stage, a variety of concentrations (2, 10 and 20 ug/mL) was superfused to the neurons, under constant flux. IK amplitude values were normalized to their maximum (I/Imax) and plotted against time (min) (Figure 4.7A; Arrows indicate the beginning of the superfusion).

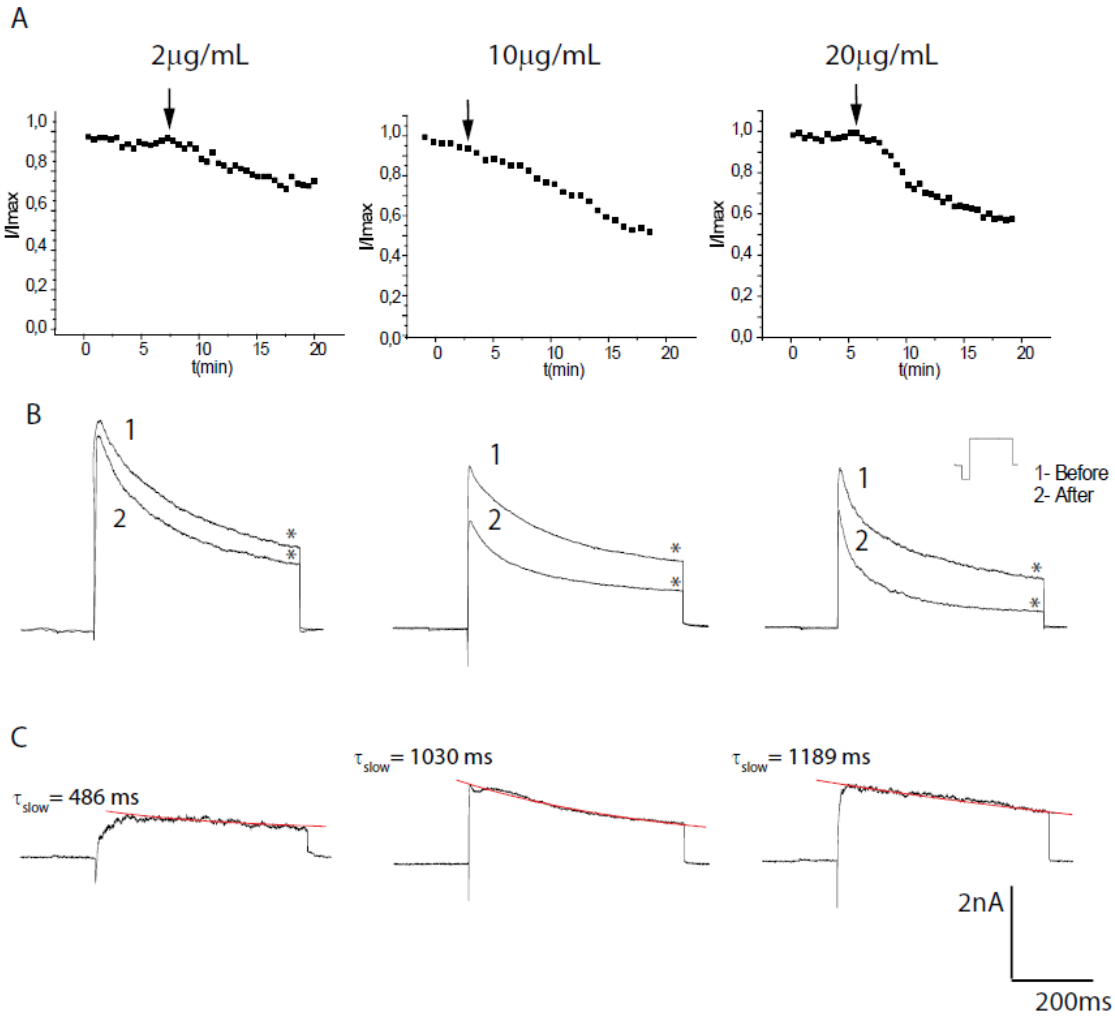

Figure 4.7 S4U1 decreases whole-cell K^+ current amplitude in a dose-dependent fashion. A) Time-course illustrative examples of the effect of S4U1 over I_K. Current amplitude was normalized to the maximum value (I/Imax) and plotted as a function of the total effect time. Arrows indicate the beginning of the superfusion with S4U1, at three different concentrations (2µg/mL; 10ug/mL and 20ug/mL). B) Respective whole-cell K^+ currents before (1) and after (2) superfusion with S4U1. K^+ currents were evoked by a depolarizing command pulse to +20mV (10740ms in duration), preceded by a hyperpolarizing pulse to -120mV, (1930 ms in length). Holding potential was set at -70mV (see inset). '*' marks the region of the K^+ currents subjected to the analysis in A). C) Current traces sensitive to the effect of S4U1, resulting from the subtraction 'trace 1 - trace 2' (in B). Subtraction traces were fitted with an exponential function (Equation 5; red traces) to obtain the time-constants of the decay

phase. Inactivation of the subtraction currents was better described by a single exponential: 2ug/mL (τ_{slow}= 486ms), 10ug/mL (τ_{slow}= 1030ms) and 20ug/mL (τ_{slow}= 1189ms)

Figure 4.7A shows IK inhibition in three individual neurons under the application of 2, 10 and 20 µg/mL S4U1. The examples illustrate an increasing effect of S4U1 along the concentrations used. Indeed, S4U1 provoked an IK inhibition of 19%, at 2µg/mL, and around 59%, at 20µg/mL. A current run-down, observed in the example taken for 10µg/mL, obstructs a straightforward calculation of the current inhibition. However, the highest effect of S4U1 was observed at 20µg/mL. This result is visually demonstrated in the respective current traces (Figure 4.7B). Figure 4.7C depicts the current sensitive to the effect of S4U1, determined by subtracting the current traces before and after S4U1 application (Figure 4.7B). The resulting subtraction traces were best fitted into a single exponential function (equation 6). The time constant of inactivation values (τ(ms)) suggests S4U1 mainly affects the slow currents, as follows: 486ms, 1030ms and 1189ms, for 2µg/mL, 10µg/mL and 20µg/mL S4U1, respectively.

The mean percentage values of current inhibition demonstrate an increased inhibition on phase slow currents (IK) when compared to the fast one (IA) for all S4U1 concentrations applied. Furthermore, 20µg/mL S4U1 presents the highest effect (in %): 36 and 60 for IA and IK (n=5), respectively (Figure 4.8). The effect of S4U1 varies in a dose-dependent manner, especially on IK. These results also led me to select the highest concentrations (20µg/mL) to further investigate the effect of S4U1 on the voltage dependence of activation and inactivation of K^+ currents.

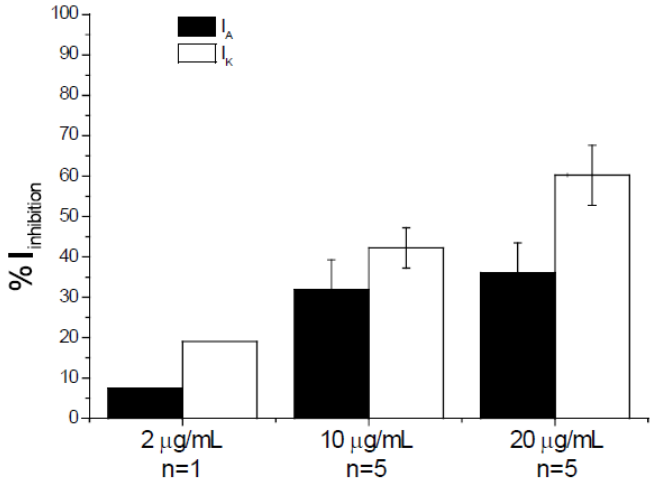

Figure 4.8 Effect of S4U1 over I_A and I_K. Mean K^+ current inhibition percentage values, analyzed for the fast currents (I_A- black) and slow currents (I_K- white), for all concentrations used: 2µg/mL (n=1), 10µg/mL (n=5) and 20µg/mL (n=5). The effect is more notorious on I_K. Error bars ±S.E.M. values.

4.4.2. Voltage dependence of Activation

The study of the effects of 20µg/mL S4U1 on the voltage dependence of activation of potassium currents in small DRG neurons. Whole-cell currents were elicited by the same voltage protocol as previously used in figure 4.5 (Figure 4.9 A), and analyzed accordingly, with a separate analysis of IA and IK.

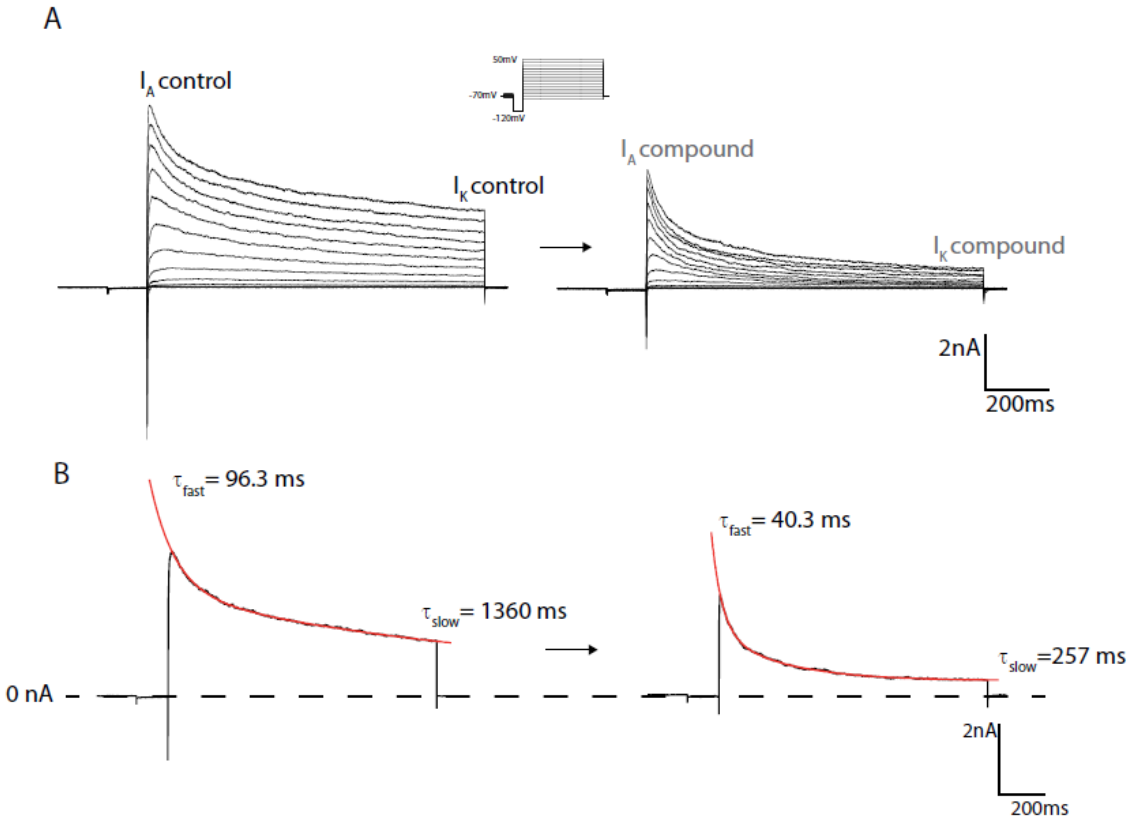

Figure 4.9 Effect of S4U1 over the whole-cell K^+ currents of acutely isolated rat sdDRG neurons from naïve animals. A) Illustrative K^+ current traces evoked following the activation protocol as explained in Figure 3.5 A (see inset), before (control; left panel) and after (compound; right panel) the application of S4U1 at 20µg/mL. Fast (I_A) and slow (I_K) components of the total K^+ current are highlighted to point the regions where voltage dependence of activation was analyzed (see figure 3.10). B) Isolation of the current traces obtained with a depolarizing command pulse at +20mV, fitted with an exponential function (equation 5; red trace). Both decay phases were described by a double exponential, with the following time-constants of inactivation: control (left panel), τ_{fast}= 96.3ms, τ_{slow}= 1360ms, and compound (right panel), τ_{fast}= 40.3ms, τ_{slow}= 257ms) In the presence of S4U1, the inactivation of the currents is rather faster, proposing a greater influence the slow component of the inactivation.

Figure 4.9A illustrates representative current traces evoked from a cell that went through the application of S4U1 (control; left panel, and after compound; right panel), at the elected concentration of 20µg/mL. A significant reduction on IA and IK amplitude is observed upon the superfusion of S4U1. The decaying phase of K^+ currents was analyzed as a measure of the kinetics of inactivation. Figure 4.9B shows the time constant of inactivation values, at +20mV, in both conditions (Control and S4U1 compound), as a result of a double exponential fitting of the respective traces (in ms): τfast = 96.3 and τslow = 1360 (for control neurons), and τfast = 40.3 and τslow = 257 (for neurons in the presence of

S4U1 20µg/mL). These results explain the change observed on the decaying phase of K^+ currents (Figure 4.9A).

Mean IA and IK amplitude values obtained for S4U1 compound (open squares) were normalized for the cell capacitance (pA/pF), plotted against voltage (I-V) and compared to control (filled squares) (Figure 4.10(i)). Subsequentially, mean IA and IK were converted into conductance(G), using equation 3, normalized to the maximum value (G/Gmax), and plotted against the command pulse voltage potentials (Figure 4.10(ii)).

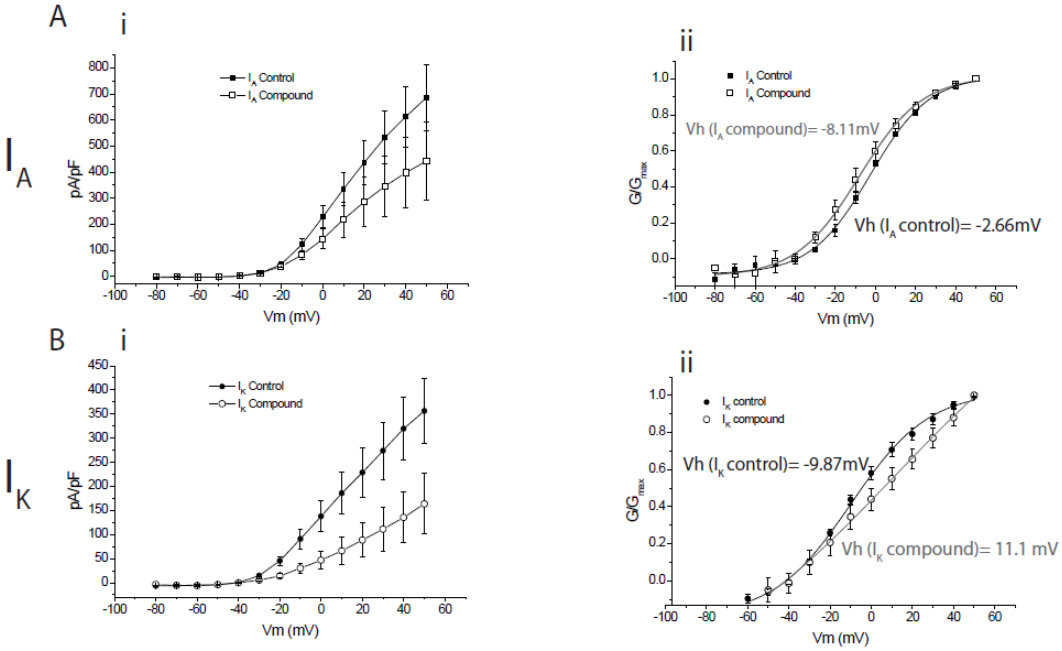

Figure 4.10 Effect of 20µg/mL S4U1 on the voltage dependence of activation of I_A and I_K. Activation curves relate to K^+ currents like those illustrated in figure 3.9. Ai) *I–V* curves depicting mean I_A normalized to cell capacitance, as a measure of current density (pA/pF; equation 2) and Aii) activation curves illustrating mean I_A conductance normalized to the maximum value (G/Gmax), in the presence (open squares; n=4) and absence (control; filled squares, n=4) of S4U1. Bi) Mean I_K density and Bii) mean I_K G/Gmax, in the presence (open circles, n= 4) and absence (control; filled circles, n= 4) of S4U1. Data points in Aii) and Bii) were fitted with a Boltzmann function (equation 4; in Aii: Vh =-2.66 mV, for control neurons, and Vh=-8.11 mV, in the presence of S4U1; in Bii: Vh= -9.87mV, for control neurons, and Vh=11.1 mV, for neurons in the presence of S4U1). Lines in Ai) and Bi) were added for better understanding of the data points. Error bars are ± S.E.M. values.

Figure 4.10 compares mean current density(i) and conductance(ii) values obtained for control neurons and for neurons under the presence of 20 µg/mL S4U1 on IA (Figure 4.10A) and IK (Figure 4.10B). The minor differences observed on I-V curves reveal that S4U1 may mainly impacts IK (Figure 4.10 Bi), whose mean current density values in control and 'S4U1' neurons, at +50mV, differ as follows: 356.2 ± 68.1pA/pF and 163.5± 62.7 pA/pF, for control and S4U1 neurons, respectively. Indeed, there this difference is not statistically significant (p-value >0.05), maybe due to the small sample size (n=4). The Vh values retrieved from fitting the activation curves (Aii and Bii) with a Boltzmann function unravel slight differences on IA and IK, assigned to the influence of S4U1. The mean Vh values, taken for every S4U1 compound concentrations tested in this thesis, are quantified in Figure 4.11. In

the presence of S4U1 there is a tendency for a small hyperpolarizing shift of the activation curves, observed both in IA and IK. There was significant difference observed only for IK, at 10µg/mL S4U1: Vh = -3.5 ± 2.1 mV, for control, and Vh = -34.5 ± 13.2mV, with S4U1 compound, (0.01 <p-value <0.05, n=5). The remaining differences are not statistically significant (p >0.05), which, once again, might be explained by the small sample size. Overall, these results indicate S4U1 influences the voltage dependence of activation of K^+ currents, especially those characterized by slow inactivating properties (IK), by shifting the opening of the channels that mediate such currents towards more hyperpolarized potentials.

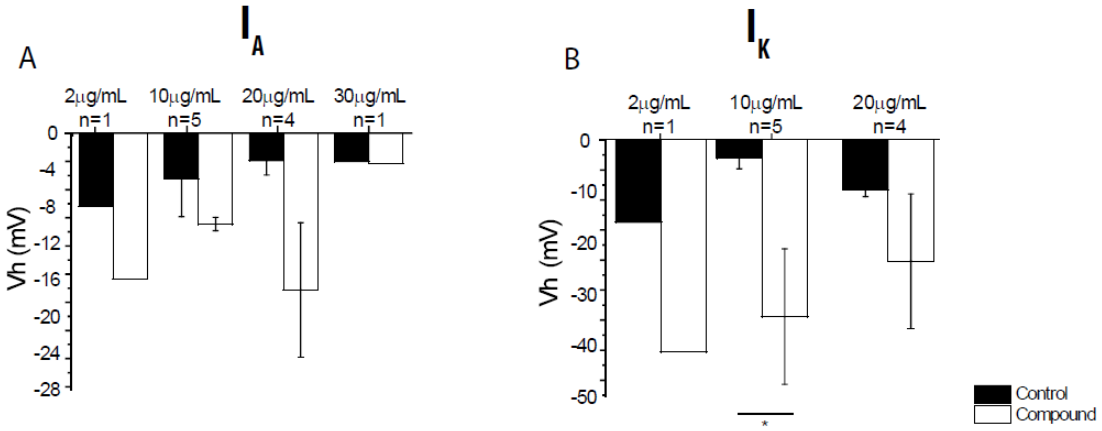

Figure 4.11 Influence of S4U1 on half-maximal activation voltage (V_h) of I_A and I_K. Mean Vh values obtained before (control; black bars) and after (compound; white bars) application of S4U1 at a range of concentrations in I_A (A; 2, 10, 20, 30 µg/mL S4U1) and I_K (B; 2, 10 and 20 µg/mL S4U1). The significant shift in V_h was observed for I_K at a concentration of 10µg/mL S4U1 (Vh control = -3,542 mV and Vh compound = -34,45mV, n= 5). Non-parametric Mann–Whitney U-test was used for statistical procedures (0.05> *p*-value > 0.01). Error bars are ±S.E.M. values.

4.4.3. Voltage dependence of Inactivation

The influence of S4U1 over the voltage dependence of steady state inactivation of K^+ currents was studied by evoking currents that followed a double pulse inactivation protocol. Such protocol included a command pulse of +10mVpreceded by conditioning pre pulses ranging from -140mV until +10 mV, in steps of +10mV, with a holding potential set at -70mV. The voltage dependence of inactivation was studied at two different instants of the command pulse, resembling the IA vs IK analysis performed in the activation process: at the beginning (peak current) and at the end (steady state current) of the command pulse (Figure 4.12).

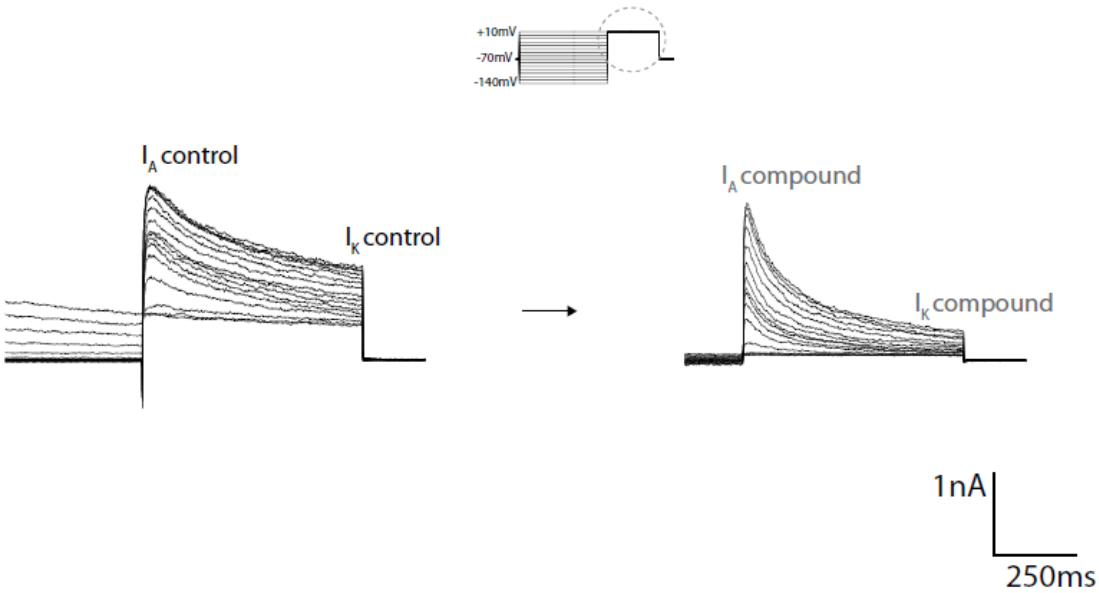

Figure 4.12 Influence of S4U1 on the steady state of inactivation of K^+ currents. Illustrative K^+ current from sdDRG neurons of naïve animals evoked by the inactivation voltage protocol as explained in figure 3.6, before (control, left panel) and after (compound, right panel) the superfusion with S4U1 at 20µg/mL. The traces correspond to the currents elicited at the command pulse (see dashed circle on the inset). Fast (I_A) and slow (I_K) components of the total K^+ current of the command pulse are highlighted to point the regions where voltage dependence of inactivation was analyzed.

Figure 4.12 illustrates whole-cell K^+ current traces of a single cell before (left panel) and after (right panel) the application of S4U1, at the elected concentration of 20µg/mL. Upon the application of S4U1 there was a reduction of the current amplitudes, in both current components. IA and IK amplitude values were normalized to their maximum (I/Imax) and subsequent mean values were plotted against the voltage potentials of the conditioning pre-pulse. The consequent inactivation curves were fitted with either single (equation 4) or double (equation 6) Boltzmann functions (Figure 4.13).

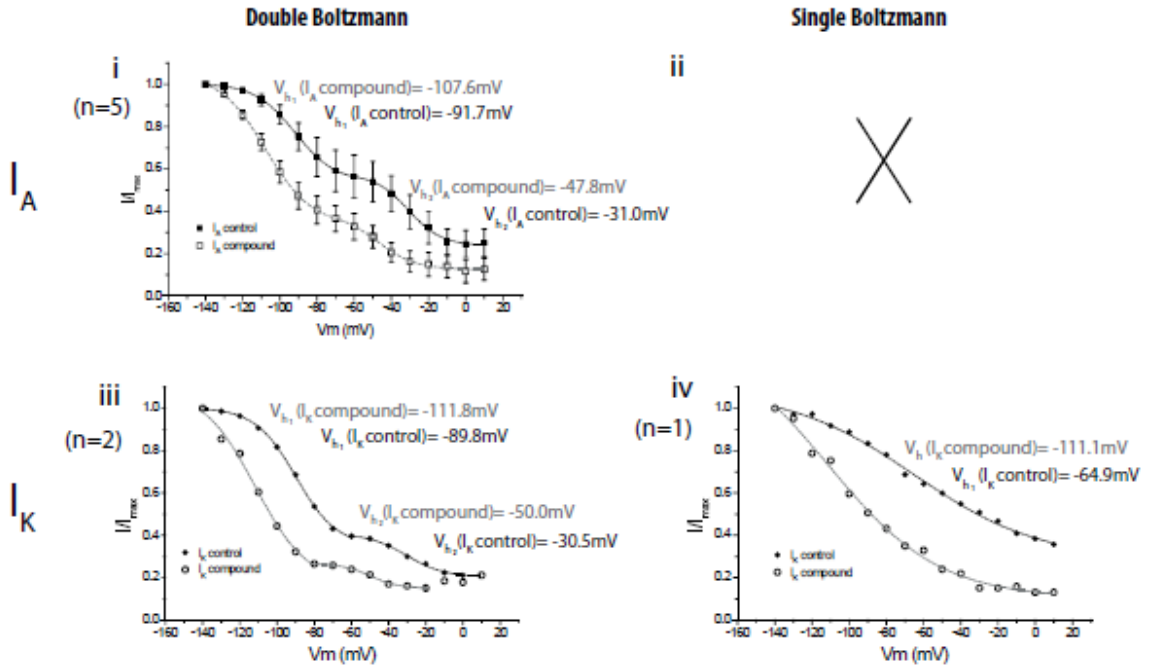

Figure 4.13 Effect of 20µg/mL S4U1 on the voltage dependence of steady state of inactivation of K^+ currents. Mean I_A (i) and I_K (ii) current values were normalization to the maximum value (I/Imax). i) I_A inactivation curves were described by a double Boltzmann function (Equation 6; V_{h1} = -91.7mV and Vh2 = -31.0mV, for control neurons – filled squares -, and Vh1 = -107.6mV and Vh2 = -47.8mV, for neurons in the presence of S4U1 – open squares -, n=5). iii) I_K inactivation curves were fitted either by a double Boltzmann function (Vh1 = -89.8mV and Vh2 = -50.0mV, for control neurons – filled circles -, and Vh1 = -111.8mV and Vh2 = -30.5mV, for neurons in the presence of S4U1 – open circles-, n= 2). or by a single Boltzmann function (Equation 4; Vh = -64.9mV, for control neurons – filled circles -, and Vh = -111.1mV, for neurons in the presence of S4U1 – open circles-, n=1). Error bars are ±S.E.M.

Figure 4.13 depicts the influence of S4U1 on the voltage dependence of inactivation of K^+ currents. Here, important to notice that the S4U1 effect are split on the recordings that expressed single vs double fittings, both quantified for IA and IK. Accordingly, the analysis conducted for IA exclusively rendered inactivation curves with a biphasic response (two-component curves; Figure 4.13i), whereas, for IK, both types of response were encountered (two-component curves; Figure 4.13iii, and one-component curves; Figure 4.13iv). Notwithstanding, in all these cases, the presence of S4U1 provoked a hyperpolarizing shift in the inactivation curves of IA and IK. The mean Vh values, obtained for every S4U1 compound concentrations applied in the present work, are quantified in Figure 4.14.

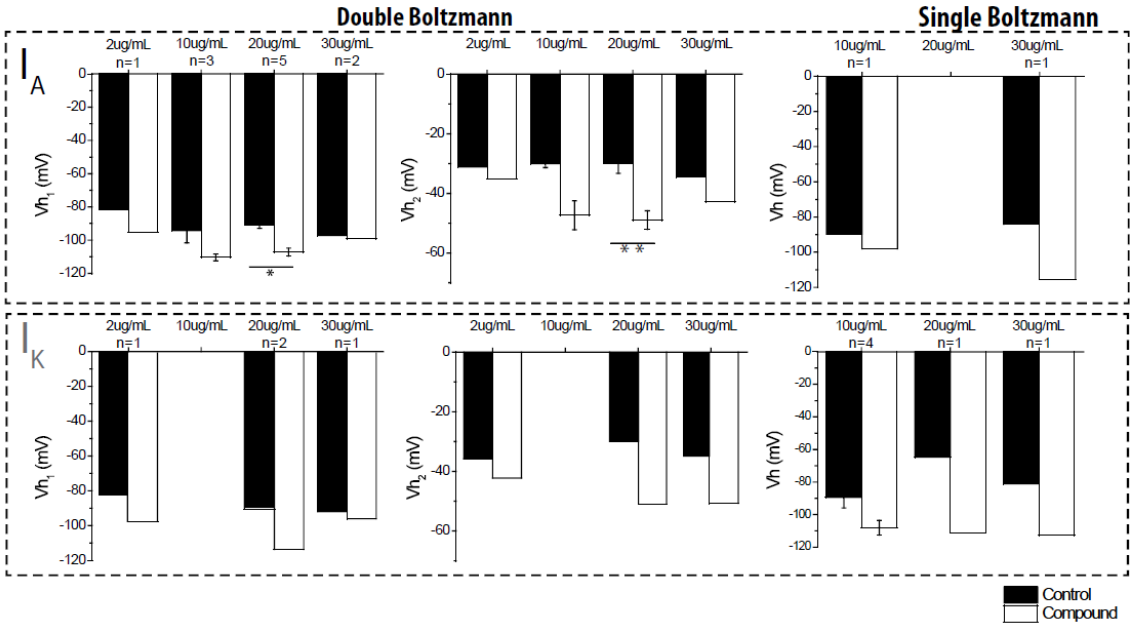

Figure 4.14 Influence of S4U1 on half-maximal inactivation voltage (V_h) of I_A and I_K inactivation curves. Mean Vh values obtained before (control; black bars) and after (compound; white bars) application of S4U1 at a range of concentrations (2, 10, 20, 30 µg/mL). The top panel relates to the results obtained for I_A and the bottom panel relates to I_K. The sample size, and the nature of inactivation curve responses (Single-component vs Double-component Boltzmann), is presented. The significant differences in V_h were observed at a concentration of 20µg/mL S4U1, both in the first component (Vh1 control = -90.72 ± 2.1mV and Vh1 compound = -107.30 ± 2.5mV, n= 5; * 0.05 > *p*-value > 0.01) and in the second component (Vh2 control = -29.75 ±3.5mV and Vh2 compound = -48.97 ±3.1mV, n=5; ** 0.01 > *p*-value > 0.001) of the inactivation curves. Non-parametric Mann–Whitney U-test was used for statistical procedures. Error bars are ±S.E.M

Figure 4.14 comprises mean Vh values of the inactivation curves of IA and IK before (black bars) and after (white bars) the superfusion with S4U1 at different concentrations. In all cases, S4U1 causes a hyperpolarizing shift of the inactivation curves, indicating a facilitation of the inactivation process. Overall, the fraction of K^+ channels available to conduct as a response to activation at a given membrane potential is decreased upon the effect of S4U1. This effect was particularly verified under a concentration of 20µg/mL S4U1, in first and second components of IA inactivation curves: mean Vh1 control = -90.72 ± 2.14mV and Vh1 S4U1 = -107.3 ± 2.49 V; mean Vh2 control =-29.75 ± 3.54 mV and Vh2 S4U1 = -48.97 ± 3.12 mV. The differences are statistically significant (0.05 > *p*-value > 0.01, for Vh1, and 0.01 > *p*-value > 0.001, for Vh2, n=5).

4.5. Characterization of Na^+ currents

Prior to the experiments done in the presence of S4U1, an electrophysiological characterization of Na^+ currents was conducted in control rat sdDRG neurons, acutely isolated from naïve animals. The

following results concern the study of the voltage dependence of activation and inactivation of whole--cell Na^+ currents.

4.5.1. Voltage dependence of Activation

Whole-cell voltage-clamp Na^+ currents were recorded in rat sdDRG neurons, following two activation voltage protocols, aiming at evoking two types of currents: Total (INa TOTAL) and TTX-resistant (INa TTX-R) currents (Figure 4.15A). Despite an analogous pool of command pulses, ranging from -50mV up to +40mV, the differentiation observed between both protocols relies on the voltage potential of the pre-pulse applied to the resting holding cell potential (-70mV). With a pre-pulse of -110mV one can record INa TOTAL, whereas at -50mV one can isolate INa TTX-R (Akopian et al., 1999; Wang et al., 2017). Figure 3.15A depicts an illustrative example of the whole-cell voltage clamp Na^+ currents recorded in this study with such protocols (see inset). Contrary to the results observed for K^+ currents, Na^+ currents were only taken at the peak (INa peak), as a measure of the current amplitude of the fast spontaneous decay current, described by one exponential, figure 3.7 (methods, for more information). Current amplitude was analyzed through a normalization of the cell capacitance values (pA/pF), measuring the cell membrane size (1μF – 1cm2;), with the consequent I-V relation-ship curve (Figure 4.15B). Afterwards, conductance was determined from the current values (equation 3), normalized to the maximum value (G/Gmax), allowing the study of voltage dependence of activation, and plotted against the corresponding voltage potentials of the conditioning pre-pulse (Figure 4.5C).

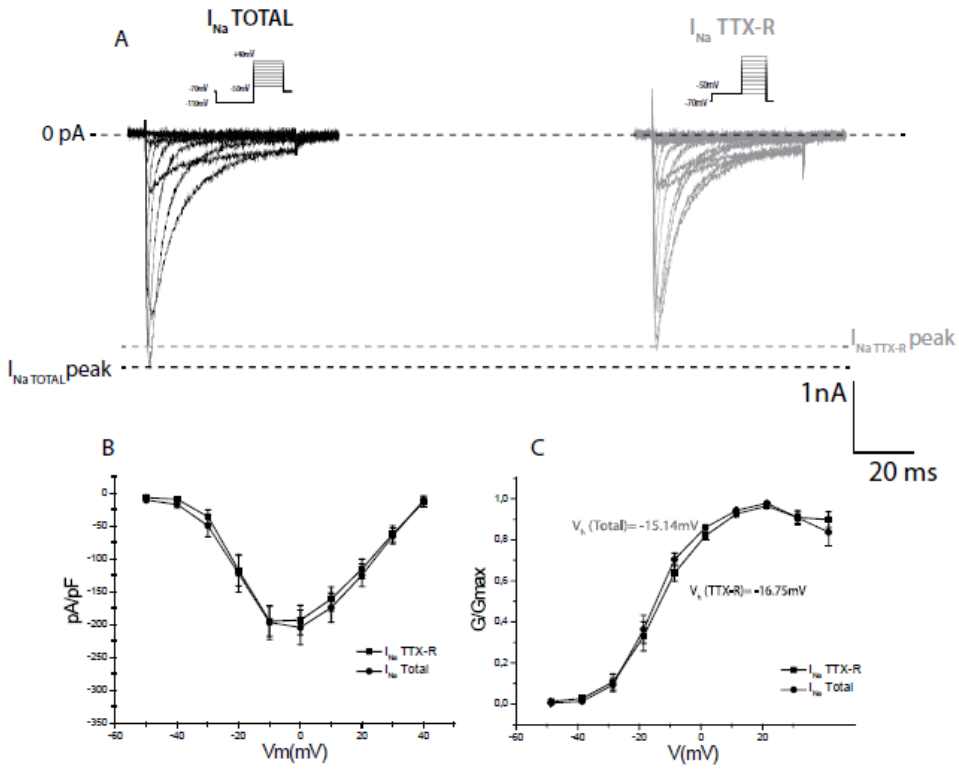

Figure 4.15 Voltage dependence of activation of voltage-gated sodium (Na^+) channels by whole-cell voltage clamp recordings in small diameter DRG neurons of naïve rats. Activation protocols: Whole-cell Na^+ currents were evoked by a set of depolarizing command pulses, from -50mV up to +40mV, in steps of +10mV, with a holding potential of -70 mV. A) At the same neuron, two protocols were used (see inset voltage protocols) to isolate TTX-resistant currents (I_{Na}TTX-R; right panel; pre-pulse at -50mV) from the Na^+ total currents (I_{Na}Total; left panel; pre-pulse at -110mV, to fully remove inactivation of the channels). The similar peak current amplitude observed for I_{Na}Total and I_{Na}TTX-R suggests that the Na^+ currents recorded are largely mediated by TTX-resistant channels. B) Peak current amplitude values were normalized to the cell capacitance (pA/pF), as a measure of current density. Mean pA/pF values were plotted as a function of voltage potential of the command pulses. C) Conductance values were normalized to the maximal value (G/Gmax) and data points of the activation curves

Figure 4.15A provides an illustrative visualization of the whole-cell Na^+ currents recorded in this study INaTOTAL (left traces) and INaTTX-R (right traces) peak values are similar suggesting that the currents evoked in both protocols might be mediated by equivalent Na^+ channels, namely those resistant to tetrodotoxin (TTX) drug, not presenting any statistical significance, with, however, a small nature of the experiment (p-value >0.05). This outcome can be supported by the mean current density values plotted in the I-V relationship curves (Figure 4.15B). Note that the Na^+ peak current density values retrieved from both protocols are superimposed. Finally, in Figure 4.15C, the results obtained from fitting the voltage dependence of activation curves with Boltzmann functions (equation 4), corroborate the results in which there is no considerable difference observed for the half-maximal activation potential for both current components (Vh (Total)= -15.43 ± 2.1mV and Vh (TTX-R) = -16.75 ± 1.74mV, n=6; see also table 4.4).

Table 4.4 Activation fitting parameters Vh (mV) and Vs (mV/e-fold), and corresponding *p*-values (Equation 4) for total Na^+ and TTX-R Na^+ currents of rat sdDRG neurons from naïve animals. Values are mean ± S.E.M.

	Voltage dependence of activation of sodium currents		
	V_h (mV)	V_s (mV/*e*-fold)	*n*
I_{Na}	-15.43 ± 2.1	6.92 ± 0.34	6
I_{Na}	-16.75 ± 1.7	6.25 ± 0.61	
P-value	0.7166	0.4779	-

4.5.2. Voltage dependence of Inactivation

The study of the voltage dependence of inactivation enables to assess the fraction of voltage dependent channels available to conduct at a range of membrane potentials. Whole-cell Na^+ channels inactivation was investigated by studying Na^+ currents evoked with a command pulse of +10 mV, preceded by a pool of conditioning pre-pulses, ranging from -120 m V to 0mV (in steps of +10 mV), from a holding potential set at -70 mV (Figure 4.16A).

Subsequently, the peak current amplitude values, were normalized to the maximum value (I/Imax), being the mean values plotted against the corresponding pre-pulse potentials (Figure 4.16B).

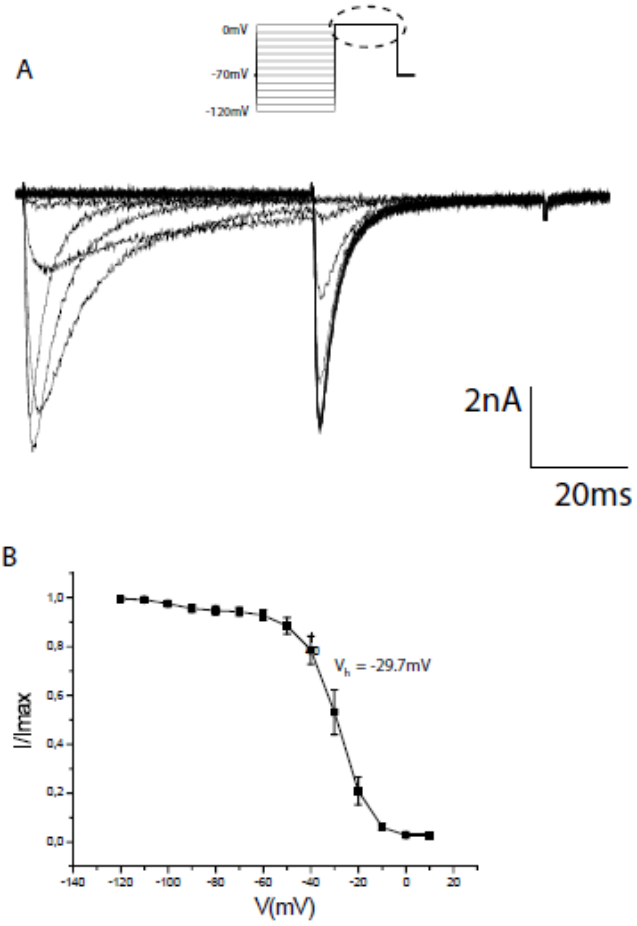

Figure 4.16 Voltage dependence of steady state of inactivation of voltage-gated sodium currents by whole-cell voltage clamp recordings in small DRG neurons from naïve rats. A) Illustrative example of current traces, evoked by a command pulse of 0 mV (see dashed circle on inset protocol), preceded by a pre-pulse of depolarizing steps, ranging from -120mV up to 0mV, in steps of +10mV, from the holding potential set at -70mV. B) Mean peak Na^+ current obtained in the test pulse normalized to the maximum value (I/Imax) as a function of pre-pulse potentials. The steady state inactivation curve was fitted with equation 4 (Vh = −29.7 mV, n=5). Error bars are ± SEM values.

Figure 4.16A exemplifies the Na^+ currents of a rat sdDRG neuron, detailed in the present study. The voltage dependence of the steady state inactivation was studied by plotting the peak current amplitude to the maximal (I/Imax) against the pre pulse voltage potential, fitting the respective inactivation curves with single Boltzmann function (equation 4). The parameters of the inactivation curves are as follows: mean half-maximal inactivation potential (Vh = -29.48 ± 2.52 mV), and mean slope constant of inactivation (Vs = 5.76 ± 0.19 mV/e-fold, n=5; see Table 4.5).

Table 4.5 Steady state inactivation fitting parameters Vh (mV) and Vs (mV/e-fold) (equation 4) for rat sdDRG neurons isolated form naïve animals. Values are mean ± S.E.M.

	Voltage dependence of inactivation of sodium currents		
	V_h (mV)	V_s (mV/*e*-fold)	*n*
I_{Na}	-29,48 ± 2,52	5,76 ± 0,19	5

4.6. Neuronal bioactivity – Effect of S4U1 on Na^+ currents

The bioactivity of S4U1 over Na^+ currents was pursued by following the same experimental procedure developed for K^+ currents. In that sense, this part of the results section analyses the Na^+ current functional expression, the voltage dependence of activation and the voltage dependence of steady state of inactivation of Na^+ currents, before and during the application of S4U1.

4.6.1. Inhibition of Na^+ currents

Firstly, to study the effect of S4U1 on Na^+ current inhibition, an activation voltage protocol with a single command pulse at 0mV, preceded by a pre-pulse at -110mV (from a holding potential of -70mV), was applied. This permitted a simplified view of the current inhibition in the presence of S4U1. This protocol was repeated, in intervals of 30 s, until the stabilization of peak Na current amplitude (visually settled), which was usually ensured after 5min without current run-down. At this stage, S4U1 was continuously superfused to the neurons, at two different concentrations (10 and 20 μg/mL) each time, under constant flux. Peak Na^+ current amplitude values were normalized to the maximum values (I/Imax) and plotted against time (min) (Figure 4.17A).

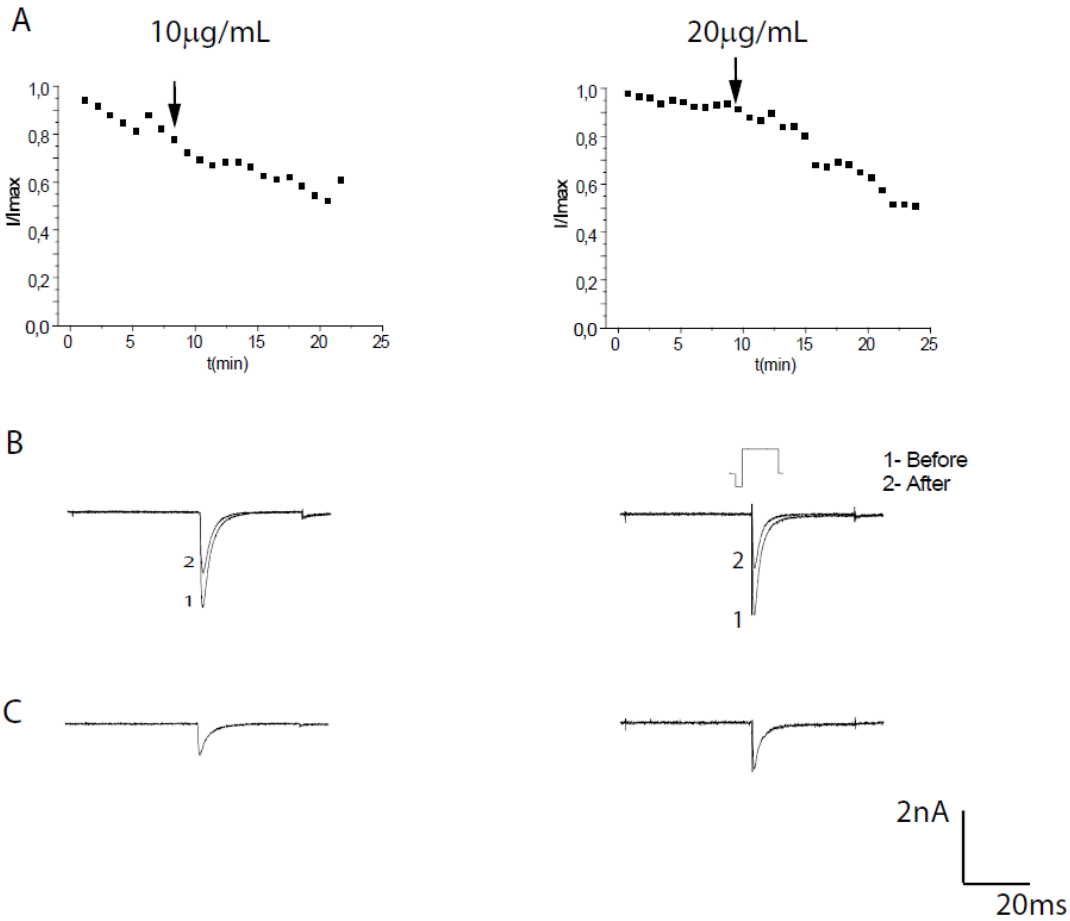

Figure 4.17 S4U1 decreases whole-cell Na^+ current amplitude upon the application of S4U1 (pointed by the arrow). A) Time-course illustrative examples of the effect of S4U1 over I_{Na}. Peak current amplitude was normalized to the maximum value (I/Imax) and plotted as a function of the total effect time. Arrows indicate the beginning of the superfusion with S4U1, at two different concentrations (10µg/mL and 20µg/mL). B) Respective whole-cell Na^+ currents before (1) and after (2) superfusion with S4U1. Na^+ currents were evoked by a depolarizing command pulse to +0mV, preceded by a hyperpolarizing pulse to -110mV. Holding potential was set at -70mV (see inset). C) Current traces sensitive to the effect of S4U1, resulting from the subtraction 'trace 1 - trace 2' (in B).

Figure 4.17A illustrates the inhibition of peak Na currents analyzed in two single neurons, each subjected to different S4U1 concentrations. The examples illustrate an increasing effect of S4U1 along the concentrations used. At 10µg/mL S4U1 provoked a current inhibition of 35%, and around 50%, at 20µg/mL. A current run-down, observed for the example taken for 10µg/mL, hinders a straightforward calculation of the current inhibition. However, one might assume that the highest effect of S4U1 was observed at 20µg/mL. This result is visually demonstrated in the respective current traces, before and after S4U1 superfusion (Figure 4.7B). The resulting subtraction traces were then presented to compare the amplitude of current sensitive to S4U1 effect (Figure 4.17C). The sensitive current assigned to the neuron superfused with 20µg/mL showed the highest current amplitude. The individual percentage inhibition values of all experiments are depicted in Figure 4.18. Notwithstanding the small sample size, it seems that S4U1 varies in a dose-dependent manner. Altogether, these results led me to select the

concentration of 20µg/mL to further investigate the effect of S4U1 on the voltage dependence of activation and inactivation of Na^+ currents.

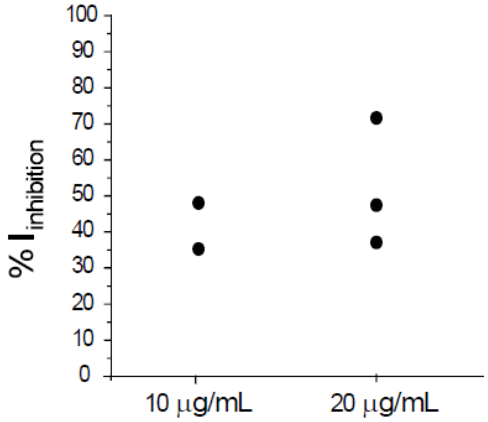

Figure 4.18 Effect of S4U1 over I_{Na}. Individual Na^+ current inhibition percentage values, obtained for the concentrations used: 10µg/mL (n=2) and 20µg/mL (n=3).

4.6.2. Voltage dependence of Activation

The study of the effect of S4U1 over the voltage dependence of activation was conducted by evoking whole-cell total Na^+ currents with the voltage protocol previously used in the left panel of figure 4.15A (Figure 4.19 A). Mean peak currents amplitude values were normalized for the cell capacitance (pA/pF) and plotted against voltage (I-V) (Figure 4.19B). Subsequentially, mean peak currents were converted into conductance(G), using equation 3, normalized to the maximum value (G/Gmax), and plotted against the command pulse voltage potentials, to obtain the activation curves (Figure 4.19C).

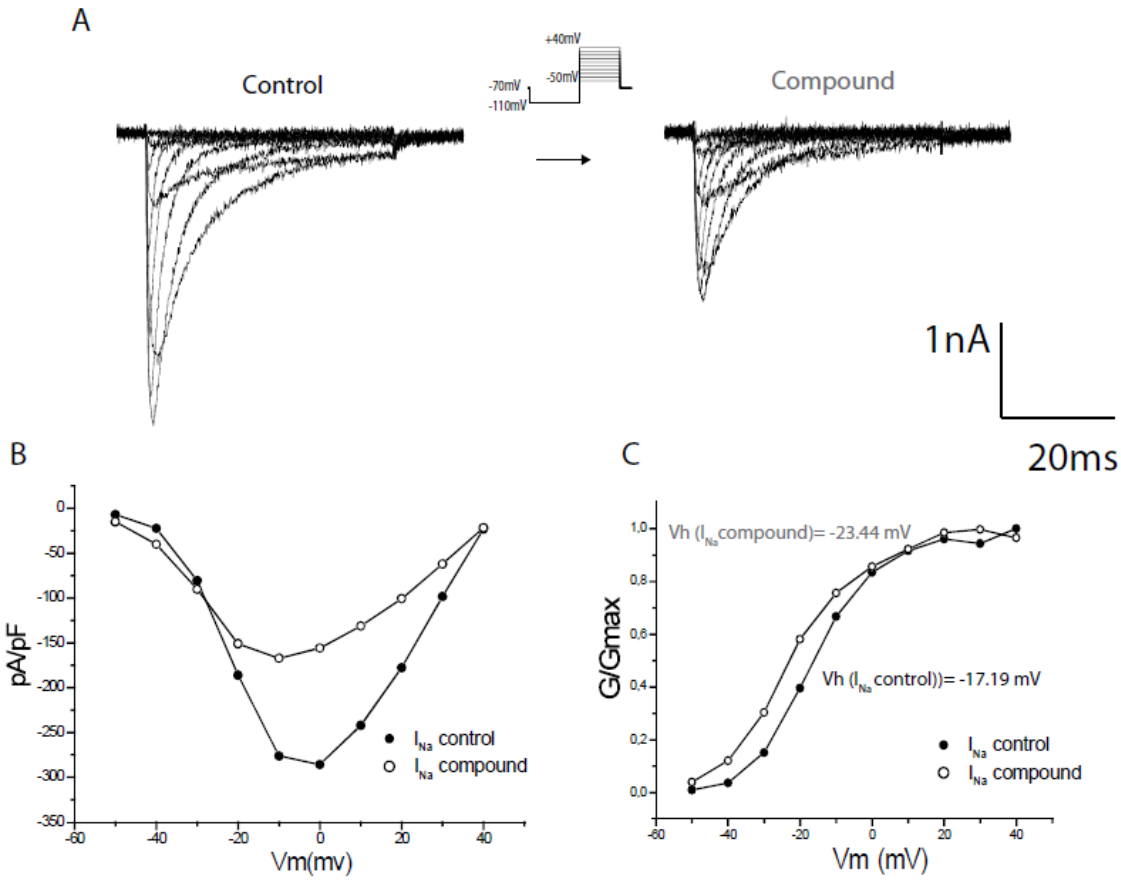

Figure 4.19 Effect of 20µg/mL S4U1 over the whole-cell Na^+ total currents of acutely isolated rat DRG neurons. A) Representative whole-cell voltage clamp Na^+ currents, recorded in the absence (control, left traces) and in the presence (compound, right traces) of S4U1, were evoked in series of depolarizing command pulses (48 ms in duration), in steps of 10 mV, from −50 mV to +40 mV, following a hyperpolarizing conditioning pulse at −110 mV (59ms in duration). Holding potential was set at −70 mV. Traces depict a decrease in peak Na^+ current amplitude in a neuron submitted to the application of S4U1 at 20µg/mL. B) I–V curves related to mean peak Na^+ current normalized to cell capacitance (pA/pF). Note the reduction of mean peak current density in the presence of the compound (open circles, n=2), when compared to control neurons (filled circles, n=2). C) Conductance values were normalized for the maximal response (G/Gmax) and the respective mean values were plotted against the pulse command potentials. Lines in the activation curves (C) are the solution of equation 4 (Vh control = -17.19mV and Vh compound = -23.44mV).

Figure 4.19A shows the whole-cell current traces recorded in a single neuron before and after the application of S4U1, (control; left panel, and after compound; right panel), with a 20ug/mL concentration. The reduction of the peak current amplitude is observed on the I-V curve (Figure 4.19B). At 0mV, the mean current density values differ as follows: -285.9 pA/pF and -155.84 pA/pF, for neurons in the absence and presence of S4U1, respectively. This small difference appears to be not significant. Also, it is important to take into consideration the small sample size (n=2) The Vh values retrieved from fitting the activation curves (Figure 4.19C) with a Boltzmann function may unravel a slight hyperpolarizing shift of ~6mV, assigned to the influence of S4U1. The individual Vh values, taken for every S4U1 compound concentrations tested, are quantified in Figure 4.20. Overall, these results suggest S4U1 influences the voltage dependence of activation of Na^+ currents, by show a small shifting the

opening of the channels towards more hyperpolarized potentials, however requiring further investigation.

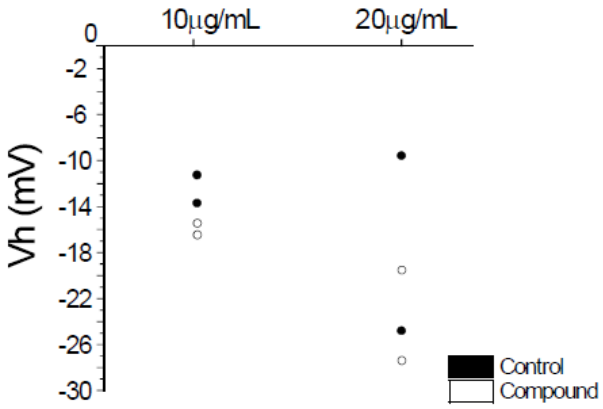

Figure 4.20 Influence of S4U1 on half-maximal activation voltage (V_h) of Na^+ total currents. Individual Vh values obtained before (control; black circles) and after (compound; white circles) application of S4U1 at 10 µg/mL (n=2) and 20µg/mL (n=2).

4.6.3. Voltage dependence of Inactivation

The influence of S4U1 upon the steady state inactivation of Na^+ channels was studied by evoking currents that followed a double pulse inactivation protocol with a command pulse of 0mV, and conditioning pre pulses ranging from -120mV until 0 mV, in steps of +10mV, with a holding potential set at -70mV. The voltage dependence of inactivation was studied at the beginning (peak current) of the command pulse (Figure 4.21). INa amplitude values were normalized for the maximum (I/Imax) and subsequent mean values were plotted against the voltage potentials of the conditioning pre pulse. The inactivation curves were fitted with a single Boltzmann function (equation 4) (Figure 4.21B).

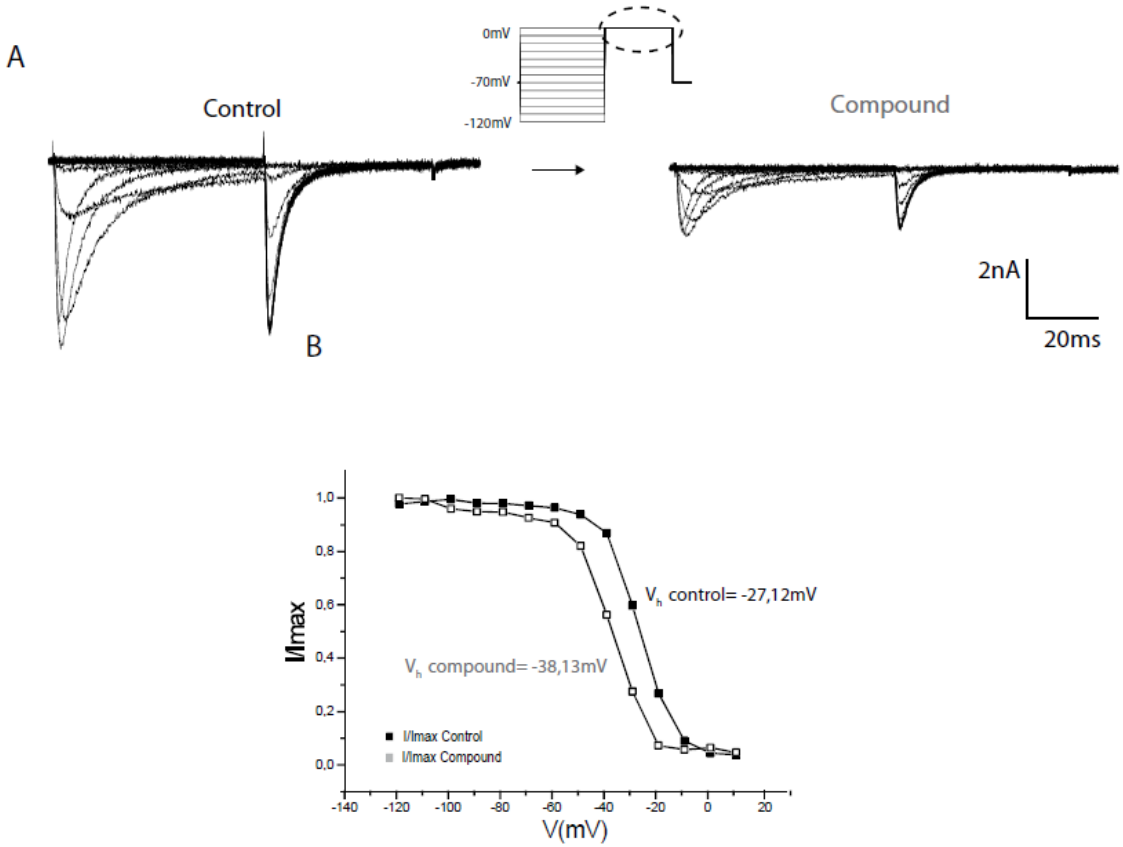

Figure 4.21 Influence of S4U1 on the voltage dependence of steady state of inactivation of whole-cell Na^+ current. A) Illustrative current traces recorded in rat DRG neurons, in the absence (control, left traces) and presence (compound, right traces) of 20µg/mL S4U1, were evoked as explained in figure 3.16 (see inset). B) Peak current amplitude values were normalized to the maximum current (I/Imax) and the respective mean values were plotted as a function of the pre-pulse potentials. The inactivation curves were described by a Boltzmann function (equation 4; Vh control =-27.12 mV – filled squares -, n=2; Vh compound = -38.13mV – open squares -, n=2).

Figure 4.21A presents an example of sodium current traces, recorded from an individual cell, before and under the effect of 20ug/mL S4U1. The presence of the compound led to a reduction of the peak current amplitude, and, also, to a hyperpolarizing shift of about 11mV in the inactivation curves. The Vh values obtained from each individual cell, before and after the application of 10µg/mL and 20µg/mL S4U1 (Figure 4.22), indicate that the fraction of Na^+ channels available to respond to activation at a given membrane potential is decreased upon the effect of S4U1. Nevertheless, as in the activation process, few considerations can be drawn from these results as the sample size of these experiments are too small. Nevertheless, there is enough suggestion that demand further research.

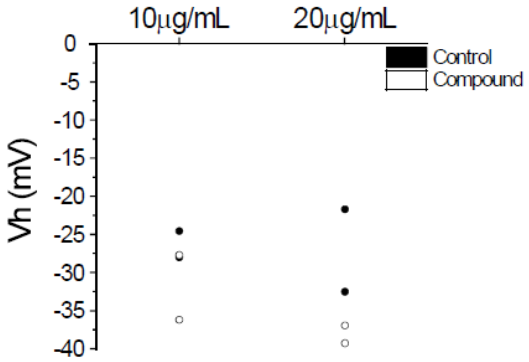

Figure 4.22 Influence of S4U1 on half-maximal inactivation voltage (V_h) of Na^+ total currents. Individual Vh values obtained before (control; black circles) and after (compound; white circles) application of S4U1 at 10 µg/mL (n=2) and 20µg/mL (n=2).

4.7. MTS experiments evaluation

The MTS method was carried out with the intent of determining possible toxic effect associated with S4U1. 96-well plates were used to evaluate S4U1 in an increasing range of concentrations (Merlin et al., 1992; O'Toole et al., 2003). In this study, two different human cell lines were used: MRC-5, a cell line of human fibroblast adherent cells derived from 'normal' lung tissue, in order to determine any noxious effect on the metabolic action of the upper respiratory cells, and Melanoma A2058, a cell line from human skin adherent cells derived from metastatic site, allowing also the knowledge of toxic effects on epithelium cell lines. The results concerning cell survival are shown in figure 4.23 (cell line MRC-5) and figure 4.24 (A2058 cell line).

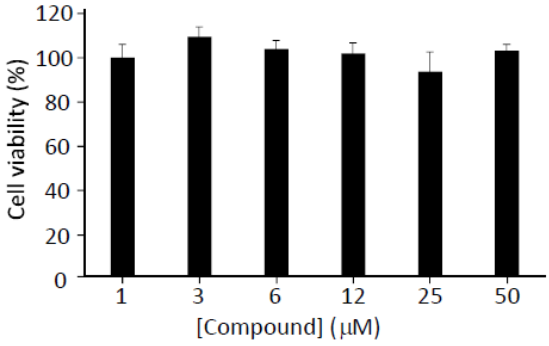

Figure 4.23 MTS assay to measure viability of MRC-5 cells after application of S4U1 at 1, 3, 6, 12, 25 and 50 µM. As presented the results show no changes in cell viability, with any of the doses used, with a high percentage above 90% in MRC-5 model cells (n=3 for each sample concentration). Error bars are ±S.E.M.

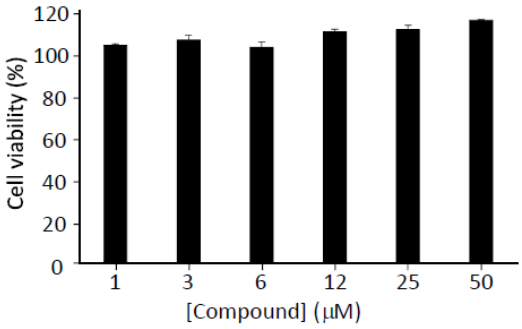

Figure 4.24 MTS assay to measure viability of A2058 cells after application of S4U1 at 1, 3, 6, 12, 25 and 50 µM. As presented the results show a clear cell viability with a high percentage above 90% in A2058 model cells (n=3 for each sample concentration). Error bars are ±S.E.M.

From the data presented in the graphs above (Figure 4.23 & 4.24), both in MCR-5 and A2058 model cells, one can infer that the metabolic activity of both cell lines does not suffer any variation even for the highest compound concentration tested. Therefore, S4U1 does not seem to induce any noxious effect over these cell lines, more specifically over the respiratory system and epithelium, envisaging a possible application of S4U1 over the skin. Complementarily, a similar method was applied on neonatal (P2-3) cardiac cells, determining levels of toxicity in cardiomyocytes from three different samples: negative control of DMSO, S4U1 purified fraction and S4U1 impure fraction, both with (50 mg/mL) (Figure 4.25).

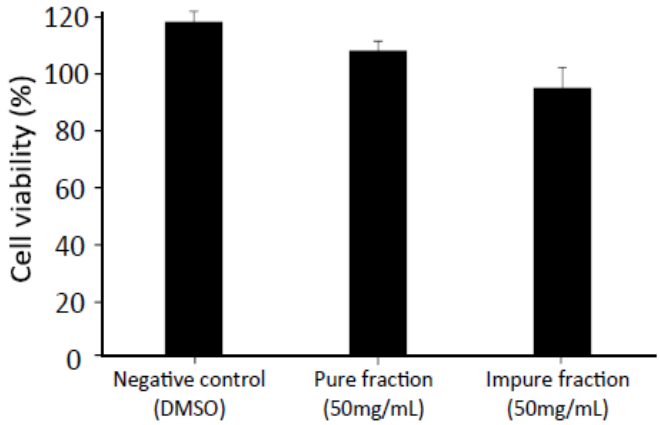

Figure 4.25 In vitro MTS assay to measure viability of cardiac cells upon application of a pure and impure samples of S4U1, at 50µg/mL, and DMSO, as a negative control. The results show S4U1 did not exert any toxicity over cardiomyocyte model cells used. Error bars are± S.E.M.

Figure 4.25 illustrates the MTS viability tests done in cardiac cell models. The similarity observed between the mean percentage values of cell viability obtained for negative control (100% cell

survival) and remaining S4U1 (pure and impure) samples determine that S4U1 do not cause cardiomyocytes death at a concentration of 50mg/mL. Furthermore, the results attained for the pure and impure fractions are highly relevant as they confirm the importance of S4U1 compound in the overall cell safety conditions.

4.8. *In vivo* testing

The result of the toxicity evaluation tests led me to take a step forward in my thesis project, as opened a possibility of administering S4U1 in laboratory animals. The next and last stage of this work presents the preliminary results that might confer to S4U1 potential analgesic properties, envisaging the possibility of developing a drug-like molecule.

With the intent of determining the possible analgesic effect of S4U1, *in vivo* testing was carried out inducing a CCI pain model on two individual rats, procedure carried out by certified operators (SPCAL). The von Frey monofilaments (vFF) were preferred as the reference method for an indirect pain evaluation, as hypersensitivity to mechanical stimuli is a readout common in pain syndromes. The development of mechanical hypersensitivity (here termed 'pain level' for simplicity) endured over a span of 35 days. Once a week, the 'pain level' was assessed with the vFF (Figure 4.26 Ai and Bi). On the 35th day of the pain model, S4U1 was intravenously injected in animals and the ease of pain was addressed by calculating the percentage of maximum possible effect (%MPE) of the compound over the ipsilateral (injured) leg. The recovery of the injured leg was compared to the withdrawal threshold scores registered for contralateral (non-injured) leg. High %MPE values mean that ipsilateral leg threshold levels are close to the ones verified for contralateral leg. Such conditions give a good indication of S4U1 as a potential analgesic drug. The data points in Figure 4.26Aii and Bii relate to the assessment of pain levels with vFF after the administration of S4U1, every 15 min, within the first hour, and every 30min, until reaching 120min.

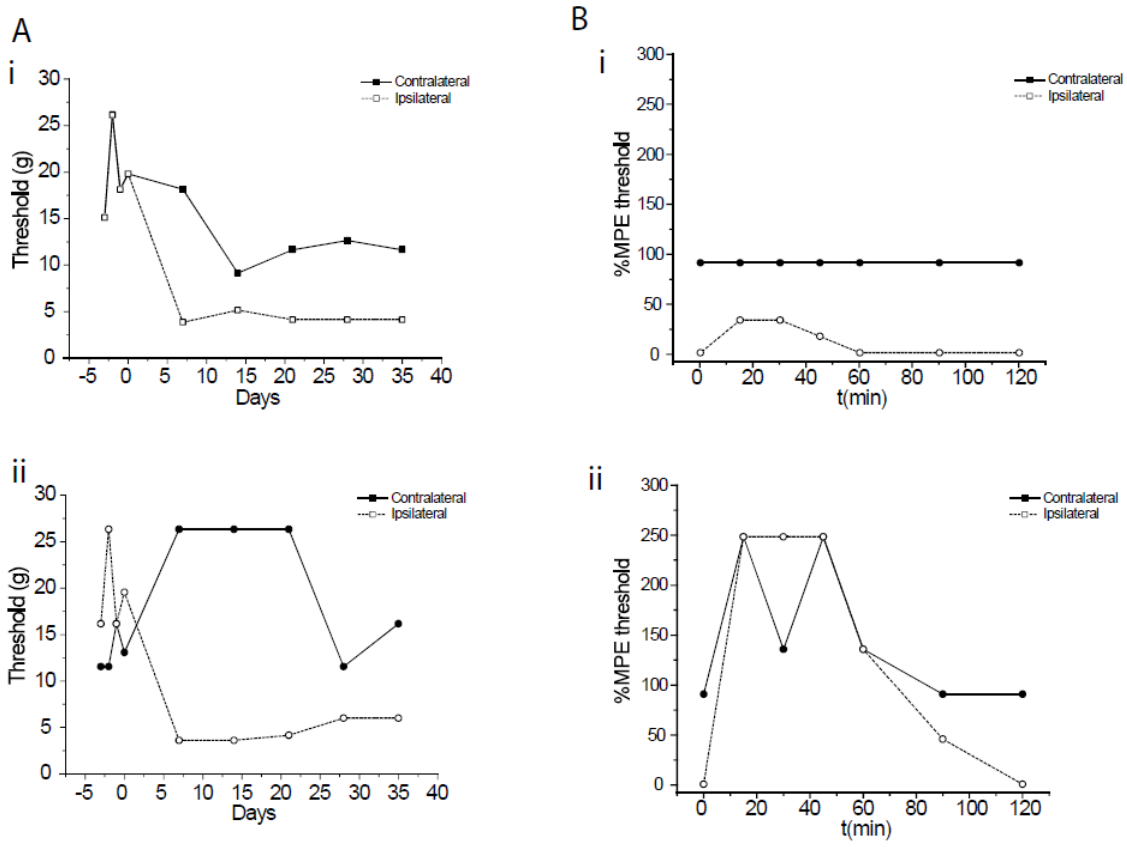

Figure 4.26 Sensitivity to mechanical stimulation as a measure of hyperalgesia in CCI pain models with further analysis of the S4U1 potential analgesic effect. Two rats were subjected to CCI of the sciatic nerve (A and B). A) after CCI surgery, pain threshold was established on the right paw (ipsilateral, injured leg) and on the left paw (contralateral, non-injured leg), throughout a period of 35 days. The withdrawal threshold (defined as the weakest monofilament (g) that induced a pain behavior in rats) of contralateral paws (filled squares), ipsilateral (open squares) from pain model rats are presented against the days after injury. B) Once determining a stable withdrawal threshold on the ipsilateral paw, S4U1 was intravenously administered at a concentration of **10 ug/mL,** that corresponds to a dose of 0,6 mg/kg. The percentage of Maximum Possible Effect (%MPE; Equation 8) was used as an indicator to evaluate the efficiency of the S4U1 as a potential analgesic drug. In Bi) the analgesic effect of S4U1 lasted for 60min and reached 40% MPE value 15 min after the administration of the compound. In Bii), despite the unsteady mechanical sensitivity levels observed on the contralateral paw, S4U1 effect on the ipsilateral paw lasted for 120min, with higher %MPE values, reaching a peak 45min after the administration of S4U1.

Figure 4.26 shows the effect of 0.6mg/Kg S4U1 administered into two individual rats under chronic pain conditions. In Figure 4.26Aii the analgesic effect of S4U1 lasted for 60min and reached 50% MPE value 30min after the administration of the compound. In figure 4.26Bii, despite the unsteady mechanical sensitivity levels observed on the contralateral paw, S4U1 effect on the ipsilateral paw lasted for 120min, with higher %MPE values, reaching a peak 45min after the administration of S4U1. The results suggest S4U1 contains analgesic properties. However, there results lack statistical relevance due to the small number of experiments involved.

5. Discussion

The project of the present thesis fits well within the scope of the Blue Biotechnology research field, aiming at further investigating the potential of marine sponges as important source of new lead molecules for treatment of unmet medical needs (Hentschel et al., 2003). The main goal of the study was to explore the potential biotechnological value of secondary metabolites from marine sponges sampled off the coast of Sagres, Portugal. The biological activity of these metabolites was tested from a neuronal activity perspective, by studying their effect over the functioning of voltage-gated potassium (K^+) and sodium (Na^+) channels encountered at the surface of rat small diameter dorsal root ganglion (sdDRG) neurons. Such ionic currents are relevant for Chronic Pain. The results confirmed the existence of a fraction (here termed 'S4U1'), purified from a crude extract of a marine sponge, which embodies compound(s) that disclose(s) neuronal bioactivity properties with a translational potential analgesic value. The results here discussed envisage the possibility of developing a drug-like molecule for the treatment of chronic pain.

Given the multidisciplinary scientific approach of the present work, this discussion will be staged into two major themes: biotechnology production and biological activity assessment. The former merges 1) the maritime prospection inside the Cave 'Cathedral', off the coast of Sagres, and 2) the extraction and isolation of the compound of interest (S4U1). The latter includes 1) S4U1 bioactivity testing done on K^+ and Na^+ currents of sdDRGs, 2) the toxicity assessment of S4U1 on animal and human cell models and 3) the potential analgesic effect evaluation in *in vivo* chronic pain rat models.

This thesis gathers a series of experimental procedures, since the sample collection until the bioactive testing in the whole animal. An attentive and rigorous experimental planning was required to minimize the underlying risks associated with the goal of this study. The first stage of the present study involved the diving session in which two sponges (designated as 'grey sponge' and 'black sponge') were collected from the "Cathedral" Cave, in Sagres, southwest coast of Portugal, at depths between 9 and 12 meters. The *underwater drug screening* methodology developed and practiced by the host company, based on ecological knowledge of the marine species found at the sea of Sagres, is perceived as

an important factor to the success rate of discovering bioactive molecules. Indeed, previous research done in that specific diving site had already led to the discover of secondary metabolites containing bioactive properties. This kind of knowledge was important for the development of the work here presented. The following steps comprised the biotechnological extraction of the secondary metabolites. Given the natural low abundance, in weight, of these chemical entities within sponges (it is estimated that sponges have less than 0.4% of secondary metabolites in dried weight (Bayona et al., 2018), two extraction methods were used to optimize the quantity of crude extracts retrieved from the grey sponge, the chosen one to be processed, due to its analogy to previous sponges studied in the host company. maceration and total extraction (percolation) methods are described in the literature as box standard techniques to isolate extracts from marine sponges. Here, the maceration method presented higher extraction yields (16%, as opposed to 10% obtained from the total extraction method), which can be explained by a) the combination of ethanol 96% and H2O (3:1) solution used, allowing an ampler polarity range extraction, when compared to a solvent only containing ethanol (Cheng et al., 2021), and b) mechanical procedure imposed by the lodestone. Afterwards, the molecular constituents of the resulting crude extracts were separated into different fractions according to their chemical polarity. For such, a mobile phase consisting of 5 different solvents was sequentially added into a reverse phase chromatography column. Thus, the elution of the crude extract molecules followed a polarity gradient, starting from the most polar and ending with the least polar solvent, forcing collection of the loaded sample into 5 different fractions. Two types of columns were used in this study considering the composition and manufacturing of the stationary phase: a homemade column packed with poly (styrene-co-divinylbenzene) resin and premade silica-based bonded cartridge columns (Sep-Pak® C18 Cartridges). The HPLC chromatograms of the fractions obtained from premade cartridges columns showed a greater resolution of the peaks, implying an accurate separation of the molecular compounds. Additionally, the usage of a prepacked column withdraws the error linked to the manual packing of the column, which may account to the reproducibility assigned to 'fractionation 2' method (see Figure 3.2). On the contrary, in what concerns 'fractionation 1' method, the ill-defined peak separation and low reproducibility shown between separation procedures might be associated with poorly packed homemade columns. Accordingly, these results confirm column packing in chromatography as a critical step in fractionation procedure.

The five collected fractions were screened against a platform of Na^+ and K^+ channels of rat sdDRG neurons dissected from naïve animals to test the putative bioactivity of the respective prominent peaks. By using electrophysiological patch-clamp technique, under whole-cell voltage clamp configuration, all fractions were tested to determine their effect on Na^+ and K^+ currents. The greater bioactivity was attributed to the fraction MeOH/H2O (7:3), as the one that provoked the highest current inhibition. The HPLC chromatogram of this fraction revealed the presence of a standout peak of interest, well defined and with high absorbance intensity. Assuming this peak contained the compound(s) accounta-

ble for Na^+ and K^+ current inhibition, it was essential to isolate it to refine the purity grade. The purification process was attained through a HPLC run with fraction MeOH/H2O (7:3), in which the majority target peak was collected in a narrow retention time interval around 30min. At the end, a purified peak sample (here termed 'S4U1') was obtained with ~99% purity grade. The identification, isolation and collection of the target peak was an important breakthrough of this thesis, as it permitted to establish a straightforward cause/effect interpretation of the results. In other words, every experimental response variation brough up by the presence of S4U1 could be solely assigned to the action of S4U1.

Before studying S4U1, an electrophysiological characterization of whole-cell voltage-gated Na^+ and K^+ channels of naïve rat sdDRG neurons was performed. The currents mediated by these channels are of the utmost importance, as they are involved in the initiation, propagation and firing frequency of APs (Hille, 2001; Kress & Mennerick, 2009). Hence, any small variation over the features of these currents, either exclusively or cumulatively, has the potential to affect the membrane excitability, which, ultimately, impacts the neuronal functioning, thus, interfering with the signal propagation and communication between neurons. In the context of the neurons used in the present study, the relevance is associated with peripheric nociception control, hence, 'pain control'. Here, activation and inactivation processes of whole-cell currents were analyzed in sdDRG neurons from the pain-sensing unmyelinated C-fibers of naïve animals. This neuronal categorization was ensured by the small mean cell capacitance values of the neurons patched in this work (9.5 ± 3.1 pF; Gentet et al., 2000). The biophysical properties of K^+ and Na^+ currents were studied by fitting the respective activation and inactivation curves with a Boltzmann function which describes the distribution of the voltage-gated ion channel populations between non-conducting and conducting states (Sontheimer & Ransom, 2002; Bezanilla & Villalba-Galea, 2013).

In what concerns whole-cell K^+ currents, the analysis was separately done in two time points of the traces: at the beginning of the command pulse, as a measure of the fast, transient A-type K^+ currents (IA), and at the end of the pulse, in a steady state condition of the current trace, as a measure of delayed rectifier, slow inactivating potassium currents (IK). The activation curves of both types of K^+ currents were described by one Boltzmann function and almost overlayed. However, IA presented slightly higher voltage sensitivity (smaller mean Vs value; see Table 3.2), neatly supporting a faster current activation process (Standen & Stanfield, 1978; Costa et al., 1994). The voltage dependence of steady state of inactivation analysis followed the double-pulse protocol originally devised by Hodgkin and Huxley (1952), permitting the assessment of the fraction of channels available to respond to activation. By normalizing the current values for the maximal response, we can assess the extension of inactivation that is happening at the equilibrium (steady state) of the pre-conditioning pulse. The inactivation curves were either fitted by a single or a double Boltzmann function. The presence of a biphasic response is consistent with either the expression of different types of channel population (fast and slow- inactivating) or with more than one inactivation process for a single channel population (Ribeiro & Costa, 2000; Godazgar et al., 2018). In this case, the patch clamp configuration used (whole-cell) implies that there

must have been a recruitment of more than one type of K^+ channel population, each one of which with different sensitivities to voltage in terms of inactivaction.

Regarding whole-cell Na^+ currents of control rat sdDRG neurons, the analysis was performed only at the beginning of the test pulse, as a measure of the peak current. The striking similarity observed between the mean peak current density values obtained for total (INaTOTAL) and TTX- resistant (INa TTX-R) Na^+ currents clearly indicates that Na^+ currents here studied are largely attributed to TTX-R sodium currents. This conclusion is reinforced by further results: a) the mean half maximal activation values of INaTOTAL and INa TTX-R are superimposed, and b) the mean Vh inactivation value calculated (Vh = -29.5mV) corroborates well with the values described in the literature for TTX-R channels (Vh ~ -30mV; Cummins & Waxman, 1997; Akopian et al., 1999; Renganathan et al., 2001; Brien et al., 2008; Mischel et al., 2018;). This stack of evidence attests to the fact that sodium currents recorded in the studied neurons are largely mediated by TTX-R channels, pointing out to a large expression of these ion channels on the surface of the patched neurons, which, once again, is aligned with previous reports mentioning DRG neurons, particularly C-type neurons (the cell model under study on this thesis), as unique in expressing high levels of TTX-R Na current (Gold, Reichling, et al., 1996; Cummins & Waxman, 1997; Shah et al., 2010). The molecular entities responsible for the expression of these TTX-resistant currents are the isoforms Nav1.8 and Nav1.9 (Hong & Wiley, 2006;Ma et al., 2019). However, one may assume that the TTX-R currents recorded in this study are mainly supported by Nav1.8, as Nav1.9 is usually linked to persistent currents (Hong & Wiley, 2006; Israel et al., 2017), which were not detected in this dissertation.

As stated above, whole-cell voltage-gated K^+ and Na^+ currents of naïve rat sdDRG neurons were used as a matrix to explore the potential biotechnological value of S4U1 in a context of neuronal activity. To ensure the complete understanding of possible effects of the compound in those cell currents measured in sdGRG neurons, a dosage evaluation was conducted, firstly in K^+ currents, using 2, 10, 20 and 30µg/mL S4U1, aiming at determining the optimal bioactive effect concentration and, similarly, with 10 and 20µg/mL S4U1 for Na^+. For comparison, recordings before, during and after the application of S4U1 were carried out, therefore allowing a better understanding of its effect on K^+ and Na^+ currents present in cell membrane. The results concerning current inhibition showed S4U1 followed a dose-dependent manner effect. Still, this dose-response relationship study presented here contributed to the small sample size observed in most cases, which might explain the lack of statistically significant results concerning the effect of S4U1 either in activation or inactivation processes of both currents. Hence, any considerations towards the neuronal activity of S4U1 must be carefully undertaken as further tests are required for clarification. Notwithstanding, the results here shown clearly demonstrate S4U1 affected the biophysics of K^+ currents recorded and a suggestion of effect on Na^+ currents.

The individual analysis of IA and IK enabled me to assess whether and how S4U1 affected K^+ currents. By doing so, it was possible to anticipate on what type of K^+ channels the compound acted upon. Current density reduction was mainly observed in IK, which indicates a specific effect on slow

K^+ currents. Moreover, the currents sensitive to the effect of S4U1 display a rather slow decaying profile, with slow time constants of inactivation (see figure 3.7 C). Thus, the K^+ currents affected by S4U1 present slow kinetics of inactivation which is consistent with the results taken from the activation curves (the hyperpolarizing shift observed in the voltage dependence of activation is only significant for IK). In view of validating the biochemical target of S4U1, and thus exploring further its biotechnological potential, this result enables to focus the upcoming stages of investigation in a narrower set of K^+ channels.

The data here also suggested that S4U1 possibly affect the conductance of Na^+ currents, by decreasing the peak current density. The presence of S4U1 reduced the influx of Na^+ ions through the pore of the channels. Additionally, S4U1 provoked hyperpolarizing shifts of the activation and inactivation curves.

By combining the effect of S4U1 over K^+ and Na^+ currents one must draw a conclusive statement: S4U1 affects membrane excitability of sdDRG neurons. These cells are primary sensory neurons that convey nociceptive pain signaling to the spinal cord, from where second order neurons carry the same pain signals to the brain, where occurs the pain perception and consequent physiological response (Marchand, 2008; Garland & Ph, 2013). Hence, considering the importance of sdDRG cells on nociception pain transmission phenomena, I sought for scaling up S4U1 effect in a pathophysiological context, by administering it in animals under chronic pain conditions. Beforehand, cell viability assays were performed to study possible toxicity effects of S4U1 that could compromise the intravenous administration in animals. The results indicated S4U1 did not produce any toxic effects in lung and cancer human cell lines at a range of concentrations from 1μM to 50μM, also being innocuous when applied in *ex vivo* cardiomyocytes preparations, which ensured overall safety conditions for S4U1 to be tested *in vivo*.

In the last step of this dissertation, I intended to conduct a preliminary proof-of-concept study aiming at confirming the translational application of S4U1 in a context of chronic pain. The results show that S4U1 decreases pain sensitivity threshold in rats from a CCI pain model, thus, suggesting an analgesic effect. Once again, the sample size being too small (n=2), but consistent with the exploratory nature of this work, hampers a full comprehension of this analgesic effect. Nevertheless, as stated above, the data suggests an analgesic effect in chronic pain, as it is important to stress the fact that S4U1 was tested in day 35, after surgery (induction of the model). In rats, 21 days after nerve insult, it is considered Chronic Pain, which is believed to have a neurophysiological rational quite different from 'Acute Pain'. (Kuphal et al., 2007)

The results showed here demand further studies, namely increasing the sample size to obtain more robust results and conducting experimental procedures to elucidate the molecule liable for the modulation of neuronal excitability and reduction of pain levels. Despite these unsolved issues, the results presented here enable me to stress out some important considerations regarding the chemical characteristics and mode of action of this molecule. Firstly, the fractionation process gave insights into the polarity of the molecule of interest. Since it was eluted by a solvent in the middle of an increasing polarity gradient solvent scale, one can assume the molecule has amphipathic nature. Secondly, the

molecule of interest acts mainly upon slow inactivating K^+ currents and suggested possible effects on TTX-R (Nav1.8 and Nav1.9) Na^+ currents. Thirdly, the results observed for the viability tests indicate the non-toxicity safety measurements of S4U1 in a wide range of concentrations. These are very promising results in a perspective of drug development, as they mitigate the risk of S4U1 administration in rodents and humans. Finally, *in vivo* studies suggest an important clinical application of S4U1 in the chronic pain context, envisaging a potential analgesic effect of S4U1. Bridging the *ex vivo* and *in vivo* effects of S4U1, it is tempting to outline Nav1.8/Nav1.9 and IK conducting potassium channels as promising therapeutic targets for the potential analgesic role of the molecule of interest. In fact, Nav1.8/Nav1.9 is known for being a therapeutic target for chronic pain, given its essential role in mediating spontaneous activity in sensitized nociceptors (Dong et al., 2007; Daou et al., 2016).

This thesis arises from the combination of essentially three main scientific fields, namely marine biology, analytical biochemistry, and neurophysiology. The biotechnological value of a marine natural compound was demonstrated by assessment its effect over the functioning of potassium and sodium voltage-gated channels of rat sdDRG neurons. The modulation of neuronal activity through the alteration of membrane excitability, was translated into a potential analgesic effect, paving the way for developing a drug-like molecule for the treatment of chronic pain.

6. Conclusion

Analysis of the multidisciplinary methodologies associated with Blue Biotechnology studies was inherently studied throughout this present dissertation. For such, collected marine organism (Porifera) off the Coast of Sagres, south of Portugal, were hypothesized as possible sources of neuronal bioactive secondary metabolites. Subsequently, resorting to extraction methods and bio-guided fractionations procedures, the separation of the molecules was attained, and bioactive properties were investigated in a pain sensing cell model (sdDRG neurons). Furthermore, a detailed neuronal effect of the selected purified fraction (S4U1) in channels involved in ionic neuronal transmission (K^+ and Na^+) was assessed with patch clamp technique, under whole-cell voltage clamp configuration. Additionally, upon determining non-toxicity safety conditions in human cell lines and rat cardiomyocytes, a possible analgesic effect of S4U1 was accessed, testing S4U1 in *in vivo* surgical induced CCI pain rat model. Regarding the results obtained, subsequent conclusion arose:

6.1. Biotech procedure:

- Biotechnological value was found on marine derived molecules from sponges off the Coast of Sagres;
- Regarding the extraction protocols used, aiming for molecules separation from the sponge matrix - “Maceration” and “Total extraction”-, the former provided better extraction yield;
- With the intention of simplifying the extraction amalgamates, prepacked commercially available columns positively influence the efficiency of compounds separation, also contributing to reproducible results;
- Additionally, S4U1 might be an amphipathic molecule given the polarity nature of the fraction where S4U1 was embedded in upon elution through the chromatography column fraction (MeOH/H2O (7:3)).

6.2. Bioactivity:

Regarding the bioactive properties of S4U1 on potassium currents:

- S4U1 effect over current inhibition follows a dose-dependent fashion;
- Reduction of mean current density values, mainly of IK, suggests a specific effect on K^+ channels with slow kinetics of inactivation;
- Similarly, S4U1 significantly hyperpolarizes inactivation curves of potassium currents.

- Regarding bioactive properties over sodium currents:
- INa total currents are largely mediated by TTX-R channels, supposedly mainly by Nav1.8 isoform;
- Presence of S4U1 influences the reduction of mean current density values;
- S4U1 altered the voltage dependence of activation and inactivation by shifting both curves to hyperpolarizing membrane potentials;
- Concerning the effect of S4U1 on both currents, one may conclude that S4U1 modulates the neuronal excitability of rat sdDRG neurons from sensory C-fibers.

Toxicity

- MTS results indicate S4U1 does not produce any toxic effects in lung and human cancer cell lines, at concentrations ranging from 1 µM up to 50 µM;
- S4U1 does not negatively impact *ex vivo* cardiomyocytes, ensuring overall safety conditions for S4U1 to be tested *in vivo*.

In vivo

- S4U1 decreases pain sensitivity threshold in rats from CCI pain model, exhibiting potential analgesic effects.

7.
Future Prospects

The conclusion of my thesis brought up some questions and ideas that should be addressed in the future. Foremost, it subsists the sample size issue, specially verified on Na^+ currents in the presence of S4U1 and *in vivo* results. These results demand robustness which can be attained by increasing the sample size of the experiments. Doing so, the tendencies observed in this thesis might turn out statistically significant differences. Additionally, it would be interesting to repeat the electrophysiological analysis, this time, using sdDRG neurons from a CCI pain model (pain model cells), to address any intrinsic biochemical/molecular and electrophysiological variation and, subsequently, evaluate the effect of S4U1 on such environment. By comparing the results obtained from CCI cells with those presently reported (from naïve cells) one will be capable of responding to some important questions: What are the shared and specific biophysical mechanisms of Na^+ and K^+ currents between model cells? S4U1 effect potency is greater in any of the model cells? The magnitude of the shifts observed for activation and inactivation curves should be higher in any of the model cells? These and other questions need to be answered to better understand the molecular and electrophysiological profiles of the effect of S4U1 within a pathophysiological context, as opposed to a naive physiological condition. Other considerations will be useful for future work, as follows:

Extraction of the compounds from the organism matrix

There are a wide range of available new methods to acquire these metabolites, regarding pressurized and temperature control machinery, such as Microwave-assisted extraction (MAE) and ultrasound-assisted extraction (UAE), for example. Their utilization would probably allow a greater variety of compounds, therefore increasing the probability of discovering novel compounds that could be leading to the development of new pharmaceutical drugs.

Elucidation of the molecular structure of the compounds of Interest

From the methods used in this study it is only possible the collection and isolation of a purified fraction. However, to fully understand the therapeutical impact of the sample, posterior to the purification of the fraction, it should be done an identification of the molecular formula of the compound by resorting to spectroscopy techniques, such as Nuclear Magnetic Resonance and Mass Spectrometry.

Electrophysiological studies

As mentioned, from the present studies within this thesis, although positive results confirming the existence of bioactive compounds, there are some doubts regarding the significance of S4U1 effect, especially over Na^+ currents. Thus, expanding the experimental sample size of the studies would allow a precise understanding of the full effect of S4U1 on the currents. Moreover, the designing of new voltage clamp protocols would enable to better comprehend the influence of S4U1 over other biophysical processes, other than activation and inactivation here addressed. For example, it would be interesting to assess the deactivation and remove from inactivation as complementary processes of activation and inactivation, respectively. To confirm the neuroexcitability modulation outlined here for S4U1, one needs to study of the neuronal output of sdDRG neurons by running current clamp electrophysiological recordings. With this technique, it is possible to record APs and study the firing frequency of the neurons (number of AP's) as a measure of the neuronal activity.

In vivo testing

As regarded with the electrophysiological studies, there is a need to improve the number of experiments to achieve a viable conclusion. Nevertheless, such increase must be framed in a sustainable experimental design having in mind animal ethical issues. Moreover, different types of pain evaluation can be considered (other than Von Frey monofilaments), allowing a wider understanding of the possible analgesic derived from to the fraction. As an example, hot and cold plate analyses are a well-studied method used on neuropathic pain models which may bring interest, considering the analgesic potential of S4U1.

References

Acharya, D. U., Shekhar, Y. C., Aggarwal, A., & Anand, I. S. (1991). Lack of pain during myocardial infarction in diabetics -Is autonomic dysfunction responsible? *The American Journal of Cardiology*, *68*(8), 793–796. https://doi.org/10.1016/0002-9149(91)90657-7

Agarwal, A., Dong, Z., Harris, R., Murray, P., Parikh, S. M., Rosner, M. H., Kellum, J. A., & Ronco, C. (2016). Cellular and molecular mechanisms of AKI. *Journal of the American Society of Nephrology*, *27*(5), 1288–1299. https://doi.org/10.1681/ASN.2015070740

Ahimsadasan, N., Reddy, V., & Kumar, A. (2021). Neuroanatomy, Dorsal Root Ganglion. In *StatPearls*. StatPearls Publishing.

Akins, P. T., & McCleskey, E. W. (1993). Characterization of potassium currents in adult rat sensory neurons and modulation by opioids and cyclic AMP. *Neuroscience*, *56*(3), 759–769. https://doi.org/10.1016/0306-4522(93)90372-M

Akopian, A. N., Souslova, V., England, S., Okuse, K., Ogata, N., Ure, J., Smith, A., Kerr, B. J., McMahon, S. B., Boyce, S., Hill, R., Stanfa, L. C., Dickenson, A. H., & Wood, J. N. (1999). The tetrodotoxin-resistant sodium channel SNS has a specialized function in pain pathways. *Nature Neuroscience*, *2*(6), 541–548. https://doi.org/10.1038/9195

Austin, P. J., Wu, A., & Moalem-Taylor, G. (2012). Chronic constriction of the sciatic nerve and pain hypersensitivity testing in rats. *Journal of Visualized Experiments : JoVE*, *61*, 2–7. https://doi.org/10.3791/3393

Aziz, Q., Barke, A., Bennett, M. I., Benoliel, R., Cohen, M., Evers, S., Finnerup, N. B., First, M. B., Giamberardino, M. A., Kaasa, S., Kosek, E., Lavand'homme, P., Nicholas, M., Perrot, S., Rief, W., Scholz, J., Schug, S., Smith, B. H., Svensson, P., … Wand, S.-J. (2015). A classification of chronic pain for ICD-11. *Pain*, *156*(6), 1003–1007.

Babcock, D. F., Bosma, M. M., Battaglia, D. E., & Darszon, A. (1992). Early persistent activation of sperm K+ channels by the egg peptide speract. *Proceedings of the National Academy of Sciences of the United States of America*, *89*(13), 6001–6005. https://doi.org/10.1073/pnas.89.13.6001

Baron, M. J., & McDonald, P. W. (2006). Significant pain reduction in chronic pain patients after detoxification from high-dose opioids. *Journal of Opioid Management*, *2*(5), 277–282. https://doi.org/10.5055/jom.2006.0041

Baron, R. (2006). Mechanisms of disease: Neuropathic pain - A clinical perspective. *Nature Clinical Practice Neurology*, *2*(2), 95–106. https://doi.org/10.1038/ncpneuro0113

Basbaum, A. I., Bautista, D. M., Scherrer, G., & Julius, D. (2009). Cellular and Molecular Mechanisms of Pain. *Cell*, *139*(2), 267–284. https://doi.org/10.1016/j.cell.2009.09.028

Baskozos, G., Dawes, J. M., Austin, J. S., Antunes-Martins, A., Mcdermott, L., Clark, A. J., Trendafilova, T., Lees, J. G., Mcmahon, S. B., Mogil, J. S., Orengo, C., & Bennett, D. L. (2019). Comprehensive analysis of long noncoding RNA expression in dorsal root ganglion reveals cell-type specificity and dysregulation after nerve injury. *Pain*, *160*(2), 463–485. https://doi.org/10.1097/j.pain.0000000000001416

Bayona, L. M., Videnova, M., & Choi, Y. H. (2018). Increasing metabolic diversity in marine sponges extracts by controlling extraction parameters. *Marine Drugs*, *16*(10). https://doi.org/10.3390/md16100393

Becker, F. G., Cleary, M., Team, R. M., Holtermann, H., The, D., Agenda, N., Science, P., Sk, S. K., Hinnebusch, R., Hinnebusch A, R., Rabinovich, I., Olmert, Y., Uld, D. Q. G. L. Q., Ri, W. K. H. U., Lq, V., Frxqwu, W. K. H., Zklfk, E., Edvhg, L. V, Wkh, R. Q., …)2015. (ح, فاطمی. The COST Manual of Laboratory Animal Care and Use Refinement, Reduction, and Research. In *Syria Studies* (Vol. 7, Issue 1). https://www.researchgate.net/publication/269107473_What_is_governance/link/548173090cf22525dcb61443/download%0Ahttp://www.econ.upf.edu/~reynal/Civil wars_12December2010.pdf%0Ahttps://think-asia.org/handle/11540/8282%0Ahttps://www.jstor.org/stable/41857625

Bennett, D. L., Clark, X. A. J., Huang, J., Waxman, S. G., & Dib-Hajj, S. D. (2019). The role of voltage-gated sodium channels in pain signaling. *Physiological Reviews*, *99*(2), 1079–1151. https://doi.org/10.1152/physrev.00052.2017

Bennett, G. J., & Xie, Y. K. (1988). A peripheral mononeuropathy in rat that produces d... [Pain. 1988] - PubMed result. *Pain*, *33*, 87–107. http://dx.doi.org/10.1016/0304-3959(88)90209-6

Bezanilla, F. (2007). Voltage-Gated Ion Channels. *Biological Membrane Ion Channels*, 81–118. https://doi.org/10.1007/0-387-68919-2_3

Bezanilla, F., & Villalba-Galea, C. A. (2013). The gating charge should not be estimated by fitting a two-state model to a Q-V curve. *Journal of General Physiology*, *142*(6), 575–578. https://doi.org/10.1085/jgp.201311056

Bhattacharya, A., Wickenden, A. D., & Chaplan, S. R. (2009). Sodium Channel Blockers for the Treatment of Neuropathic Pain. *Neurotherapeutics*, *6*(4), 663–678. https://doi.org/10.1016/j.nurt.2009.08.001

Black, J. A., Liu, S., Tanaka, M., Cummins, T. R., & Waxman, S. G. (2004). Changes in the expression of tetrodotoxin-sensitive sodium channels within dorsal root ganglia neurons in inflammatory pain. *Pain*, *108*(3), 237–247. https://doi.org/10.1016/j.pain.2003.12.035

Blair, N. T., & Bean, B. P. (2002). Roles of tetrodotoxin (TTX)-sensitive Na+ current, TTX-resistant Na+ current, and Ca2+ current in the action potentials of nociceptive sensory neurons. *Journal of Neuroscience*, *22*(23), 10277–10290. https://doi.org/10.1523/jneurosci.22-23-10277.2002

Blunt, J. W., Carroll, A. R., Copp, B. R., Davis, R. A., Keyzers, R. A., & Prinsep, M. R. (2018). Marine natural products. *Natural Product Reports*, *35*(1), 8–53. https://doi.org/10.1039/c7np00052a

Brien, B. J. O., Caldwell, J. H., Ehring, G. R., Brien, K. M. B. O., Luo, S., & Levinson, S. R. (2008). *Sodium Channels Na v 1 . 8 and Na v 1 . 9 Are Expressed in the Retina*. *951*(October 2007), 940–951.

Buchanan, C. (2015). FUTURE OCEAN CHALLENGES FOR PORTUGAL. In *NEW CHALLENGES OF THE ATLANTIC An Approach from Portugal* (pp. 67–75). Institute of Social and Political Sciences of the University of Lisbon. https://doi.org/10.13140/RG.2.1.4065.6727

Buckton, K. S., Legon, A. C., & Millen, D. J. (1969). Microwave spectrum and structure of nitrosyl fluoride. *Transactions of the Faraday Society*, *65*, 1975–1984. https://doi.org/10.1039/TF9696501975

Campbell, J. N., & Meyer, R. A. (2006). Mechanisms of Neuropathic Pain. *Neuron*, *52*(1), 77–92. https://doi.org/10.1016/j.neuron.2006.09.021

Cao, Y., Jin, X., Huang, H., Derebe, M. G., Levin, E. J., Kabaleeswaran, V., Pan, Y., Punta, M., Love, J., Weng, J., Quick, M., Ye, S., Kloss, B., Bruni, R., Martinez-Hackert, E., Hendrickson, W. A., Rost, B., Javitch, J. A., Rajashankar, K. R., … Zhou, M. (2011). Crystal structure of a potassium ion transporter, TrkH. *Nature*, *471*(7338), 336–341. https://doi.org/10.1038/nature09731

Chaplan, S. R., Bach, F. W., Pogrel, J. W., Chung, J. M., & Yaksh, T. L. (1994). Quantitative assessment of tactile allodynia in the rat paw. *Journal of Neuroscience Methods*, *53*(1), 55–63. https://doi.org/10.1016/0165-0270(94)90144-9

Cheng, W., Zhou, F., Zhu, B., Ding, X., Lu, J., Qian, C., Ye, X., & Ding, Z. (2021). Characterization and evaluation of Bletilla striata polysaccharide/ethanol extract composite multifunctional sponges. *Materials and Design*, *206*, 109806. https://doi.org/10.1016/j.matdes.2021.109806

Colloca, L., Ludman, T., Bouhassira, D., Baron, R., Dickenson, A. H., Yarnitsky, D., Freeman, R.,

Truini, A., Attal, N., Finnerup, N. B., Eccleston, C., Kalso, E., Bennett, D. L., Dworkin, R. H., & Raja, S. N. (2017). Neuropathic pain. *Nature Reviews Disease Primers*, *3*, 1–20. https://doi.org/10.1038/nrdp.2017.2

Comissão das Comunidades Europeias. (2008). *Pt Pt Pt*. *2014*, 12.

Cooper, M. K., Porter, J. A., Young, K. E., & Beachy, P. A. (1998). Teratogen-mediated inhibition of target tissue response to Shh signaling. *Science*, *280*(5369), 1603–1607. https://doi.org/10.1126/science.280.5369.1603

Costa, P. F., Santos, A. I., & Ribeiro, M. A. (1994). Potassium currents in acutely isolated maturing rat hippocampal CA1 neurones. *Developmental Brain Research*, *83*(2), 216–223. https://doi.org/10.1016/0165-3806(94)00140-5

Costigan, M., & Woolf, C. J. (2000). Pain: Molecular mechanisms. *Journal of Pain*, *1*(3 SUPPL.), 35–44. https://doi.org/10.1054/jpai.2000.9818

Coward, K., Plumpton, C., Facer, P., Birch, R., Carlstedt, T., Tate, S., Bountra, C., & Anand, P. (2000). Immunolocalization of SNS/PN3 and NaN/SNS2 sodium channels in human pain states. *Pain*, *85*(1–2), 41–50. https://doi.org/10.1016/S0304-3959(99)00251-1

Cummins, T. R., & Waxman, S. G. (1997). Downregulation of tetrodotoxin-resistant sodium currents and upregulation of a rapidly repriming tetrodotoxin-sensitive sodium current in small spinal sensory neurons after nerve injury. *Journal of Neuroscience*, *17*(10), 3503–3514. https://doi.org/10.1523/jneurosci.17-10-03503.1997

Cutignano, A., Nuzzo, G., Ianora, A., Luongo, E., Romano, G., Gallo, C., Sansone, C., Aprea, S., Mancini, F., D'Oro, U., & Fontana, A. (2015). Development and application of a novel SPE-method for bioassay-guided fractionation of marine extracts. *Marine Drugs*, *13*(9), 5736–5749. https://doi.org/10.3390/md13095736

Daou, I., Beaudry, H., Ase, A. R., Wieskopf, J. S., Ribeiro-da-silva, A., Mogil, J. S., & Séguéla, P. (2016). *Optogenetic Silencing of Na v 1 . 8-Positive Afferents Alleviates Inflammatory and Neuropathic Pain*. *3*(February), 1–12.

De Hert, S., De Baerdemaeker, L., & De Maeseneer, M. (2014). What the phlebologist should know about local anesthetics. *Phlebology*, *29*(7), 428–441. https://doi.org/10.1177/0268355513501303

De Sousa, M. V. P., Ferraresi, C., De Magalhães, A. C., Yoshimura, E. M., & Hamblin, M. R. (2014). Building, testing and validating a set of home-made von Frey filaments: A precise, accurate and cost effective alternative for nociception assessment. *Journal of Neuroscience Methods*, *232*, 1–5. https://doi.org/10.1016/j.jneumeth.2014.04.017

Dib-Hajj, S. D., Black, J. A., & Waxman, S. G. (2009). Voltage-gated sodium channels: Therapeutic targets for pain. *Pain Medicine*, *10*(7), 1260–1269. https://doi.org/10.1111/j.1526-4637.2009.00719.x

Dib-Hajj, S. D., Yang, Y., Black, J. A., & Waxman, S. G. (2013). The Na v 1.7 sodium channel: From molecule to man. *Nature Reviews Neuroscience*, *14*(1), 49–62. https://doi.org/10.1038/nrn3404

Dong, X. W., Goregoaker, S., Engler, H., Zhou, X., Mark, L., Crona, J., Terry, R., Hunter, J., & Priestley, T. (2007). Small interfering RNA-mediated selective knockdown of NaV1.8 tetrodotoxin-resistant sodium channel reverses mechanical allodynia in neuropathic rats. *Neuroscience*, *146*(2), 812–821. https://doi.org/10.1016/j.neuroscience.2007.01.054

Doyle, D. A., Cabral, M., Pfuetzner, R. A., Kuo, A., Gulbis, J. M., Cohen, S. L., Chait, B. T., & Mackinnon, R. (1998). The Structure of the PotassiumChannel: Molecular Basis of K. *Science*, *280*(April), 1–9. papers2://publication/uuid/054C4FA3-F61C-4B97-92F6-7707970FA7F6

Du, X., & Gamper, N. (2013). Potassium Channels in Peripheral Pain Pathways: Expression, Function and Therapeutic Potential. *Current Neuropharmacology*, *11*(6), 621–640. https://doi.org/10.2174/1570159x113119990042

Everill, B., Rizzo, M. A., & Kocsis, J. D. (1998). Morphologically identified cutaneous afferent DRG neurons express three different potassium currents in varying proportions. *Journal of Neurophysiology*, *79*(4), 1814–1824. https://doi.org/10.1152/jn.1998.79.4.1814

Faulkner, D. J., Harper, M. K., Haygood, M. G., Salomon, C. E., & Schmidt, E. W. (2004). Symbiotic Bacteria in Sponges: Sources of Bioactive Substances. *Drugs from the Sea*, 107–119. https://doi.org/10.1159/000062486

Fernando, I. P. S., Fernando, P. W. P., Kim, T., & Ahn, G. (2021). Structural diversity, biosynthesis, and health-promoting properties of brown algal meroditerpenoids. *Critical Reviews in*

Biotechnology, *0*(0), 1–22. https://doi.org/10.1080/07388551.2021.2001639
Fitzgerald, M. (1991). Development of pain mechanisms. *British Medical Bulletin*, *47*(3), 667–675. https://doi.org/10.1093/oxfordjournals.bmb.a072499
Garland, E. L., & Ph, D. (2013). Pain Processing in the Nervous System. *Prim Care*, *39*(3), 561–571. https://doi.org/10.1016/j.pop.2012.06.013.Pain
Gemes, G., Koopmeiners, A., Rigaud, M., Lirk, P., Sapunar, D., Bangaru, M. L., Vilceanu, D., Garrison, S. R., Ljubkovic, M., Mueller, S. J., Stucky, C. L., & Hogan, Q. H. (2013). Failure of action potential propagation in sensory neurons: Mechanisms and loss of afferent filtering in C-type units after painful nerve injury. *Journal of Physiology*, *591*(4), 1111–1131. https://doi.org/10.1113/jphysiol.2012.242750
Gentet, L. J., Stuart, G. J., & Clements, J. D. (2000). *10866957*. *79*(July), 1–7. http://www.ncbi.nlm.nih.gov/pmc/articles/PMC1300935/pdf/10866957.pdf%5Cnpapers2://publication/uuid/0FF7A1BB-786B-46B7-83F2-C5A4626D3121
Gilchrist, J., Olivera, B. M., & Bosmans, F. (2014). Animal toxins influence voltage-gated sodium channel function. *Handbook of Experimental Pharmacology*, *221*, 203–229. https://doi.org/10.1007/978-3-642-41588-3_10
Godazgar, M., Zhang, Q., Chibalina, M. V., & Rorsman, P. (2018). Biphasic voltage-dependent inactivation of human Na V 1.3, 1.6 and 1.7 Na + channels expressed in rodent insulin-secreting cells. *Journal of Physiology*, *596*(9), 1601–1626. https://doi.org/10.1113/JP275587
Goiris, K., Muylaert, K., Fraeye, I., Foubert, I., De Brabanter, J., & De Cooman, L. (2012). Antioxidant potential of microalgae in relation to their phenolic and carotenoid content. *Journal of Applied Phycology*, *24*(6), 1477–1486. https://doi.org/10.1007/s10811-012-9804-6
Gold, M. S., Reichling, D. B., Shuster, M. J., & Levine, J. D. (1996). Hyperalgesic agents increase a tetrodotoxin-resistant Na+ current in nociceptors. *Proceedings of the National Academy of Sciences of the United States of America*, *93*(3), 1108–1112. https://doi.org/10.1073/pnas.93.3.1108
Gold, M. S., Shuster, M. J., & Levine, J. D. (1996). Characterization of six voltage-gated K+ currents in adult rat sensory neurons. *Journal of Neurophysiology*, *75*(6), 2629–2646. https://doi.org/10.1152/jn.1996.75.6.2629
Haefeli, M., & Elfering, A. (2006). Pain assessment. *European Spine Journal*, *15*(SUPPL. 1), 17–24. https://doi.org/10.1007/s00586-005-1044-x
Hardoim, C. C. P., & Costa, R. (2014). Microbial communities and bioactive compounds in marine sponges of the family irciniidae-A review. *Marine Drugs*, *12*(10), 5089–5122. https://doi.org/10.3390/md12105089
Helber, S. B., Hoeijmakers, D. J. J., Muhando, C. A., Rohde, S., & Schupp, P. J. (2018). Sponge chemical defenses are a possible mechanism for increasing sponge abundance on reefs in Zanzibar. *PLoS ONE*, *13*(6), 7–10. https://doi.org/10.1371/journal.pone.0197617
Hille, B. (2001). *Ion Channels of Excitable Membranes* (3rd ed.). Sinauer Associates Inc.
Hodgkin, A., & Huxley, A. (1952). A quantitative description of membrane current and its application to conductance and excitation. *Journal of Physiology*, *117*, 500–544.
Hong, S., & Wiley, J. W. (2006). Altered expression and function of sodium channels in large DRG neurons and myelinated A-fibers in early diabetic neuropathy in the rat. *Biochemical and Biophysical Research Communications*, *339*(2), 652–660. https://doi.org/10.1016/j.bbrc.2005.11.057
Hori, Y., Goto, G., Arai-Iwasaki, M., Ishikawa, M., & Sakamoto, A. (2013). Differential expression of rat hippocampal microRNAs in two rat models of chronic pain. *International Journal of Molecular Medicine*, *32*(6), 1287–1292. https://doi.org/10.3892/ijmm.2013.1504
Hudspith, M., Rix, L., Achlatis, M., Bougoure, J., Guagliardo, P., Clode, P. L., Webster, N. S., Muyzer, G., Pernice, M., & de Goeij, J. M. (2021). Subcellular view of host–microbiome nutrient exchange in sponges: insights into the ecological success of an early metazoan–microbe symbiosis. *Microbiome*, *9*(1), 1–15. https://doi.org/10.1186/s40168-020-00984-w
Hulse, R. P., Wynick, D., & Donaldson, L. F. (2011). Activation of the galanin receptor 2 in the periphery reverses nerve injury-induced allodynia. *Molecular Pain*, *7*, 1–12. https://doi.org/10.1186/1744-8069-7-26
index @ www.marinepharmacology.org. (n.d.). https://www.marinepharmacology.org/

Isbn, C., Pdf, T., Press, N. A., Press, N. A., Academy, N., Academy, N., & Press, N. A. (1991). Recognition and Alleviation of Pain and Distress in Laboratory Animals. In *ILAR Journal* (Vol. 33, Issue 4). https://doi.org/10.1093/ilar.33.4.71

Ishikawa, K., Tanaka, M., Black, J. A., & Waxman, S. G. (1999). Changes in expression of voltage-gated potassium channels in dorsal root ganglion neurons following axotomy. *Muscle and Nerve*, *22*(4), 502–507. https://doi.org/10.1002/(SICI)1097-4598(199904)22:4<502::AID-MUS12>3.0.CO;2-K

Israel, M. R., Tay, B., Deuis, J. R., & Vetter, I. (2017). Sodium Channels and Venom Peptide Pharmacology. In *Advances in Pharmacology* (1st ed., Vol. 79). Elsevier Inc. https://doi.org/10.1016/bs.apha.2017.01.004

Jänig, W. (2009). Pain and the Sympathetic Nervous System. In L. R. Squire (Ed.), *Encyclopedia of Neuroscience* (pp. 371–383). Academic Press. https://doi.org/https://doi.org/10.1016/B978-008045046-9.00703-8

Jonas, R., Klusch, A., Schmelz, M., Petersen, M., & Carr, R. W. (2015). Assessment of TTX-s and TTX-r action potential conduction along neurites of NGF and GDNF cultured porcine DRG somata. *PLoS ONE*, *10*(9), 1–16. https://doi.org/10.1371/journal.pone.0139107

Keyhanfar, F., Meymandi, M. S., Sepehri, G., Rastegaryanzadeh, R., & Heravi, G. (2013). Evaluation of antinociceptive effect of pregabalin in mice and its combination with tramadol using tail flick test. *Iranian Journal of Pharmaceutical Research*, *12*(3), 483–493. https://doi.org/10.22037/ijpr.2013.1340

Klugbauer, N., Lacinova, L., Flockerzi, V., & Hofmann, F. (1995). Structure and functional expression of a new member of the tetrodotoxin-sensitive voltage-activated sodium channel family from human neuroendocrine cells. *EMBO Journal*, *14*(6), 1084–1090. https://doi.org/10.1002/j.1460-2075.1995.tb07091.x

Krames, E. S. (2015). The dorsal root ganglion in chronic pain and as a target for neuromodulation: A review. *Neuromodulation*, *18*(1), 24–32. https://doi.org/10.1111/ner.12247

Kress, G. J., & Mennerick, S. (2009). Action potential initiation and propagation: Upstream influences on neurotransmission. *Neuroscience*, *158*(1), 211–222. https://doi.org/10.1016/j.neuroscience.2008.03.021

Kubo, Y., Adelman, J. P., Clapham, D. E., Jan, L. Y., Karschin, A., Kurachi, Y., Lazdunski, M., Nichols, C. G., Seino, S., & Vandenberg, C. A. (2005). International union of pharmacology. LIV. Nomenclature and molecular relationships of inwardly rectifying potassium channels. *Pharmacological Reviews*, *57*(4), 509–526. https://doi.org/10.1124/pr.57.4.11

Kumar, S. P., & Ravikumar, S. (2014). In vitro antiplasmodial activity of marine sponge Clathria vulpina extract against chloroquine sensitive Plasmodium falciparum. *Asian Pacific Journal of Tropical Disease*, *4*(S1). https://doi.org/10.1016/S2222-1808(14)60433-3

Kuphal, K. E., Fibuch, E. E., & Taylor, B. K. (2007). Extended Swimming Exercise Reduces Inflammatory and Peripheral Neuropathic Pain in Rodents. *Journal of Pain*, *8*(12), 989–997. https://doi.org/10.1016/j.jpain.2007.08.001

Laedermann, C. J., Cachemaille, M., Kirschmann, G., Pertin, M., Gosselin, R. D., Chang, I., Albesa, M., Towne, C., Schneider, B. L., Kellenberger, S., Abriel, H., & Decosterd, I. (2013). Dysregulation of voltage-gated sodium channels by ubiquitin ligase NEDD4-2 in neuropathic pain. *Journal of Clinical Investigation*, *123*(7), 3002–3013. https://doi.org/10.1172/JCI68996

Lavand'Homme, P. (2011). The progression from acute to chronic pain. *Current Opinion in Anaesthesiology*, *24*(5), 545–550. https://doi.org/10.1097/ACO.0b013e32834a4f74

Li, C. L., & Bak, A. (1976). Excitability characteristics of the A- and C-fibers in a peripheral nerve. *Experimental Neurology*, *50*(1), 67–79. https://doi.org/10.1016/0014-4886(76)90236-3

Lindquist, N., Hay, M. E., & Fenical, W. (1992). Defense of Ascidians and Their Conspicuous Larvae : Adult vs . Larval Chemical Defenses Author (s): Niels Lindquist , Mark E . Hay , William Fenical Reviewed work (s): Published by : Ecological Society of America Stable URL : http://www.jstor.org/stab. *Ecological Monographs*, *62*(4), 547–568.

Liu, M., & Wood, J. N. (2011). The Roles of Sodium Channels in Nociception : *Pain Medicine*, *12*, 93–99.

Luján, R. (2010). Organisation of potassium channels on the neuronal surface. *Journal of Chemical Neuroanatomy*, *40*(1), 1–20. https://doi.org/10.1016/j.jchemneu.2010.03.003

Ma, R. S. Y., Kayani, K., Whyte-Oshodi, D., Whyte-Oshodi, A., Nachiappan, N., Gnanarajah, S., & Mohammed, R. (2019). Voltage gated sodium channels as therapeutic targets for chronic pain. *Journal of Pain Research*, *12*, 2709–2722. https://doi.org/10.2147/JPR.S207610

Malin, S. A., Davis, B. M., & Molliver, D. C. (2007). Production of dissociated sensory neuron cultures and considerations for their use in studying neuronal function and plasticity. *Nature Protocols*, *2*(1), 152–160. https://doi.org/10.1038/nprot.2006.461

Manzano, G. M., Giuliano, L. M. P., & Nóbrega, J. A. M. (2008). A brief historical note on the classification of nerve fibers. *Arquivos de Neuro-Psiquiatria*, *66*(1), 117–119. https://doi.org/10.1590/S0004-282X2008000100033

Marchand, S. (2008). The Physiology of Pain Mechanisms: From the Periphery to the Brain. *Rheumatic Disease Clinics of North America*, *34*(2), 285–309. https://doi.org/10.1016/j.rdc.2008.04.003

Mazzocchio, R., & Caleo, M. (2015). More than at the Neuromuscular Synapse: Actions of Botulinum Neurotoxin A in the Central Nervous System. *The Neuroscientist*, *21*(1), 44–61. https://doi.org/10.1177/1073858414524633

McCormick, T., & Law, S. (2016). Assessment of acute and chronic pain. *Anaesthesia and Intensive Care Medicine*, *17*(9), 421–424. https://doi.org/10.1016/j.mpaic.2016.06.007

Merlin, J. L., Azzi, S., Lignon, D., Ramacci, C., Zeghari, N., & Guillemin, F. (1992). MTT assays allow quick and reliable measurement of the response of human tumour cells to photodynamic therapy. *European Journal of Cancer*, *28*(8–9), 1452–1458. https://doi.org/10.1016/0959-8049(92)90542-A

Michels, P. J., Adams, D. B., & McBride, P. (1983). Chronic pain. *Journal of Family Practice*, *17*(4), 591–610.

Minett, M. S., Eijkelkamp, N., & Wood, J. N. (2014). Significant determinants of mouse pain behaviour. *PLoS ONE*, *9*(8). https://doi.org/10.1371/journal.pone.0104458

Mischel, R. A., Dewey, W. L., & Akbarali, H. I. (2018). Tolerance to Morphine-Induced Inhibition of TTX-R Sodium Channels in Dorsal Root Ganglia Neurons Is Modulated by Gut-Derived Mediators. *IScience*, *2*, 193–209. https://doi.org/10.1016/j.isci.2018.03.003

Mogil, J. S. (2015). Social modulation of and by pain in humans and rodents. *Pain*, *156*(4), S35–S41. https://doi.org/10.1097/01.j.pain.0000460341.62094.77

O'Toole, S. A., Sheppard, B. L., McGuinness, E. P. J., Gleeson, N. C., Yoneda, M., & Bonnar, J. (2003). The MTS assay as an indicator of chemosensitivity/resistance in malignant gynaecological tumours. *Cancer Detection and Prevention*, *27*(1), 47–54. https://doi.org/10.1016/S0361-090X(02)00171-X

Ocaña, M., Cendán, C. M., Cobos, E. J., Entrena, J. M., & Baeyens, J. M. (2004). Potassium channels and pain: Present realities and future opportunities. *European Journal of Pharmacology*, *500*(1-3 SPEC. ISS.), 203–219. https://doi.org/10.1016/j.ejphar.2004.07.026

Pasquet, V., Morisset, P., Ihammouine, S., Chepied, A., Aumailley, L., Berard, J. B., Serive, B., Kaas, R., Lanneluc, I., Thiery, V., Lafferriere, M., Piot, J. M., Patrice, T., Cadoret, J. P., & Picot, L. (2011). Antiproliferative activity of violaxanthin isolated from bioguided fractionation of Dunaliella tertiolecta extracts. *Marine Drugs*, *9*(5), 819–831. https://doi.org/10.3390/md9050819

Pogatzki-Zahn, E., Kranke, P., Winner, J., Weyland, W., Reich, A., Vigelius-Rauch, U., Paland, M., Löhr, T., & Eberhart, L. (2020). Real-world use of the sufentanil sublingual tablet system for patient-controlled management of acute postoperative pain: a prospective noninterventional study. *Current Medical Research and Opinion*, *36*(2), 277–284. https://doi.org/10.1080/03007995.2019.1681133

Powley, T. L. (2021). Brain-gut communication: vagovagal reflexes interconnect the two "brains." *American Journal of Physiology-Gastrointestinal and Liver Physiology*, *321*(5), G576–G587. https://doi.org/10.1152/ajpgi.00214.2021

Raffaeli, W., & Arnaudo, E. (2017). Pain as a disease: An overview. *Journal of Pain Research*, *10*, 2003–2008. https://doi.org/10.2147/JPR.S138864

Raj, A. A., & Birring, S. S. (2007). Clinical assessment of chronic cough severity. *Pulmonary Pharmacology and Therapeutics*, *20*(4), 334–337. https://doi.org/10.1016/j.pupt.2006.10.002

Ramachandra, R., Mcgrew, S. Y., Baxter, J. C., Kiveric, E., & Elmslie, K. S. (2012). Tetrodotoxin-resistant voltage-dependent sodium channels in identified muscle afferent neurons. *Journal of Neurophysiology*, *108*(8), 2230–2241. https://doi.org/10.1152/jn.00219.2012

Ramachandran, R. (2018). Neurogenic inflammation and its role in migraine. *Seminars in Immunopathology*, *40*(3), 301–314. https://doi.org/10.1007/s00281-018-0676-y

Rasband, M. N., Park, E. W., Vanderah, T. W., Lai, J., Porreca, F., & Trimmer, J. S. (2001). Distinct potassium channels on pain-sensing neurons. *Proceedings of the National Academy of Sciences of the United States of America*, *98*(23), 13373–13378. https://doi.org/10.1073/pnas.231376298

Renganathan, M., Cummins, T. R., & Waxman, S. G. (2001). Contribution of Nav 1.8 sodium channels to action potential electrogenesis in DRG neurons. *Journal of Neurophysiology*, *86*(2), 629–640. https://doi.org/10.1152/jn.2001.86.2.629

Renthal, W. (2020). Chapter 23 - Pain genetics. In R. N. Rosenberg & J. M. Pascual (Eds.), *Rosenberg's Molecular and Genetic Basis of Neurological and Psychiatric Disease (Sixth Edition)* (Sixth Edit, pp. 397–410). Academic Press. https://doi.org/https://doi.org/10.1016/B978-0-12-813866-3.00023-0

Ribeiro, M. A., & Costa, P. F. (2000). Kinetic parameters of calcium currents in maturing acutely isolated CA1 cells. *Developmental Brain Research*, *124*(1–2), 11–23. https://doi.org/10.1016/S0165-3806(00)00099-7

Rigaud, M., Gemes, G., Barabas, M. E., Chernoff, D. I., Abram, S. E., Stucky, C. L., & Hogan, Q. H. (2008). Species and strain differences in rodent sciatic nerve anatomy: Implications for studies of neuropathic pain. *Pain*, *136*(1–2), 188–201. https://doi.org/10.1016/j.pain.2008.01.016

Roberts, W. J., & Kramis, R. C. (1990). Sympathetic nervous system influence on acute and chronic pain. In *Pain Syndromes in Neurology*. Butterworth & Co. (Publishers) Ltd. https://doi.org/10.1016/b978-0-407-01124-3.50010-1

Rocha, J., Peixe, L., Gomes, N. C. M., & Calado, R. (2011). Cnidarians as a source of new marine bioactive compounds - An overview of the last decade and future steps for bioprospecting. *Marine Drugs*, *9*(10), 1860–1886. https://doi.org/10.3390/md9101860

Rush, A. M., Cummins, T. R., & Waxman, S. G. (2007). Multiple sodium channels and their roles in electrogenesis within dorsal root ganglion neurons. *Journal of Physiology*, *579*(1), 1–14. https://doi.org/10.1113/jphysiol.2006.121483

Russo, C. M., & Brose, W. G. (1998). Chronic Pain. *Annual Review of Medicine*, *49*(1), 123–133. https://doi.org/10.1146/annurev.med.49.1.123

Saab, C. Y. (2012). Pain-related changes in the brain: Diagnostic and therapeutic potentials. *Trends in Neurosciences*, *35*(10), 629–637. https://doi.org/10.1016/j.tins.2012.06.002

Serrão, J. M. M. (2015). *Validation of voltage-gated sodium channels from dorsal root ganglia neurons as a pharmacological target for the treatment of Chronic pain*.

Shah, K. U., Nandkishor, M., Singh, J. N. J., Sharma, S. S., Mule, N., Singh, J. N. J., & Sharma, S. S. (2010). Voltage Gated Sodium Channel Blockers: Potential Treatment for Neuropathic Pain. *Current Research & Information on Pharmaceuticals Sciences*, *11*(1), 11–16.

Sontheimer, H., & Ransom, C. B. (2002). Whole-Cell Patch-Clamp Recordings. In W. Walz, A. A. Boulton, & G. B. Baker (Eds.), *Patch-Clamp Analysis: Advanced Techniques* (pp. 35–67). Humana Press. https://doi.org/10.1385/1-59259-276-7:35

Standen, N. B., & Stanfield, P. R. (1978). A potential- and time-dependent blockade of inward rectification in frog skeletal muscle fibres by barium and strontium ions. *The Journal of Physiology*, *280*(1), 169–191. https://doi.org/10.1113/jphysiol.1978.sp012379

Suer, M., & Sehgal, N. (2021). Pain Signaling Processes. In *Questions and Answers in Pain Medicine: A Guide to Board Exams* (pp. 19–26). Springer International Publishing. https://doi.org/10.1007/978-3-030-68204-0_4

Szwarc, B. (2017). *Characterization of Voltage-Gated Potassium Channels from Dorsal Root Ganglia Neurons in Neuropathic and Inflammatory Chronic Pain*.

Tanaka, N., Goodell, H., & Karger, B. L. (1978). The role of organic modifiers on polar group selectivity in reversed-phase liquid chromatography. *Journal of Chromatography A*, *158*(C), 233–248. https://doi.org/10.1016/S0021-9673(00)89970-7

Taylor, M. W., Hill, R. T., Piel, J., Thacker, R. W., & Hentschel, U. (2007). Soaking it up: The complex lives of marine sponges and their microbial associates. *ISME Journal*, *1*(3), 187–190. https://doi.org/10.1038/ismej.2007.32

Taylor, M. W., Radax, R., Steger, D., & Wagner, M. (2007). Sponge-Associated Microorganisms: Evolution, Ecology, and Biotechnological Potential. *Microbiology and Molecular Biology*

Reviews, *71*(2), 295–347. https://doi.org/10.1128/mmbr.00040-06

The Axon Guide. (n.d.). 2500.The Axon Guide. (n.d.). *2500*.

Thomas, T. R. A., Kavlekar, D. P., & LokaBharathi, P. A. (2010). Marine drugs from sponge-microbe association - A review. *Marine Drugs*, *8*(4), 1417–1468. https://doi.org/10.3390/md8041417

Tsantoulas, C., & McMahon, S. B. (2014). Opening paths to novel analgesics: The role of potassium channels in chronic pain. *Trends in Neurosciences*, *37*(3), 146–158. https://doi.org/10.1016/j.tins.2013.12.002

Varijakzhan, D., Loh, J. Y., Yap, W. S., Yusoff, K., Seboussi, R., Lim, S. H. E., Lai, K. S., & Chong, C. M. (2021). Bioactive compounds from marine sponges: Fundamentals and applications. *Marine Drugs*, *19*(5). https://doi.org/10.3390/md19050246

Wang, G. (2006). Diversity and biotechnological potential of the sponge-associated microbial consortia. *Journal of Industrial Microbiology and Biotechnology*, *33*(7), 545–551. https://doi.org/10.1007/s10295-006-0123-2

Wang, H. J., Li, Y. L., Zhang, L. Bin, Zucker, I. H., Gao, L., Zimmerman, M. C., & Wang, W. (2011). Endogenous reactive oxygen species modulates voltage-gated sodium channels in dorsal root ganglia of rats. *Journal of Applied Physiology*, *110*(5), 1439–1447. https://doi.org/10.1152/japplphysiol.01409.2010

Wang, J., Ou, S. W., Bai, Y. F., Wang, Y. J., Xu, Z. Q. D., & Luan, G. M. (2017). Multiple Nav1.5 isoforms are functionally expressed in the brain and present distinct expression patterns compared with cardiac Nav1.5. *Molecular Medicine Reports*, *16*(1), 719–729. https://doi.org/10.3892/mmr.2017.6654

Waxman, S. G. (1980). Determinants of conduction velocity in myelinated nerve fibers. *Muscle & Nerve*, *3*(2), 141–150. https://doi.org/10.1002/mus.880030207

Waxman, S. G., & Zamponi, G. W. (2014). Regulating excitability of peripheral afferents: Emerging ion channel targets. *Nature Neuroscience*, *17*(2), 153–163. https://doi.org/10.1038/nn.3602

Wulff, H., Castle, N. A., & Pardo, L. A. (2009). Voltage-gated potassium channels as therapeutic targets. *Nature Reviews Drug Discovery*, *8*(12), 982–1001. https://doi.org/10.1038/nrd2983

Yu, F. H., Yarov-Yarovoy, V., Gutman, G. A., & Catterall, W. A. (2005). Overview of molecular relationships in the voltage-gated ion channel superfamily. *Pharmacological Reviews*, *57*(4), 387–395. https://doi.org/10.1124/pr.57.4.13

Zemel, B. M., Ritter, D. M., Covarrubias, M., & Muqeem, T. (2018). A-Type KV Channels in Dorsal Root Ganglion Neurons: Diversity, Function, and Dysfunction. *Frontiers in Molecular Neuroscience*, *11*(August), 1–17. https://doi.org/10.3389/fnmol.2018.00253

Zhang, Q. W., Lin, L. G., & Ye, W. C. (2018). Techniques for extraction and isolation of natural products: A comprehensive review. *Chinese Medicine (United Kingdom)*, *13*(1), 1–26. https://doi.org/10.1186/s13020-018-0177-x

Zhang, X. L., & Gold, M. S. (2009). Dihydropyridine block of voltage-dependent K+ currents in rat dorsal root ganglion neurons. *Neuroscience*, *161*(1), 184–194. https://doi.org/10.1016/j.neuroscience.2009.03.012

A.
Appendix

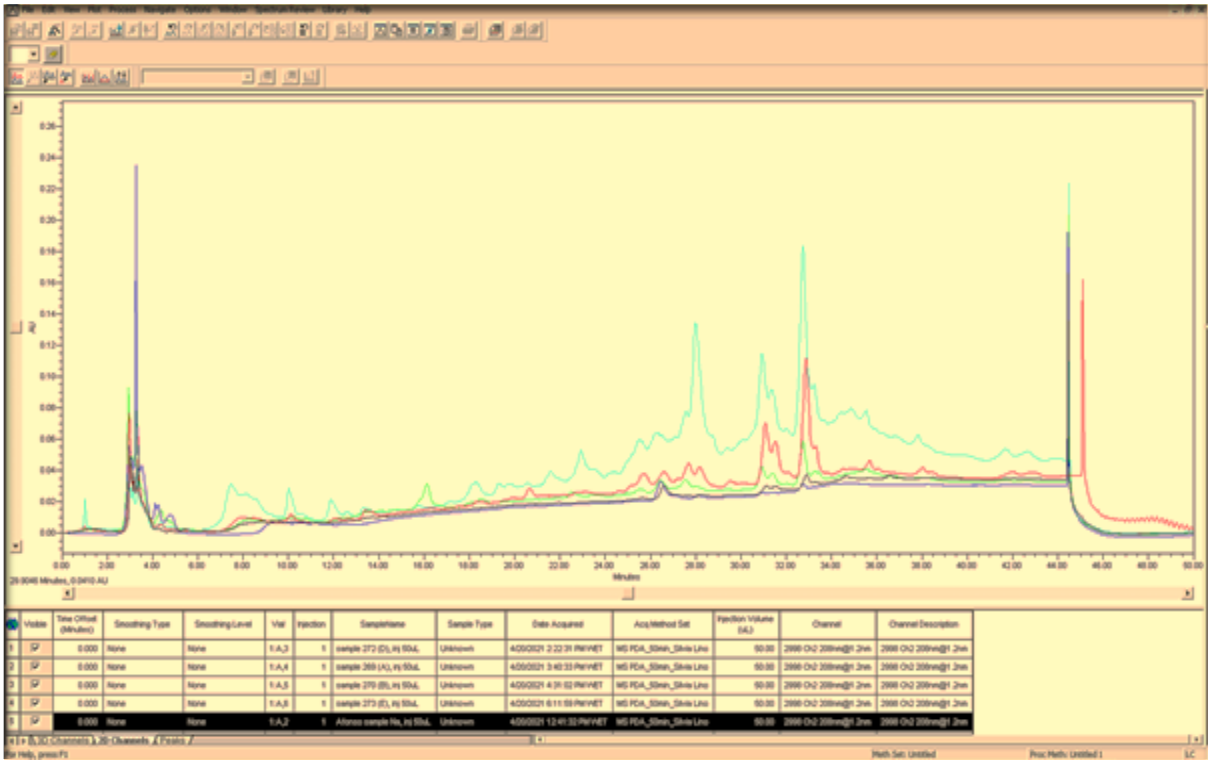

Figure A.7.1 - HPLC chromatograms of the fractions obtained with the fractionation 1 method, first experiment. The HPLC separation method was performed with a gradient elution starting at 0min with 95% ACN and 5% MeOH and ending at 40min with 100 % MeOH, with a subsequent washing of the column until the end of the protocol (lasting for up to 50min). The chromatograms of the 5 fractions collected in the fractionation method are sequentially shown from bottom to top: H2O; H2O/MeOH (1:1); MeOH/H2O (7:3); ACN; DCM/MeOH (9:1).

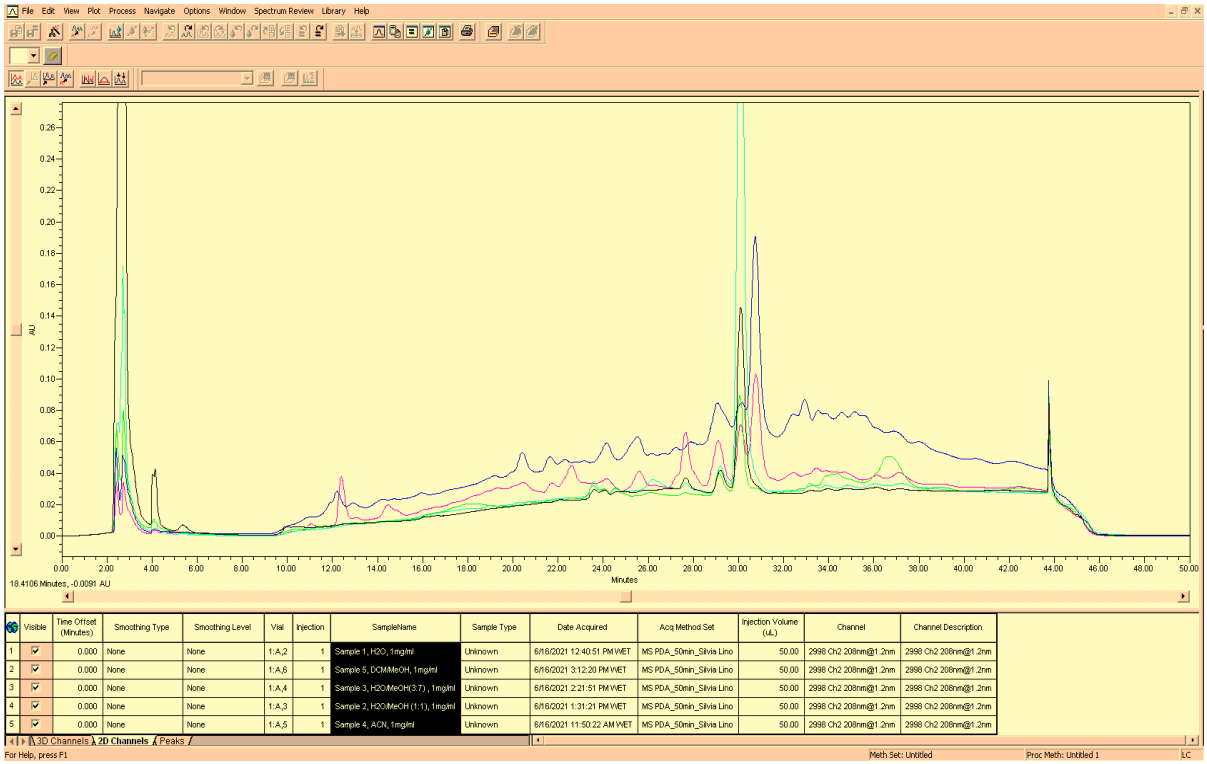

	Visible	Time Offset (Minutes)	Smoothing Type	Smoothing Level	Vial	Injection	SampleName	Sample Type	Date Acquired	Acq Method Set	Injection Volume (uL)	Channel	Channel Description
1	☑	0.000	None	None	1:A,2	1	Sample 1, H2O, 1mg/ml	Unknown	6/16/2021 12:40:51 PM WET	MS PDA_50min_Silvia Lino	50.00	2998 Ch2 208nm@1.2nm	2998 Ch2 208nm@1.2nm
2	☑	0.000	None	None	1:A,6	1	Sample 5, DCM/MeOH, 1mg/ml	Unknown	6/16/2021 3:12:20 PM WET	MS PDA_50min_Silvia Lino	50.00	2998 Ch2 208nm@1.2nm	2998 Ch2 208nm@1.2nm
3	☑	0.000	None	None	1:A,4	1	Sample 3, H2O/MeOH(3:7) , 1mg/ml	Unknown	6/16/2021 2:21:51 PM WET	MS PDA_50min_Silvia Lino	50.00	2998 Ch2 208nm@1.2nm	2998 Ch2 208nm@1.2nm
4	☑	0.000	None	None	1:A,3	1	Sample 2, H2O/MeOH (1:1), 1mg/ml	Unknown	6/16/2021 1:31:21 PM WET	MS PDA_50min_Silvia Lino	50.00	2998 Ch2 208nm@1.2nm	2998 Ch2 208nm@1.2nm
5	☑	0.000	None	None	1:A,5	1	Sample 4, ACN, 1mg/ml	Unknown	6/16/2021 11:50:22 AM WET	MS PDA_50min_Silvia Lino	50.00	2998 Ch2 208nm@1.2nm	2998 Ch2 208nm@1.2nm

Figure A.7.2 HPLC chromatograms of the fractions obtained with the fractionation 1 method, second experiment. The HPLC separation method was performed with a gradient elution starting at 0min with 95% ACN and 5% MeOH and ending at 40min with 100 % MeOH, with a subsequent washing of the column until the end of the protocol (lasting for up to 50min). The chromatograms of the 5 fractions collected in the fractionation method are sequentially shown from bottom to top: H2O; H2O/MeOH (1:1); MeOH/H2O (7:3); ACN; DCM/MeOH (9:1).

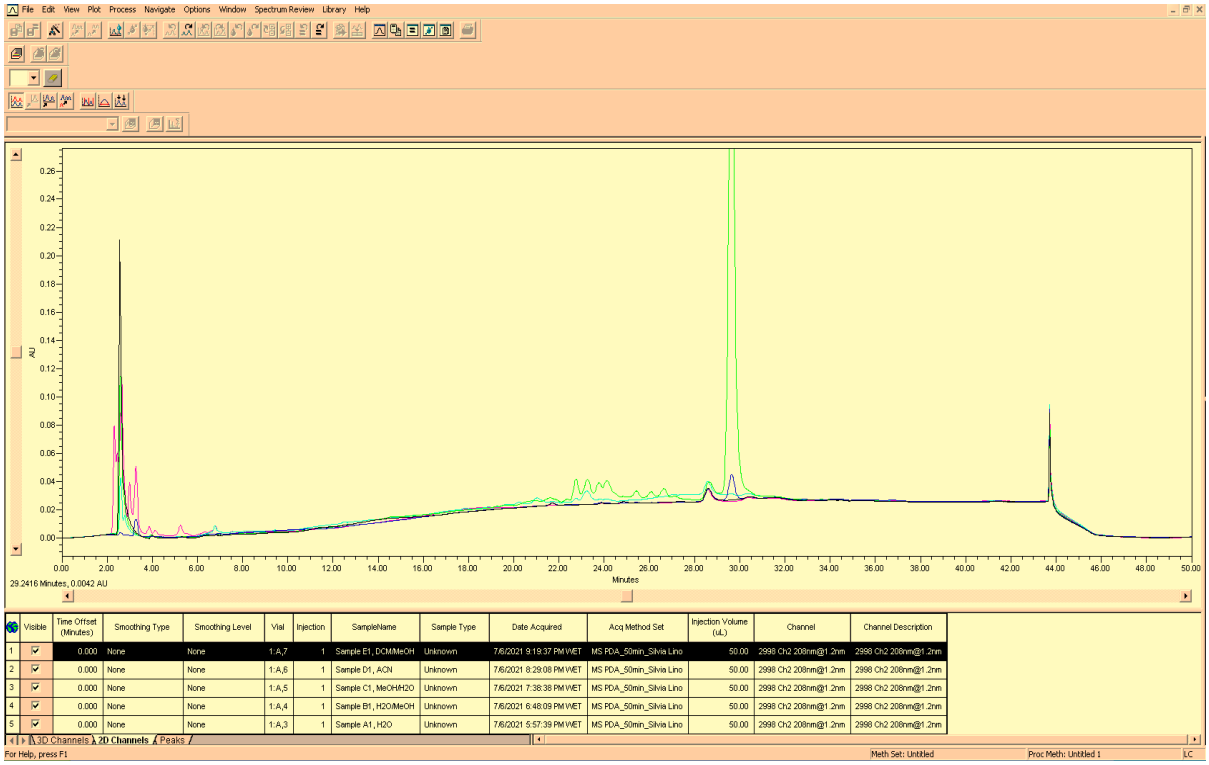

	Visible	Time Offset (Minutes)	Smoothing Type	Smoothing Level	Vial	Injection	SampleName	Sample Type	Date Acquired	Acq Method Set	Injection Volume (uL)	Channel	Channel Description
1	☑	0.000	None	None	1:A,7	1	Sample E1, DCM/MeOH	Unknown	7/6/2021 9:19:37 PM WET	MS PDA_50min_Silvia Lino	50.00	2998 Ch2 208nm@1.2nm	2998 Ch2 208nm@1.2nm
2	☑	0.000	None	None	1:A,6	1	Sample D1, ACN	Unknown	7/6/2021 8:29:08 PM WET	MS PDA_50min_Silvia Lino	50.00	2998 Ch2 208nm@1.2nm	2998 Ch2 208nm@1.2nm
3	☑	0.000	None	None	1:A,5	1	Sample C1, MeOH/H2O	Unknown	7/6/2021 7:38:38 PM WET	MS PDA_50min_Silvia Lino	50.00	2998 Ch2 208nm@1.2nm	2998 Ch2 208nm@1.2nm
4	☑	0.000	None	None	1:A,4	1	Sample B1, H2O/MeOH	Unknown	7/6/2021 6:48:09 PM WET	MS PDA_50min_Silvia Lino	50.00	2998 Ch2 208nm@1.2nm	2998 Ch2 208nm@1.2nm
5	☑	0.000	None	None	1:A,3	1	Sample A1, H2O	Unknown	7/6/2021 5:57:39 PM WET	MS PDA_50min_Silvia Lino	50.00	2998 Ch2 208nm@1.2nm	2998 Ch2 208nm@1.2nm

Figure A.3 - HPLC chromatograms of the fractions obtained with the fractionation 2 method, first experiment. The HPLC separation method was performed with a gradient elution starting at 0min with 95% ACN and 5% MeOH and ending at 40min with 100 % MeOH, with a subsequent washing of the column until the end of the protocol (lasting for up to 50min). The chromatograms of the 5 fractions collected in the fractionation method are sequentially shown from bottom to top: H2O; H2O/MeOH (1:1); MeOH/H2O (7:3); ACN; DCM/MeOH (9:1).

2022

AFONSO MIGUEL DOS SANTOS GONÇALVES

Blue biotechnology on the Coast of Portugal: a prospection of neurological bioactive compounds from marine sponges

NOVA SCHOOL OF SCIENCE & TECHNOLOGY